Titre: Title:	Formation et caractérisation physico-chimique des complexes ADN/chitosane pour la thérapie génique
Auteur: Author:	Pei Lian Ma
Date:	2010
Type:	Mémoire ou thèse / Dissertation or Thesis
Référence: Citation:	Ma, P. L. (2010). Formation et caractérisation physico-chimique des complexes ADN/chitosane pour la thérapie génique [Thèse de doctorat, École Polytechnique de Montréal]. PolyPublie. https://publications.polymtl.ca/304/

URL de PolyPublie: PolyPublie URL:	https://publications.polymtl.ca/304/
Directeurs de recherche: Advisors:	Michael D. Buschmann, & Françoise Winnik
Programme: Program:	Génie chimique

UNIVERSITÉ DE MONTRÉAL

FORMATION ET CARACTÉRISATION PHYSICO-CHIMIQUE DES COMPLEXES ADN/CHITOSANE POUR LA THÉRAPIE GÉNIQUE

PEI LIAN MA

DÉPARTEMENT DE GÉNIE CHIMIQUE

ÉCOLE POLYTECHNIQUE DE MONTRÉAL

THÈSE PRÉSENTÉE EN VUE DE L'OBTENTION

DU DIPLÔME DE PHILOSOPHIAE DOCTOR (Ph. D.)

(GÉNIE CHIMIQUE)

AVRIL 2010

UNIVERSITÉ DE MONTRÉAL

ÉCOLE POLYTECHNIQUE DE MONTRÉAL

Cette thèse intitulée:

FORMATION ET CARACTÉRISATION PHYSICO-CHIMIQUE DES COMPLEXES ADN/CHITOSANE POUR LA THÉRAPIE GÉNIQUE

présentée par : MA Pei Lian

en vue de l'obtention du diplôme de : Philosophiae Doctor

a été dûment acceptée par le jury d'examen constitué de :

M. FAVIS Basil, Ph. D., président

M. BUSCHMANN Michael, Ph. D., membre et directeur de recherche

Mme WINNIK Françoise, Ph. D., membre et codirectrice de recherche

M. DE CRESCENZO Grégory, Ph. D., membre

Mme STRAND Sabina P., Ph. D., membre

DÉDICACE

J’aimerais dédier ce travail à tous les membres de ma famille,

avec mes souhaits de bonheur.

REMERCIEMENTS

Je tiens tout d'abord à remercier mon directeur le professeur Michael Buschmann pour m'avoir donné la chance de rejoindre son groupe de recherche et de continuer mon doctorat suite à mon interruption d'études. Je le remercie également pour la confiance et les moyens qu'il a mis à ma disposition au cours des cinq dernières années dans la réalisation de mon projet de thèse.

Je remercie sincèrement ma co-directrice la professeure Françoise Winnik pour son soutien, sa confiance et son aide durant ces dernières années de thèse. Je me rappellerai toujours avec émotion de la première journée où elle m'a accueillie chaleureusement au sein de son groupe de recherche. Je lui suis très reconnaissante de m'avoir recommandée à Mike afin que je puisse poursuivre mes études et réaliser ce projet. Je lui exprime également ma profonde gratitude pour ses conseils avisés et personnels durant les moments les plus difficiles qui nous ont beaucoup rapprochées.

J'adresse mes sincères remerciements au professeur Basil Favis pour m'avoir initiée à la recherche et appris l'importance du savoir-faire et du savoir-être. Je lui suis très reconnaissante pour l'amitié et le soutien continuel qu'il m'a témoignés durant ces dernières années. Je tiens également à lui exprimer ma gratitude pour avoir accepté de présider ce jury de thèse.

Je remercie également Dr. Strand et Prof. De Crescenzo d'avoir accepté d'évaluer mon travail.

Je remercie mes collègues, du passé et présent, du groupe de Mike et de Mme Winnik. Merci en particulier à J-R, Eliza, Satu, Vladimir, Shivaji, Suri, Cyril, Florence S., Sania, Charbel et Piotr. J'apprécie énormément leur amitié, leur solidarité et tous les moments de détente et de fous rires passés ensemble.

Un grand merci à Yuan, Carol, Robert, Jacques et Louise Beaudry du département de génie chimique pour leur aide précieuse durant ces dernières années. Merci à Sevario et Christian de JAB pour leur sympathie et leur bonne humeur !

Je remercie également le FQRNT et la Fondation J. Armand Bombardier (Fondation de Polytechnique) pour l'octroi de mes bourses d'études.

Je tiens à remercier Margaret et mes *super-héros* Pierre, Florence, Emma, André et Chloé-Anne pour leur soutien chaleureux et l'amitié profonde qu'ils m'ont témoignés pendant ces années. Je vous adore! Pierre, Florence, cette amitié ne serait possible si elle n'était pas fondée sur le respect, le partage et la confiance inestimable que vous m'avez accordés.

Un grand merci à Vincent pour son aide précieuse et la relecture de cette thèse.

Je tiens surtout à remercier tous les membres de ma famille, en particulier mon *petit* chéri, pour leur amour et leur soutien inconditionnel. Aucun mot ne saurait exprimer toute ma grande reconnaissance envers mes parents qui ont beaucoup risqué et énormément donné pour nous offrir une bonne éducation et une vie meilleure.

RÉSUMÉ

La thérapie génique est un secteur biomédical en plein essor et de nombreux vecteurs non-viraux à partir de polymères cationiques ont été étudiés pour la livraison de gènes. Le système de livraison de gènes doit condenser l'ADN, le protéger contre la dégradation par les nucléases, faciliter son entrée dans les cellules et transporter l'ADN jusqu'au noyau pour permettre l'expression des gènes. Ce projet consiste à approfondir notre compréhension d'un système prometteur pour la livraison de gènes: les complexes ADN/chitosane. Les objectifs principaux de cette thèse étaient de déterminer les interactions qui régissent la formation des complexes ADN/chitosane, de caractériser leurs propriétés physico-chimiques et d'étudier leur stabilité afin d'établir une corrélation avec leur efficacité de transfection.

Dans un premier temps, l'association entre le chitosane et un ADN plasmide en fonction du pH, du degré de désacétylation (DDA) et de la masse molaire (M_n) du chitosane a été étudiée par microcalorimétrie de titrage isotherme (ITC). Cette étude nous a permis de déterminer la constante d'interaction, l'enthalpie d'interaction et la stœchiométrie des complexes. Nous avons trouvé que l'interaction chitosane-ADN est couplée avec un transfert de protons du système tampon au chitosane. Le transfert de proton est occasionné par la nature fortement anionique de l'ADN qui facilite l'ionisation des amines du chitosane lors de la complexation. De plus, nous avons démontré que l'enthalpie d'interaction mesurée était entièrement due aux changements d'ionisation du chitosane et du tampon. Nous avons trouvé une constante d'interaction chitosane-ADN de l'ordre de 10^9-10^{10} M^{-1} et qui augmente avec la diminution du pH. Ceci est attribué aux interactions électrostatiques plus intenses lorsque le degré d'ionisation du chitosane est plus élevé. Nous avons également mesuré une augmentation par dix de la constante d'affinité

pour une augmentation de la masse molaire du chitosane de 7 à 153 kDa. Cette constante varie peu pour un DDA compris entre 72% et 80% (~80 kDa). En revanche, un DDA variant de 80 à 93% augmente la constante d'affinité pour atteindre une valeur proche du chitosane avec un M_n de 153 kDa et un DDA de 80%. Ces résultats montrent qu'il est possible de contrôler l'affinité chitosane-ADN par le pH et les caractéristiques moléculaires du chitosane. Cette étude a démontré que la formation des complexes ADN/chitosane est gouvernée par des interactions électrostatiques.

Pour la transfection, les complexes ADN/polycation sont généralement formés avec un excès de polycation et utilisant des ratios N/P supérieurs à 3 (amines du polycation/phosphates de l'ADN). L'excès important de chitosane par rapport à la quantité d'ADN souvent utilisé dans la préparation des complexes pour la transfection nous a convaincu de l'importance de déterminer la fraction de chitosane libre en solution. Le but de cette deuxième étude était de développer une méthode permettant de quantifier cette fraction. Les travaux ont été réalisés en combinant la technique de fractionnement par flux-force avec flux asymétrique (AF4) avec un spectrophotomètre UV/Vis, un détecteur de diffusion de lumière multi-angles (MALS) et un détecteur de diffusion dynamique de la lumière (DLS). Ce système AF4 permet de séparer le chitosane libre des complexes, de le quantifier directement et de mesurer la taille des particules séparées. Pour une dispersion de complexes ADN/chitosane préparée avec un ratio N/P de 5, nous avons trouvé que 73% du chitosane reste sous forme libre. Les particules ADN/chitosane ont un rayon hydrodynamique (R_h) compris entre 20 et 160 nm. Ces résultats ont été confirmés par SEM et par DLS en mode « batch ». Nous avons démontré que ce système AF4 est un outil puissant pour la caractérisation de systèmes de livraison de gènes car il permet à la fois de

mesurer la taille et la distribution de taille des particules mais aussi de quantifier la proportion de chitosane libre en solution.

Le système AF4 couplé avec les détecteurs UV/Vis, MALS et DLS a ensuite été utilisé afin d'étudier des facteurs qui peuvent influencer l'efficacité de transfection des complexes ADN/chitosane, tels que la concentration d'ADN lors du mélange, le rapport N/P utilisé pour préparer les complexes, la masse molaire et le DDA du chitosane. Cette technique a permis de déterminer plusieurs propriétés physico-chimiques importantes des complexes ADN/chitosane: la taille et la distribution de taille et la conformation structurale des particules, ainsi que la composition des particules calculée à partir de la fraction de chitosane libre. Pour toutes les préparations, les particules mesurent de 15 à 160 nm de rayon hydrodynamique mais la distribution de taille varie suivant les préparations. Lorsque la concentration d'ADN ou la masse molaire du chitosane augmente, nous avons observé la formation d'une fraction importante de grosses particules (> 60 nm). Dans tous les cas, la proportion de chitosane libre est majoritaire. Nous avons constaté que la composition des complexes ADN/chitosane reste constante avec une valeur N/P de 1.4, quelque soit l'excès de chitosane utilisé par rapport à l'ADN lors du mélange. Nous avons confirmé ses résultats par ultracentrifugation des dispersions et analyse des surnageants par colorimétrie. Cette étude a révélé l'importance de quantifier le chitosane libre pour comprendre son rôle dans les mécanismes de livraison de gènes.

Après l'étude themodynamique de l'association chitosane-ADN et la caractérisation des propriétés physico-chimiques des complexes ADN/chitosane formés, leur stabilité a été étudiée en présence de différents polyanions compétiteurs afin de complèter ce projet de thèse. Ces polyanions peuvent interagir avec le chitosane et, par conséquent, induire la dissociation des complexes ADN/chitosane. L'ADN dissocié des complexes a été quantifié par spectroscopie de

fluorescence en utilisant le Picogreen comme fluorophore. Nous avons montré que la capacité de ces polyanions à déstabiliser les complexes ADN/chitosane est reliée à leur affinité pour le chitosane par rapport à l'affinité ADN-chitosane. Les complexes ADN/chitosane étaient très stables en présence de la chondroitine de sulfate ou l'acide hyaluronique. La constante d'affinité ADN-chitosane est au moins 40 fois supérieure à celle de ces polyanions pour le chitosane. Par contre, l'héparine qui a une densité de charge élevée et possède une constante d'affinité proche de celle entre l'ADN et le chitosane, peut dissocier les complexes. Cependant, la stabilité des complexes augmente avec le DDA et la masse molaire du chitosane, en accord avec les constantes d'association déterminées dans la première étude. Nous avons également démontré que le chitosane libre en quantité suffisante peut éviter la dissociation des complexes par l'héparine.

ABSTRACT

Chitosan is a prominent natural polymer used in nonviral gene delivery, due to its biocompatibility and biodegradability. It can condense DNA through electrostatic interactions to form nanoparticles that can be internalized by cells. In the first part of this thesis, the interaction of chitosan with plasmid DNA was investigated as a function of pH, buffer composition, degree of deacetylation (DDA) and molecular weight of chitosan, using isothermal titration microcalorimetry (ITC). The chitosan-DNA interaction was shown to be coupled with proton transfer from the buffer to chitosan. This proton transfer is induced by the strong polyanionic nature of DNA which facilitates the ionization of glucosamines of chitosan upon binding. The measured enthalpy of binding was almost entirely due to the ionization changes of the buffer and of chitosan. The chitosan-DNA binding constant was found in the range of 10^{9}-10^{10} M^{-1}. The binding constant was pH-dependent and was greater at lower pH due to increased electrostatic attraction to DNA when chitosan is highly charged. The binding constant between chitosan and plasmid DNA was significantly influenced by molecular weight and by DDA. The electrostatic effects were found to dictate the binding of chitosan to DNA. The results of this study provide insights into previously measured dependence of transfection efficiencies of DNA/chitosan complexes on chitosan DDA and molecular weight, where a balance between complex stability and chitosan-DNA binding strength was suggested to play a critical role.

We then report a new approach to characterize DNA/polycation complexes using asymmetrical flow field-flow fractionation (AF4) coupled online with UV/Vis spectroscopy, multi-angle light scattering (MALS), and dynamic light scattering (DLS). We demonstrated that this AF4 combined system can provide in a single measurement, three important

physicochemical parameters of the complexes: the amount of unbound polycation, the hydrodynamic size of the complexes, and their size distribution. The accuracy of the particles sizes was confirmed by comparison with data from batch-mode DLS and scanning electron microscopy. Accurate quantification of unbound polycation can provide insight into the contribution of the free polycation in the process of gene delivery.

The subsequent part of this thesis treats the characterization of different preparations of DNA/chitosan complexes by the AF4 combined system. Parameters known to influence the transfection efficiency of DNA/chitosan complexes were investigated, including the DNA concentration at mixing, the ratio of chitosan amine to DNA phosphate (N/P) used in the preparations, the chitosan molecular weight, and its degree of deacetylation. We found that all preparations yielded similar ranges of particle hydrodynamic radii ($15 \leq R_H \leq 160$ nm) but that differed in size distribution. Either an increase of the DNA concentration at mixing or an increase of chitosan molecular weight generated the formation of a higher fraction of larger particles ($R_H > 60$ nm) in the dispersions. The dispersions contained a majority of free chitosan in solution that was separated from the nanoparticles and quantified by the AF4 combined system. The free chitosan content was 53 to 92% in dispersions prepared with N/P ratios from 3 to 15, respectively, corresponding to an N/P ratio in the particles that was almost constant (1.3 to 1.6). The accuracy of the free chitosan determination by AF4 was confirmed by ultracentrifugation of the dispersion and analysis of the supernatant. This study reveals the utility of AF4 in the analysis of DNA/polycation dispersions and the importance of quantifying and understanding the role of the free polycation component in these nonviral gene delivery systems.

In the last part of our work, we assessed the stability of DNA/chitosan complexes upon exposure to hyaluronan (HA), chondroitin sulfate (CS), and heparin (Hp). Fluorescence spectroscopy was used and Picogreen was selected as the probe to quantify the release of DNA.

Only the highly charged heparin was found to destabilize the DNA/chitosan complexes and release DNA in solution. The ability of the competing polyanions to release DNA from the DNA/chitosan complexes was related to the binding affinities of chitosan with the different negatively charged polyelectrolytes (including DNA). The stability of the DNA/chitosan complexes exposed to heparin increased with chitosan DDA and molecular weight, in agreement with increasing binding affinities previously determined by ITC. Heparin was unable to dissociate the complexes in dispersions with a significant amount of free chitosan. This amount of free chitosan was found to be sufficient for binding to both DNA and heparin. These findings suggest that free polycation can prevent premature dissociation of DNA/polycation complexes upon interactions with anionic components in the extracellular matrix.

TABLE DES MATIÈRES

LISTE DES TABLEAUX

LISTE DES FIGURES

LISTE DES SIGLES ET ABRÉVIATIONS

α	Degré d'ionisation du chitosane en solution
β	Degré d'ionisation du chitosane complexé
λ	Longueur d'onde
θ	Angle de diffusion
Θ	Fraction de sites d'interaction de l'ADN occupée par le chitosane
A_2	Second coefficient de Viriel
ADN	Acide désoxyribonucléique
AF4	Fractionnement par flux-force avec flux asymétrique
AFM	Miscroscopie à force atomique
ARN	Acide ribonucléique
AUC	Ultracentrifugeuse analytique
c	Concentration massique des espèces diffusées
Ch	Chitosane
Ch-rho	Chitosane marqué avec de la rhodamine
DDA	Degré de désacétylation
DLS	Diffusion dynamique de lumière
DNA	Acide désoxyribonucléique
ESEM	Microscopie électronique à balayage en mode environnemental
FCS	Spectroscopie de corrélation de fluorescence
G	Enthalpie libre
H	Enthalpie

ITC	Microcalorimétrie de titrage isotherme
K	Constante thermodynamique d'interaction
L	Concentration molaire de chitosane libre
L_T	Concentration molaire de chitosane
M_T	Concentration molaire d'ADN
MALS	Diffusion de lumière multi-angles
MES	Acide morpholinoéthane sulfonique
MOPS	Acide morpholinopropane sulfonique
M_n	Masse molaire moyenne en nombre
M_w	Masse molaire moyenne en masse
n	Stoechiométrie des complexes (nombre de sites d'interaction de l'ADN pour le chitosane)
$n_{N/P}$	Stoechiométrie des complexes exprimée en ratio d'amines protonables du chitosane par rapport aux phosphates de l'ADN
$n_{N+/P-}$	Stoechiométrie des complexes exprimée en ratio de charges positives du chitosane par rapport aux charges négatives de l'ADN
Δn_{H+}	Nombre de moles de protons échangés entre le système tampon et le Chitosane
N/P	Ratio molaire de groupements amine protonable du chitosane par rapport aux groupements phosphate de l'ADN
$P(\theta)$	Fonction de diffusion de la particule à un angle de diffusion θ
PDEA	Polyméthacrylate de (2-dimethylamino)éthyle
PDEAEMA	Polyméthacrylate de (2-(diéthylamino)éthyle

PDMAEMA	Polyméthacrylate de (2-diméthylamino)méthyle
PEI	Polyéthylèneimine
PLL	Poly-L-Lysine
POE	Polyoxyéthylène
Q	Chaleur
r	Coefficient de régression linéaire
R_g	Rayon de giration
R_H	Rayon hydrodynamique
$R(\theta)$	Rapport de Rayleigh à un angle θ
RMN	Résonance magnétique nucléaire
S	Entropie
SEC	Chromatographie d'exclusion stérique
SEM	Microscopie électronique à balayage
SPR	Résonance plasmonique de surface
SSIS	Modèle *Single Set of Identical Sites*
TEM	Microscopie électronique à transmission
UV	Ultraviolet
V	Volume
Vis	Visible

LISTE DES ANNEXES

CHAPITRE 1 INTRODUCTION

La thérapie génique consiste à introduire du matériel génétique d'acide désoxyribonucléique (ADN) ou d'acide ribonucléique (ARN) dans les cellules où se déroulent les mécanismes de transcription et de production de protéines régulatrices. Cette approche thérapeutique a pour but de corriger un défaut génétique pouvant mettre en défaut la production ou le fonctionnement d'une protéine essentielle. Cependant, l'ADN thérapeutique injecté directement au patient est susceptible d'être dégradé par le système immunitaire. L'utilisation d'un vecteur est nécessaire pour protéger l'ADN de l'action des nucléases et le livrer efficacement dans des cellules spécifiques. Deux types de vecteurs sont utilisés en thérapie génique : les vecteurs viraux et les vecteurs non-viraux. Les vecteurs viraux tels que les rétrovirus et les adénovirus utilisent leur capacité de pénétration dans les cellules hôtes pour transférer efficacement leur matériel génétique (Thomas et Klibanov, 2003). Cependant, les problèmes associés aux vecteurs viraux sont nombreux (toxicité, réponse immunologique, risques de mutagenèse) et peuvent avoir des conséquences fatales, comme le décès d'un patient lors d'un traitement utilisant un adénovirus pendant une étude clinique (Marshall, 1999). Ces problèmes ont forcé le développement de vecteurs plus sécuritaires à partir de lipides ou de polymères cationiques. Les polymères cationiques, ou polycations, qu'ils soient naturels ou synthétiques, sont parmi les vecteurs non-viraux les plus couramment étudiés car ils sont faiblement toxiques et relativement facile à préparer (Mintzer et Simanek, 2009). Ces derniers ont la capacité de former des complexes avec l'ADN par des interactions électrostatiques, formant des particules avec des tailles nanométriques. Bien que leur taux de transfection soit moins élevé que les vecteurs viraux, la possibilité de modifier la masse molaire et la structure du polymère ou d'y attacher des

ligands ciblant des récepteurs spécifiques des cellules permet le développement de vecteurs plus efficaces pour traverser les barrières cellulaires et livrer l'ADN (Mintzer et Simanek, 2009).

Reconnu pour sa biodégradabilité et biocompatibilité, le chitosane est un des polycations naturels les plus utilisés pour la thérapie génique depuis que Mmper et al. (1995) ont découvert son potentiel comme vecteur non-viral. Les propriétés physico-chimiques (taille, charge de surface et morphologie des particules) et l'efficacité de transfection des complexes ADN/chitosane peuvent être influencées par plusieurs facteurs tels que la masse molaire et le degré de désacétylation (DDA) du chitosane, le pH, la force ionique ainsi que la concentration des deux polyélectrolytes de charges opposées (MacLaughlin et al., 1998; Koping-Hoggard et al., 2001; Sato et al., 2001; Lavertu et al., 2006; Strand et al., 2010). Le DDA et le pH sont deux paramètres qui permettent de moduler la densité de charge du chitosane. Des taux de transfection élevés ont été récemment obtenus dans notre groupe en utilisant des chitosanes avec des masses molaires et des DDA bien spécifiques (Lavertu et al., 2006). De plus, il est possible d'obtenir une efficacité de transfection élevée en combinant soit une masse molaire élevée du chitosane avec un DDA faible, ou bien une masse molaire faible avec un DDA élevé. Une tendance similaire a été également observée après une substitution des groupements chargés avec des groupements neutres pour des chitosanes hautement déacétylés (Strand et al., 2010) et pour d'autres polymères ayant une densité de charge élevée, comme le polyéthylèneimine (Gabrielson et Pack, 2006). Contrairement à ce qu'on peut attendre, cette stratégie a permis d'obtenir une meilleure efficacité de transfection alors qu'elle avait pour objectif de diminuer l'interaction entre le polycation et l'ADN. Ces résultats suggèrent que la force d'interaction entre le polycation et l'ADN doit être à la fois suffisamment élevée pour assurer la stabilité des complexes formés et assez faible pour faciliter la dissociation de l'ADN du chitosane dans la cellule et permettre l'expression du gène (Gabrielson et Pack, 2006; Lavertu et al., 2006; Strand et al., 2010). L'effet

des paramètres moléculaires d'un polycation sur son affinité avec l'ADN et sur la stabilité des complexes formés a été souvent étudié par la capacité du polycation à déplacer une molécule initialement liée à l'ADN (Rungsardthong et al., 2003; Strand et al., 2005) ou par la capacité d'un polyanion compétiteur à dissocier les complexes ADN/polycation pour se lier au polycation (Danielsen, Strand et al., 2005). Cependant, aucune étude n'a été consacrée à la quantification de l'affinité du système chitosane-ADN car les observations sont fondées sur des mesures qualitatives et ne permettent pas de mesurer l'affinité d'un polycation comme le chitosane pour l'ADN ou la force d'interaction nécessaire à la stabilité des complexes lors d'interactions compétitives avec des composantes extracellulaires avant l'entrée dans la cellule.

La fraction de polycation libre semble jouer un rôle dans le processus de livraison des gènes (Boeckle et al., 2004) qui est à déterminer. Les complexes ADN/polycation sont en effet généralement préparés avec un excès de polycation par rapport à l'ADN pour que la transfection soit efficace. Cependant, seulement une partie du polycation est complexée avec l'ADN, le reste est sous forme libre en solution. Jusqu'à présent, très peu d'études ont quantifié les fractions libre et liée du polycation ou déterminé la composition réelle des complexes (Clamme et al., 2003; Boeckle et al., 2004). La caractérisation de ces paramètres représente encore un défi car les méthodes disponibles sont limitées en détection ou bien comportent des difficultés techniques mettant en doute la précision des résultats d'analyse. Une meilleure compréhension de ces éléments pourrait offrir des indices sur les mécanismes complexes impliqués dans la livraison de gènes par les vecteurs non-viraux et permettraient de développer des vecteurs à base de polymères plus efficaces pour la transfection.

1.1 Objectifs

Le premier objectif de la thèse est de comprendre la nature des interactions régissant la formation des complexes ADN/chitosane par une étude thermodynamique. Il s'agit également de déterminer l'affinité du chitosane pour l'ADN en fonction des paramètres moléculaires du chitosane et des conditions de mélange. Un autre but consiste à déterminer l'effet de ces paramètres sur la composition, la taille et la structure des complexes ADN/chitosane. Enfin, il s'agit de comprendre la relation entre l'affinité du chitosane pour l'ADN, la stabilité des complexes et leur capacité à se dissocier pour l'expression du gène.

1.2 Structure de la thèse

Dans ce document, une revue bibliographique est présentée dans le chapitre 2 traitant des propriétés de l'ADN et du chitosane. Des études menées sur les complexes d'ADN à partir de chitosane et d'autres polymères cationiques y sont également présentées. Le chapitre 3 résume la démarche entreprise pour l'ensemble du travail qui est ensuite présenté dans les chapitres 4 à 6 sous la forme de trois articles publiés ou soumis dans des revues scientifiques. Un quatrième article qui est en cours de préparation pour soumettre à une revue scientifique est présenté à l'annexe. Une discussion générale de ces articles, une conclusion et des recommandations complètent ce travail.

CHAPITRE 2 REVUE DE LITTÉRATURE

2.1 Structure et condensation de l'ADN

L'ADN est un biopolymère présentant une structure hélicoïdale formée par deux brins antiparallèles étroitement reliés par des liaisons hydrogène. Le monomère répétitif de chaque brin est un nucléotide composé d'un sucre (le désoxyribose), d'un groupement phosphate et d'une base azotée, soit une des purines (adénine ou guanine), ou soit une des pyrimidines (cytosine ou thymine) (Rawn, 1990). La complémentarité des bases azotées fait en sorte qu'une adénine d'un brin s'associe par des liaisons hydrogène avec une thymine de l'autre brin, et qu'une guanine d'un brin se lie à une cytosine de l'autre brin de l'ADN. En raison de l'hydrophobicité des cycles aromatiques qui composent les bases azotées, ces dernières sont empilées les unes au dessus des autres à l'intérieur de l'hélice alors que les sucres et les phosphates des nucléotides sont sur la face externe et exposés à la solution. Le pK_a de ~1 de ses groupements phosphates confère à l'ADN un caractère fortement anionique (Bloomfield et al., 2000). Parmi les différentes conformations que peut adopter l'ADN à double brins, la conformation B est la plus courante dans les conditions physiologiques. La double hélice de cette conformation possède un diamètre de 2.37 nm et renferme environ 10 paires de bases par tour d'hélice. Par rapport à l'axe de la double hélice, les paires de bases sont espacées en moyenne de 0.33 nm, ce qui représente une distance moyenne entre les charges de 0.17 nm (Dickerson et al., 1982; Rawn, 1990).

En raison de sa nature fortement anionique et sa grande taille, l'ADN ne peut pas être internalisé efficacement dans les cellules. De plus, l'ADN est facilement dégradé par les nucléases. Une grande variété de polymères, naturels ou synthétiques, ont été utilisés comme

vecteur pour l'ADN, tels que le chitosane (Lavertu et al., 2006; Strand et al., 2010), le polyéthylèneimine (PEI) (Boeckle et al., 2004), la poly-L-lysine (PLL) (Miyata et al., 2004), les polyglyamidoamines (Liu, Y. et Reineke, 2010) et les dendrimères (Chen et al., 2000). Ces polymères cationiques ayant des structures linéaires, ramifiés ou dendritiques, peuvent former des complexes avec l'ADN par des interactions électrostatiques entre leurs charges positives et les groupements phosphate chargés négativement de l'ADN. La neutralisation des charges de l'ADN par les polycations peut induire la condensation de l'ADN et former des structures compactes pouvant atteindre 20 à 500 nm de diamètre (Morille et al., 2008). Les différents types de polycations utilisés pour condenser l'ADN, le protéger contre la dégradation par les nucléases et le livrer dans le noyau, se différencient par leur efficacité de transfection et leur toxicité (Mintzer et Simanek, 2009). Le chitosane est un des polymères naturels les plus utilisés pour la livraison de gènes. La biodégradabilité, la biocompatibilité et la faible cytotoxicité du chitosane ont conduit à la reconnaissance de ce polysaccharide en tant que vecteur prometteur pour la thérapie génique (Kim, T.-H. et al., 2007; Mintzer et Simanek, 2009).

2.2 Chitosane

Le chitosane est un biopolymère de la famille des polysaccharides dont la découverte a été attribuée à Rouget en 1859 (Crini et al., 2009). C'est l'un des rares polyélectrolytes naturels cationiques. Il est obtenu par modification chimique de la chitine, un biopolymère issu de la carapace de certains crustacés et insectes ainsi que des champignons. La chitine est le polysaccharide le plus abondant après la cellulose (Rinaudo, 2006).

2.2.1 Structure

La chitine et le chitosane sont identiques du point de vue chimique et sont des copolymères linéaires possédant un enchaînement de motifs 2-acétamido-2-désoxy-β-D-glucopyranose (N-acétyl-D-glucosamine, ou unité acétylée notée A, et 2-amino-2-désoxy-β-D-glucopyranose (D-glucosamine, ou unité désacétylée notée D, reliées entre elles par des liaisons glucosidiques β-(1,4) (Figure 2.1). La principale différence entre ces deux polysaccharides réside dans la proportion de ces deux motifs que l'on nomme le degré de désacétylation (DDA) et qui correspond à la proportion d'unités désacétylées par rapport au nombre total d'unités dans les chaînes.

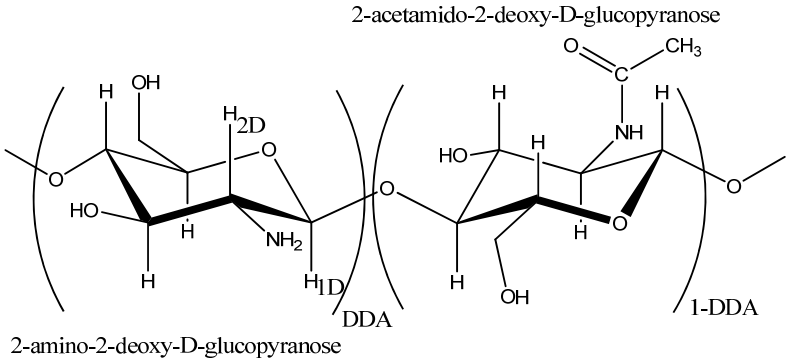

Figure 2.1. Structure chimique du chitosane

Le DDA est un paramètre qui permet de différencier le chitosane de la chitine et explique les grandes différences de propriétés entre ces deux polymères, telles que la solubilité. Le terme chitine est donné à un copolymère dont la valeur du DDA est inférieure à 50% tandis que le chitosane possède une valeur de DDA supérieure à 50%. Les deux polymères sont non toxiques, biocompatibles et biodégradables par hydrolyse grâce aux chitinases ou aux lyzosymes. Les

chitinases sont des enzymes hydrolysant les liaisons β-1,4 entre les motifs D-glucosamine dans des chitosanes partiellement hydrolysés (Izume et al., 1992).

2.2.2 Préparation du chitosane

Il existe plusieurs méthodes de préparation du chitosane à partir de la chitine traitée (Roberts, 1992). Pour ce faire, il est nécessaire de désacétyler la chitine en hydrolysant les fonctions amide des unités acétylées. Bien que cette hydrolyse se fasse en milieu acide ou alcalin, le milieu acide est à éviter car les liaisons glucosidiques entres les unités sont sensibles à l'hydrolyse acide. Une des méthodes couramment utilisées (Mima et al., 1983) consiste à désacétyler la chitine dans une solution concentrée de NaOH (jusqu'à 50% en masse) sous atmosphère inerte (généralement N_2) pendant quelques heures à 110°C. Le chitosane obtenu est ensuite lavé avec de l'eau à 80°C jusqu'à pH neutre puis séché. L'atmosphère inerte est nécessaire afin d'éviter des réactions d'oxydation qui pourraient faire diminuer la taille des chaînes de chitosane. La concentration en soude permet quant à elle de moduler le degré de désacétylation du chitosane. Cette réaction peut être réalisée plusieurs fois de suite afin d'obtenir un DDA proche de 100%.

2.2.3 Degré de désacétylation (DDA)

Le DDA du chitosane renseigne sur la proportion en amine primaire par chaîne et par conséquent influence ses propriétés. Dans le cas de la solubilité, c'est la présence de charge (par protonation des amines) qui va permettre la solubilisation du polyélectrolyte en milieu aqueux acide. D'un point de vue pratique, le chitosane est soluble dans la plupart des solutions acides organiques et celle couramment utilisée est la solution d'acide acétique dilué. Le polymère est

également soluble dans les acides minéraux dilués (HCl, HNO_3) mais une concentration trop élevée empêche l'hydratation des chaînes et risque d'hydrolyser le matériau. La solubilité est gouvernée par la protonation des fonctions amine qui participe à un équilibre acido-basique défini par le couple suivant :

$$Gluc - NH_3^+ \rightleftharpoons Gluc - NH_2 + H^+$$

Cet équilibre est décrit par l'équation de la constante de dissociation suivante :

$$pKa_{app} = pH + \log\left(\frac{\alpha}{1-\alpha}\right)$$

où α est le degré d'ionisation du chitosane (fraction de monomères glucosamine ionisés). Pour un polyélectrolyte, le p*K*a n'est pas constant du fait de la difficulté d'ajouter des charges sur la chaîne lorsque α augmente et par conséquent décroît avec α. Filion et al. (2007) ont montré que pKa_{app} dépend de la force ionique et de la concentration en chitosane du milieu mais qu'il diminue faiblement avec l'augmentation du DDA. La présence de charges sur le polymère peut également modifier la flexibilité des chaînes et donc sa conformation (Rinaudo, 2006).

Le DDA du chitosane peut être mesuré avec précision par spectroscopie RMN du proton ^1H (Varum et al., 1991; Lavertu et al., 2003). Il faut que l'échantillon soit soluble dans de l'eau deutérée. À partir du spectre du chitosane (Figure 2.2), le DDA est calculé selon l'équation suivante :

$$DDA = \frac{H1D}{H1D + \left(HAc/3\right)}$$

où H1D correspond à l'intégration du pic du proton anomérique de l'unité désacétylée (Figure 2.1) à 5.25 ppm sur la somme des protons des différents motifs (c'est-à-dire proton anomérique et les protons du groupement CH_3 des fonctions acétylées).

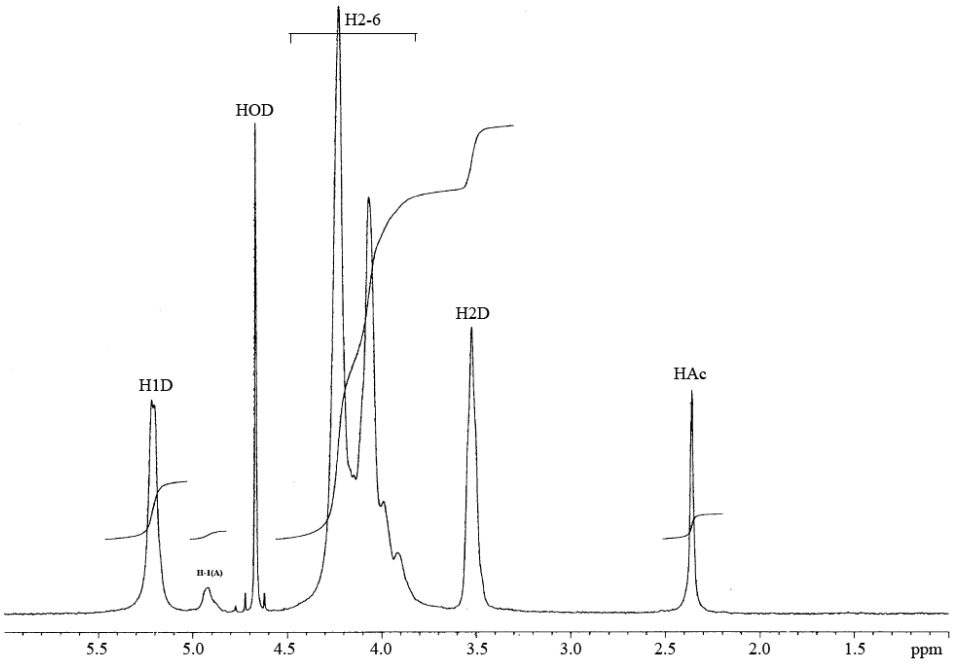

Figure 2.2. Spectre RMN ^1H du chitosane solubilisé dans D_2O + DCl (Lavertu et al., 2003).

2.2.4 Masse molaire

La masse molaire joue un rôle important dans la solubilisation et la viscosité des solutions de chitosane. Elle peut être mesurée par la chromatographie d'exclusion stérique (SEC) couplée avec des détecteurs tels que la diffusion de la lumière multi-angles et un réfractomètre. Cette méthode permet la détermination de la masse molaire moyenne en nombre (M_n) et en masse (M_w) mais aussi de la distribution des masses dans l'échantillon. Cette technique utilise une colonne dont la phase stationnaire est constituée de gel dont la taille des pores est contrôlée et connue. Cette colonne permet la séparation des chaînes de polymère, comme le chitosane, puisque les

plus grosses chaînes ne peuvent pas rentrer aussi profondément dans les pores que les chaînes plus petites. Étant donné de leur chemin plus court dans la colonne, les grosses chaînes possèdent un temps d'élution plus court que les chaînes plus petites. Il faut éviter les interactions (électrostatiques ou hydrophobes par exemple) entre le polymère et la phase stationnaire sous peine d'affecter la séparation des différentes chaînes suivant leur taille. La concentration de chaque fraction éluée de la colonne peut être mesurée en temps réel grâce à un réfractomètre. De plus, un détecteur de lumière diffusée multiangles (MALS) permet de déterminer M_w et M_n mais aussi le rayon de giration R_g. Ces paramètres sont calculés à partir des équations issues de la théorie de la diffusion de la lumière qui sont présentées dans l'annexe 1.

2.3 Mécanismes de livraison de gènes

Le passage des complexes ADN/polycation à travers la membrane plasmique et la diffusion de l'ADN jusqu'au noyau de la cellule ne se fait pas directement. Ils doivent surmonter plusieurs barrières extracellulaires et intracellulaires avant de rejoindre le noyau pour la transcription des gènes, telle que le montre la Figure 2.3. Cependant, les mécanismes impliqués dans la livraison de gènes par les polycations ne sont pas tous connus.

Tout d'abord, l'entrée d'un système non-viral dans la cellule peut se produire par plusieurs voies : endocytose, phagocytose ou macropinocytose (Morille et al., 2008; Mintzer et Simanek, 2009). L'endocytose par adsorption non-spécifique est le processus principalement emprunté par les complexes ADN/polycation (sans ligand), suivi par un mécanisme modulée par de la clathrine. Il a été démontré que l'adsorption non-spécifique avec la membrane plasmique des cellules est favorisée par des complexes chargés positivement. Ces derniers peuvent en effet interagir avec les protéoglycanes, les glycoprotéines et les glycérophosphates anioniques présents

sur la membrane plasmique (Mislick et Baldeschwieler, 1996). D'un autre côté, il est important que les complexes ADN/polycation soient assez stables durant ce processus pour éviter la dissociation par ces biomolécules anioniques. Des tailles de particules inférieures à 100 nm de diamètre sont suggérées pour favoriser l'internalisation (Mintzer et Simanek, 2009). Cependant, des études *in vitro* ont montré que des complexes ADN/chitosane avec des tailles beaucoup plus grandes peuvent également transfecter les cellules (Lavertu et al., 2006; Strand et al., 2010).

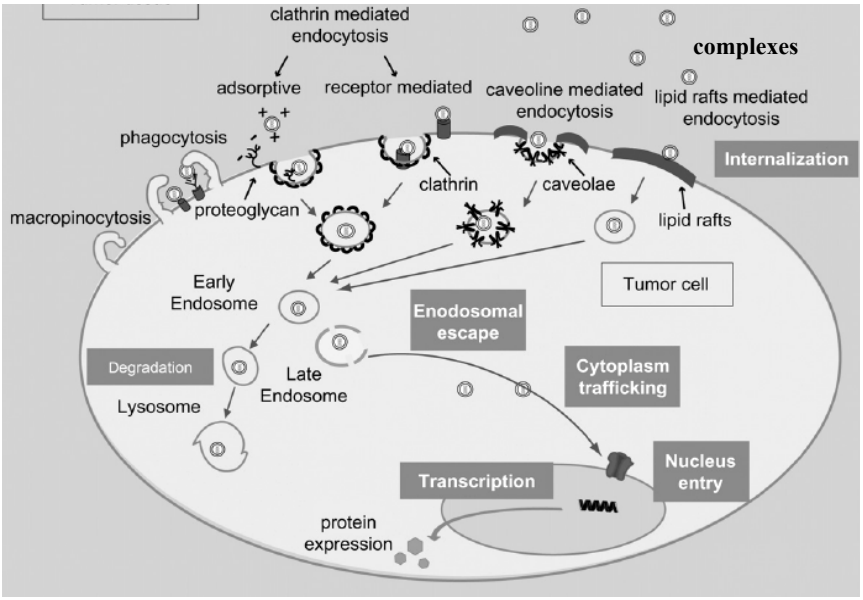

Figure 2.3. Schéma illustrant les différents barrières extracellulaires et intracellulaires que doivent passer les systèmes non-viraux lors de la transfection (Morille et al., 2008).

Après l'internalisation par endocytose, les particules sont généralement piégées dans les endosomes et ensuite dégradées par les lysosomes (Figure 2.3). Ce deuxième obstacle de la transfection doit être surmonté par les complexes, préférablement, avant que les endosomes passent d'une forme précoce à une forme mature pour finalement devenir des lysosomes dans lesquels des enzymes hydrolytiques dégradent les composés emprisonnés (Luzio et al., 2001).

Durant la maturation des endosomes, le pH à l'intérieur des vésicules passe d'environ 7 à 4.5-5.0 (Behr, 1997). Deux hypothèses ont été suggérées pour la libération des complexes ADN/polycation dans le cytoplasme. La première hypothèse est fondée sur la capacité des polycations comme les dendrimères à interagir directement avec la membrane bicouche de l'endosome et à provoquer sa rupture (Zhang et Smith, 2000). En raison de la nature anionique de la membrane bicouche contenant des phospholipides, des interactions électrostatiques avec les polycations pourraient induire localement des courbures (*bending*) à cette membrane jusqu'à causer sa rupture (Figure 2.4). Bien que ce mécanisme ait été suggéré pour les dendrimères à base de polyamidoamine et de PLL, il semble ne pas s'appliquer pour des polycations linéaires car le PLL sous forme linéaire ne peut induire de tels changements à la membrane de l'endosome (Zhang et Smith, 2000).

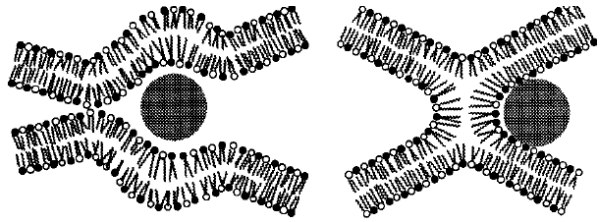

Figure 2.4. Hypothèse de rupture de l'endosome provoquée par des courbures locales de sa membrane phospholipidique qui seraient induites par des interactions électrostatiques avec des dendrimères (Zhang et Smith, 2000).

Une hypothèse alternative pour libérer les complexes ADN/polycation de l'endosome a été proposée par le groupe de Behr à partir de leurs études sur des complexes à base de PEI (Boussif et al., 1995; 1997). Selon cette hypothèse, connue sous le terme de « *proton sponge effect* », les polymères cationiques comme le PEI et les polyamidoamines, qui possèdent une

grande quantité de groupements protonables, pourraient servir de tampon lors de l'acidification du compartiment des endosomes par les enzymes ATPase qui transportent des protons du cytoplasme (Figure 2.5). Cette accumulation de protons induit en même temps un flux de contre-ions (Cl^-) pour assurer l'électroneutralité et une entrée d'eau qui fait augmenter la pression osmotique dans les endosomes, conduisant à leur gonflement et leur éclatement pour ainsi libérer les complexes. Selon un modèle de prédiction dérivé d'une étude récente, les complexes seuls ne peuvent pas provoquer une telle augmentation de la pression osmotique dans les endosomes sans une quantité suffisante de polycation libre (Yang et May, 2008). Selon d'autres études sur les systèmes de livraison de gènes à base de polymères, l'hypothèse du *proton sponge effect* n'est pas toujours valide. Par exemple, l'acétylation du PEI pour diminuer jusqu'à 57% des groupements protonables a en effet donné de meilleures efficacités de transfection par rapport au PEI non modifié (Gabrielson et Pack, 2006). Dans le cas des complexes ADN/chitosane, ce ne sont pas les chitosanes avec des valeurs de DDA les plus élevées qui sont nécessairement plus efficaces pour la transfection (Lavertu et al., 2006), tel que montre également une étude récente dans laquelle les groupements amine protonables du chitosane ont été substitués par des oligosaccharides neutres (Strand et al., 2008; Strand et al., 2010).

Les complexes libérés des endosomes doivent ensuite rejoindre le noyau des cellules par diffusion dans le cytoplasme (Figure 2.3). L'état de l'ADN dans le cytoplasme est peu connu, il peut être associé ou dissocié du polycation. Il est suggéré que le polycation doit maintenir ses fonctions assurant la protection de l'ADN contre la dégradation des nucléases du cytoplasme et la condensation de l'ADN pour faciliter la diffusion vers le noyau (Lukacs et al., 2000). Le mécanisme de pénétration dans le noyau est également peu connu et ne sera pas abordé dans le cadre de ce travail. Cependant, plusieurs études suggèrent l'importance d'avoir des complexes ADN/polycation facilement dissociables au niveau du noyau pour permettre la transcription des

gènes mais également suffisamment stables pour éviter une décomplexation prématurée (Gabrielson et Pack, 2006; Lavertu et al., 2006; Strand et al., 2010).

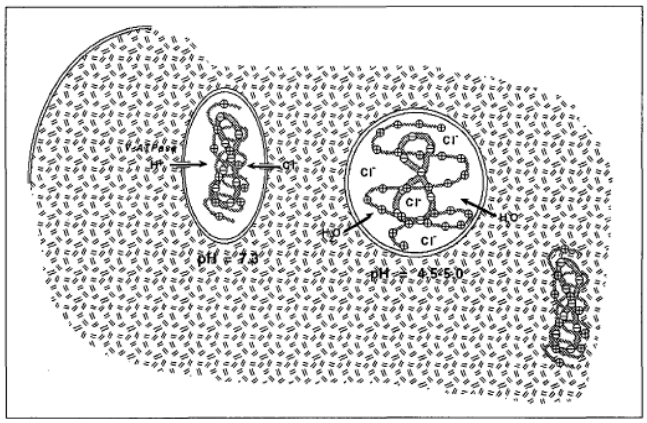

Figure 2.5. Shéma illustrant l'hypothèse du « *proton sponge effect* » (Behr, 1997).

2.4 Propriétés physico-chimiques des complexes ADN/chitosane

Le DDA et la masse molaire du chitosane sont des facteurs qui peuvent influencer les propriétés physico-chimiques des complexes formés avec l'ADN. La charge de surface et la taille des complexes résultant de l'association électrostatique peuvent en effet affecter l'efficacité de transfection. En plus des caractéristiques moléculaires du chitosane, les conditions de préparation telles que le pH, la force ionique, la concentration de l'ADN et le ratio de chitosane par rapport à l'ADN sont également des facteurs qui peuvent influencer les propriétés physico-chimiques et la transfection des complexes ADN/chitosane (MacLaughlin et al., 1998; Koping-Hoggard et al., 2001; Romoren et al., 2003; Strand et al., 2005; Lavertu et al., 2006; Strand et al., 2010).

La charge de surface des particules est un paramètre important contrôlant l'agrégation. Pour les complexes ADN/polycation, elle est estimée par les mesures du potentiel zéta. La charge de surface n'affecte pas uniquement la stabilité colloïdale des complexes mais peut également influencer les interactions avec les composantes anioniques sur la membrane plasmique des cellules, comme les protéoglycanes, qui joueraient un rôle médiateur durant le processus d'internalisation par endocytose (Mislick et Baldeschwieler, 1996). C'est pour ces raisons qu'il est généralement suggéré de préparer des complexes avec une charge de surface nette positive en utilisant un excès de polycation par rapport à l'ADN. Des ratios molaires de groupements amine protonables du polycation par rapport aux groupements phosphate de l'ADN, ou ratio N/P, supérieurs à 3 sont généralement utilisés dans la préparation des complexes à partir de chitosane ou d'autres polycations (Koping-Hoggard et al., 2001; Boeckle et al., 2004; Huang, M. et al., 2005; Lavertu et al., 2006; Strand et al., 2010). Des ratios N/P égaux à 1 ou proche de la neutralisation des charges opposées favorisent l'agrégation des particules ou la formation d'agrégats insolubles, alors que des ratios N/P inférieurs à 1 ne permettent pas de condenser l'ADN et de neutraliser ses charges négatives (Tang et Szoka, 1997).

Dans certaines études menées sur les complexes ADN/chitosane, des ratios N/P élevés entre 20 et 60 ont été même utilisés (Koping-Hoggard et al., 2004; Germershaus et al., 2008; Strand et al., 2008; Strand et al., 2010). Cependant, l'intensité du potentiel zéta mesurée dans des conditions proches de celle de la préparation de ces complexes à pH 5, n'augmente pas significativement lorsque le ratio N/P est supérieur à 2 (Strand et al., 2005). L'utilisation de ratios N/P si élevés avec des valeurs de potentiel zéta presque constantes soulèvent bien des questions. À partir de la spectroscopie de corrélation de fluorescence (FCS), les coefficients de diffusion d'un oligomère de chitosane (~6 kDa) libre et complexé avec l'ADN ont été déterminé récemment pour une dispersion préparée avec un ratio N/P de 10 et à un pH proche de 5 (Reitan

et al., 2009). L'analyse de la courbe de corrélation obtenue dans ces conditions par un modèle à deux composantes a montré que près de 50% du chitosane est en effet libre en solution. Deux autres études sur la caractérisation de complexes ADN/PEI ont montré que la majorité du PEI est à l'état libre en solution (Clamme et al., 2003; Boeckle et al., 2004). D'après Boeckle et al. (2004), le PEI libre jouerait un rôle important dans le processus de livraison de gènes en contribuant au *proton sponge effect*. Dans le cas du chitosane comme vecteur pour l'ADN, quelle serait le rôle de la fraction libre ? Quel serait l'effet du ratio N/P sur la composition de ces complexes ou sur les fractions de chitosane libre et complexé ? On peut également se questionner sur l'effet du DDA et de la masse molaire du chitosane sur ces paramètres.

Afin de pouvoir pénétrer à travers la membrane plasmique des cellules et avoir une bonne mobilité pour diffuser dans le cytoplasme jusqu'à noyau, il faut que les complexes soit de petites tailles. Pour l'internalisation par endocytose, il est suggéré que la taille des particules soit inférieure à 100 nm de diamètre (Mintzer et Simanek, 2009). Cependant, plusieurs études ont montré que des complexes à base de chitosane ou de PEI avec des tailles de particules au delà des centaines de nanomètres, même après agrégation, sont capables de transfecter efficacement des cellules (Ogris et al., 1998; Ishii et al., 2001; Lavertu et al., 2006; Strand et al., 2010). Ces résultats montrent que la transfection n'est pas nécessairement plus efficace avec des particules de petites tailles. Il est probable que les grosses particules sédimentent plus facilement à la surface des cellules (Strand et al., 2010) et favorisent une internalisation par endocytose forcée (Mintzer et Simanek, 2009).

D'autre part, MacLaughlin et al. (1998) ont trouvé que la taille des particules augmente de 100 à 500 nm lorsque la masse molaire du chitosane augmente de 7 à 540 kDa. La taille des particules peut également augmenter avec la concentration de l'ADN utilisée lors de préparation de ces complexes à un ratio N/P constant (MacLaughlin et al., 1998; Koping-Hoggard et al.,

2004). Des résultats similaires ont été obtenus avec d'autres polycations (Ogris et al., 1998; Oupicky et al., 2000).

2.5 Études de l'affinité polycation-ADN

Des taux de transfection faibles ont été souvent associés à une stabilité trop faible ou trop élevée des systèmes polycationiques de livraison de gènes (MacLaughlin et al., 1998; Koping-Hoggard et al., 2004; Gabrielson et Pack, 2006; Lavertu et al., 2006; Strand et al., 2010). Il est reconnu que l'affinité du polycation pour l'ADN constitue un facteur déterminant de la stabilité des complexes (Strand et al., 2005). Une interaction trop faible entre le polycation et l'ADN entraînerait la formation de complexes peu stables pouvant être facilement dissociés dans le milieu extracellulaire avant même de pénétrer dans la cellule, alors qu'une interaction trop forte empêcherait la dissociation intracellulaire de l'ADN pour l'expression du gène. Les différentes approches d'analyses de l'affinité d'un polycation pour l'ADN sont abordées ci-dessous et peuvent être classées de la manière suivante : les méthodes qualitatives regroupant l'électrophorèse sur gel et la perte de fluorescence du bromure d'éthidium, ainsi que les méthodes quantitatives fondées sur la mesure de la constante d'interaction, telles que la résonance plasmonique de surface et la microcalorimétrie de titrage isotherme (ITC).

2.5.1 Gel d'électrophorèse

Cette méthode consiste à incuber les complexes dans une solution saline ou en présence de molécules anioniques, telles que les protéines de sérum, l'héparine ou l'acide hyaluronique, qui peuvent induire la dissociation de l'ADN pour se lier au polycation (Bertschinger et al., 2006). L'ADN libéré peut être ensuite révélé et visualisé après électrophorèse sur un gel trempé

dans une solution de bromure d'éthidium (Figure 2.6). L'affinité du polycation pour l'ADN est reliée à la stabilité des complexes avant et après leur exposition à des molécules compétitrices. Bien que cette méthode soit fréquemment utilisée pour sa facilité et sa rapidité, elle ne permet pas de quantifier avec précision l'ADN dissocié des complexes à cause de sa limite de détection et ne donne aucune information quantitative sur l'affinité entre les composantes.

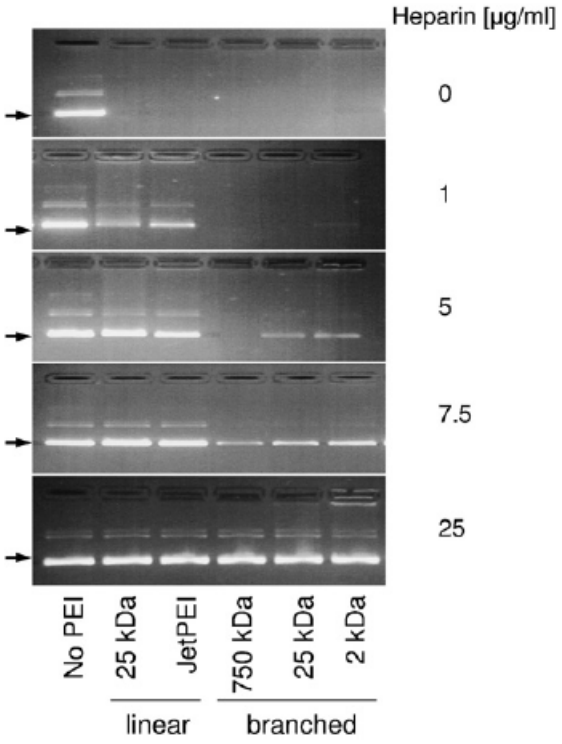

Figure 2.6. Électrophorèse en gel d'agarose montrant de l'ADN dissocié des complexes ADN/PEI par l'héparine (Bertschinger et al., 2006).

2.5.2 Méthodes de fluorescence avec un marqueur pour l'ADN

La méthode de fluorescence la plus utilisée est celle fondée sur la perte de fluorescence causée par le déplacement du bromure d'éthidium initialement lié à l'ADN (Izumrudov et al., 2002; Rungsardthong et al., 2003; Zelikin et al., 2003; Strand et al., 2005). Le bromure d'éthidium est une molécule cationique (Figure 2.7A) qui s'intercale entre les paires de bases de l'ADN et émet de la fluorescence. L'intensité de la fluorescence mesurée est donc proportionnelle à la quantité de bromure d'éthidium lié à l'ADN et diminue jusqu'à extinction

lorsque cet agent est expulsé de l'ADN par les interactions électrostatiques entre le polycation et l'ADN. En effet, le bromure d'éthidium libre en solution ne fluoresce pas car la désexcitation (retour de l'état excité à l'état fondamental) se fait de façon non-radiative impliquant le transfert de proton d'un groupement amine au solvant aqueux. L'intensité de la fluorescence est donc beaucoup plus élevée lorsque le cation d'éthidium est isolé du solvant aqueux en s'intercalant entre les paires de bases de l'ADN puisque l'élimination du transfert de proton entraine une augmentation de la durée de vie de l'état excité de 1.8 ns (dans l'eau) à 23 ns (Le Pecq et Paoletti, 1967; Pasternack et al., 1991).

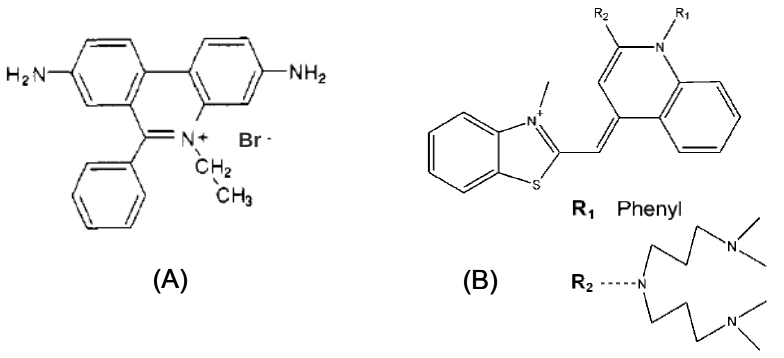

Figure 2.7. Structure chimique du bromure d'éthidium (A) (Pasternack et al., 1991) et du Picogreen (B) (Zipper et al., 2004).

Généralement, on procède au titrage d'une solution d'ADN contenant du bromure d'éthidium par une solution de polycation. L'intensité de la fluorescence du bromure d'éthidium diminue progressivement avec l'augmentation de la concentration du polycation dans la solution indiquant l'expulsion du bromure d'éthidium de l'ADN et la formation de complexes ADN/polycation. La perte de fluorescence du bromure d'éthidium est donc une conséquence d'une meilleure affinité entre le polycation et l'ADN. Lorsque le point de neutralisation des

charges (N/P ~ 1) est atteint, on remarque souvent que l'ajout subséquent de polycation ne diminue pas davantage l'intensité de fluorescence et l'extinction complète du bromure d'éthidium n'est jamais atteinte (Figure 2.8). Une étude utilisant cette méthode rapporte que la capacité du chitosane à déplacer le bromure d'éthidium augmente avec le DDA pour une masse molaire d'environ 140 kDa (Strand et al., 2005). Par contre, cette capacité d'expulsion du bromure d'éthidium ne change pas avec des chitosanes complètement désacétylés (DDA = 100%) pour des masses molaires variant de ~ 2 à 150 kDa. Ces résultats obtenus avec une méthode d'analyse qui mesure plutôt une affinité apparente soulèvent bien des questions. Quelles sont les limites de détection de cette méthode ? Lors du titrage, les complexes qui ont précipité proche du point de neutralisation deviennent en effet insolubles, ce qui affecterait l'accès du polycation à l'ADN. En d'autres termes, comment la précipitation de l'ADN complexé affecte-t-elle les mesures, surtout lorsqu'il s'agit de comparer différents systèmes ? Est-ce que les mesures sont uniquement reliées à la capacité du polycation à déplacer le bromure d'éthidium ?

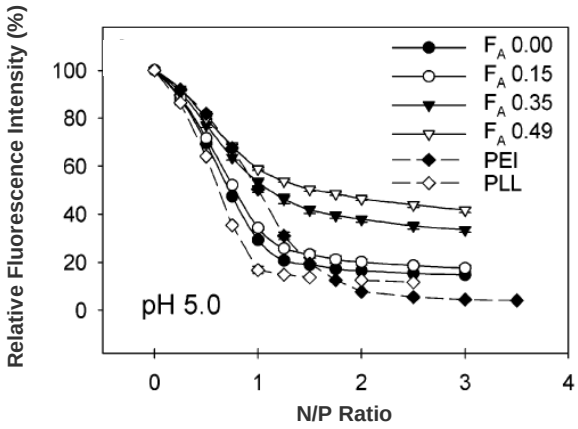

Figure 2.8. Titrage d'une solution ADN-bromure d'éthidium par une solution de chitosane de DDA différents (F_A = 1 – DDA), de PEI et de PLL. L'intensité de fluorescence est relative à la fluorescence mesurée pour une solution ADN-bromure d'éthidium sans ajout de polycation (Strand et al., 2005).

Le problème de précipitation de l'ADN complexé par titrage peut être contourné en préparant séparément chaque échantillon à des ratios N/P différent par la méthode de mélange rapide. L'affinité du polycation pour l'ADN peut être également étudiée indirectement par la stabilité des complexes exposés à des polyanions compétiteurs, comme l'héparine. L'ADN dissocié peut être ensuite détecté par l'ajout du bromure d'éthidium et mesuré par la spectroscopie de fluorescence. Cette méthode a été utilisée dans une étude sur la stabilité des complexes ADN/chitosane où il a été démontré que la masse molaire du chitosane et le ratio N/P augmente la stabilité des complexes en présence de l'héparine (Danielsen, Strand et al., 2005). Cette méthode a été également utilisée pour déterminer la stabilité d'autres systèmes de livraison de gènes à partir de PEI ou de lipide cationique en présence de l'héparine (Moret et al., 2001). Dans cette étude, l'ADN dissocié des complexes a été quantifié par le bromure d'éthidium mais aussi par le Picogreen (Figure 2.7B), un marqueur qui émet également de la fluorescence en

s'intercalant entre les paires de bases de l'ADN. Comparé au bromure d'éthidium, le Picogreen possède un coefficient d'absorption environ 12 fois plus élevé, ce qui lui confère une meilleure sensibilité pour la détection et la quantification de l'ADN dissocié (Singer et al., 1997; Ren et Xu, 2008). Il peut permettre la détection jusqu'à 0.025 ng/mL d'ADN double brins (Singer et al., 1997),et il est moins affecté par la présence de molécules anioniques, comme l'héparine (Singer et al., 1997), et par le ratio fluorophore/paire de bases de l'ADN qui peut entraîner l'extinction d'un fluorophore à de fortes doses (Yan et al., 1999).

2.5.3 Résonance plasmonique de surface

La technique de résonance plasmonique de surface (SPR) a été utilisée pour la première fois par Wink et al. (1999) pour étudier les interactions d'ADN plasmidique avec du PLL et du polyméthacrylate de (2-dimethylamino)éthyle (PDMAEMA). Le principe de cette technique est fondé sur la détection optique des variations de masse à la surface métallique (or) d'un biocapteur sur lequel les auteurs de cette étude ont immobilisé les polycations de façon non-covalente par adsorption, et covalente par thiolation du polymère. L'ADN a été ensuite injecté en flux continu à la surface du biocapteur et la masse fixée a été mesurée en temps réel. Les changements de masse induits par l'association ou la dissociation des complexes à la surface du biocapteur modifient l'indice de réfraction du milieu et décalent la position de l'angle de résonance qui est en effet mesuré. À partir des courbes de suivi en temps réel (Figure 2.9), les constantes cinétiques d'association et de dissociation entre l'ADN et les différents polycations ont été déterminées et ont permis de calculer les constantes d'affinité. Les constantes d'affinité déterminées à pH 7.4 sont respectivement 1×10^{10} et 5×10^{8} M^{-1} pour les interactions PLL-ADN et PDMAEMA-ADN. La meilleure affinité de l'ADN pour le PLL a été attribuée au degré

d'ionisation plus élevé du PLL à ce pH. Même si les auteurs n'ont pas observé une influence significative de la thiolation partielle des polymères sur la constante d'affinité, cette modification est nécessaire afin d'obtenir une immobilisation homogène et reproductible des polymères sur la surface d'or des biocapteurs.

La technique SPR peut se révéler très utile pour étudier les interactions polycation-ADN et déterminer leur constante d'affinité. Cependant, elle est fondée sur la formation d'une couche à partir d'une composante immobilisée à une surface alors que les deux composantes sont en solution dans la formation de complexes ADN/polycation pour la thérapie génique. La conformation des composantes et la structure des complexes résultants sont en effet différentes dans les deux cas.

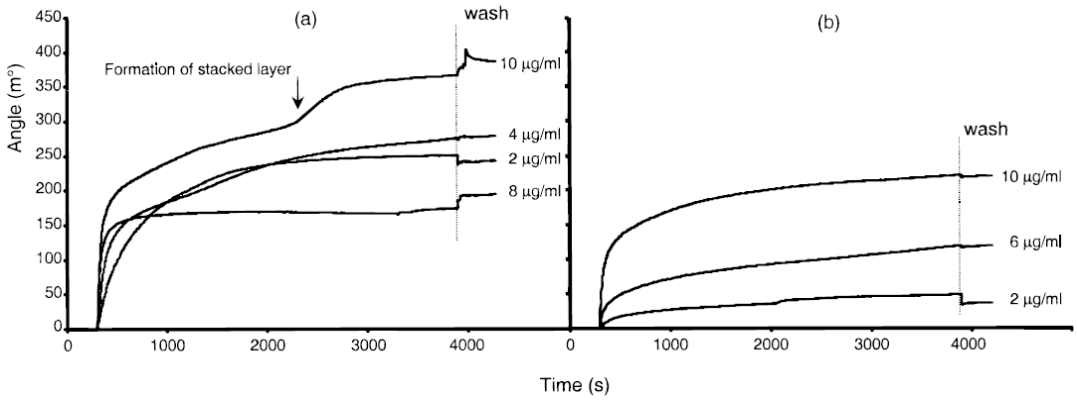

Figure 2.9. Courbes d'interaction d'ADN avec du PLL non-modifié (a) et du PDMAEMA thiolé à 5% (b) obtenues par SPR. Différentes concentrations d'ADN ont été injectées à la surface des biocapteurs (Wink et al., 1999).

2.5.4 Microcalorimétrie de titrage isotherme

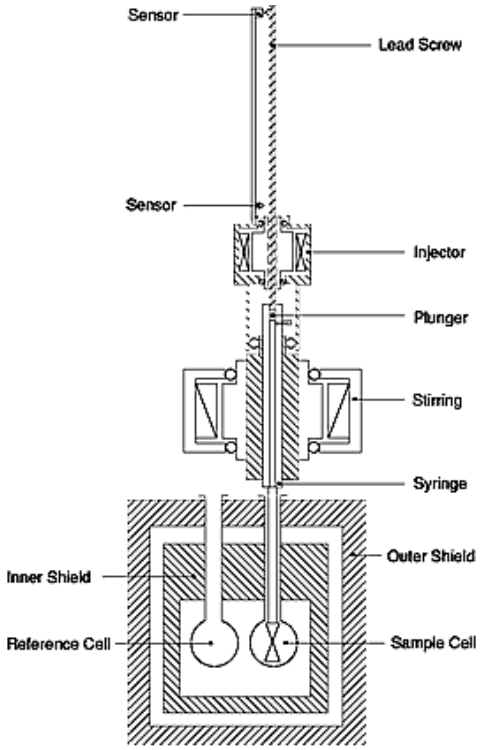

Figure 2.10. Schéma de l'ITC (VP-ITC, Microcal)

La microcalorimétrie de titrage isotherme (ITC) est une technique très utile pour étudier les interactions entre deux composantes en solution comme le montrent plusieurs études récentes sur les interactions polycation-ADN (Bronich et al., 2001; Ehtezazi et al., 2003; Rungsardthong et al., 2003; Kim, W. et al., 2006; Tan et al., 2006; Prevette et al., 2007; Huang, D. et al., 2008; Prevette et al., 2008; Yin et al., 2008). Le principe de l'ITC est fondé uniquement sur la mesure de la chaleur dégagée ou absorbée au cours d'une interaction entre deux composantes. Dans le cas d'une étude d'interaction entre un ADN et un polycation, une solution d'ADN placée dans la cellule de mesure de l'ITC est titrée à température constante par l'injection d'une solution de polycation au moyen d'une seringue qui assure également l'agitation du mélange (Figure 2.10).

La quantité de chaleur mesurée est proportionnelle à la quantité de complexes formés. Au cours du titrage, l'ADN est progressivement neutralisé par l'ajout de polycation jusqu'à la saturation. Les quantités de chaleur mesurées permettent d'obtenir une isotherme d'interaction qui peut être analysée à l'aide d'un modèle en adéquation avec les données pour déterminer la constante d'affinité, l'enthalpie d'interaction et la stoechiométrie d'interaction.

Dans une étude de systèmes complexes par ITC, comme le cas de l'ADN avec un polycation, plusieurs phénomènes peuvent contribuer à la chaleur mesurée et ne sont pas explicitement indiqués par une simple équation d'équilibre (Liu, Yufeng et Sturtevant, 1997): ADN + polycation ⇌ complexe ADN/polycation. Les changements d'ionisation des composantes, la libération de contre-ions et de molécules d'eau ainsi que le changement de conformation sont des phénomènes qui peuvent contribuer à la chaleur mesurée. Plusieurs études ont rapporté que l'interaction de l'ADN avec un polycation est accompagnée d'un transfert de protons entre les réactifs et le système tampon (Choosakoonkriang et al., 2003; Ehtezazi et al., 2003; Prevette et al., 2007; Prevette et al., 2008). L'utilisation de différentes solutions tampon à un pH spécifique permet de déterminer les changements d'ionisation puisque l'enthalpie d'interaction mesurée, ΔH_{obs}, est directement proportionnelle au nombre de protons échangés avec le système tampon par la relation suivante (Hinz et al., 1971):

$$\Delta H_{obs} = \Delta H_{o} + \Delta n_{H^+} \Delta H_{buffer}$$

où Δn_{H^+} est le nombre de moles de protons échangés avec le système tampon, et ΔH_o est l'enthalpie d'interaction polycation-ADN si l'enthalpie d'ionisation du système tampon, ΔH_{buffer}, est nulle. Cependant, le terme ΔH_o a été jusqu'à présent interprété comme étant l'enthalpie intrinsèque d'interaction entre le polycation et l'ADN. Des valeurs calculées de ΔH_o, positives ou négatives, ont été directement associées à des interactions endothermiques ou exothermiques

qui ont mené à des conclusions hâtives. Par exemple, des valeurs de ΔH_o négatives ont été attribuées à la formation de liaisons hydrogène au cours de la complexation entre un ADN et des polyglycoamidoamines (Prevette et al., 2007). Il faut savoir que le terme ΔH_o peut également contenir une contribution due au changement d'ionisation des réactifs avec lesquels l'échange de protons a lieu avec le système tampon. Cette contribution peut être importante mais a été jusqu'à présent négligée dans les études sur les interactions polycation-ADN.

CHAPITRE 3 DÉMARCHE DE L'ENSEMBLE DU TRAVAIL ET ORGANISATION GÉNÉRALE DES ARTICLES

Les parties expérimentales avec les interprétations et les discussions des résultats obtenus dans ce travail sont présentées dans les chapitres 4 à 6, sous forme de trois articles publiés ou soumis dans des revues scientifiques. Un dernier article, en cours de préparation pour soumettre dans une revue scientifique, est présenté dans l'annexe.

Le chapitre 4 présente l'étude sur les interactions chitosane-ADN par calorimétrie de titrage isotherme. L'analyse de la chaleur dégagée pendant le titrage de l'ADN par des chitosanes de masses molaires et de DDA différents nous a permis de déterminer la constante d'interaction, l'enthalpie d'interaction et la stoechiométrie des complexes formés. Nous avons effectué les titrages avec des solutions tamponnées à des valeurs de pH différentes et nous avons analysé la contribution de l'ionisation de chaque composante à l'enthalpie d'interaction mesurée. La dépendance de l'enthalpie d'interaction chitosane-ADN avec le type de solution tampon indique un transfert de protons de la solution tampon au chitosane lors de la complexation avec l'ADN. Les résultats de cette étude ont été publiés : Ma, P. L., Lavertu, M., Winnik, F. M. et Buschmann, M. D. (2009). New Insights into Chitosan-DNA Interactions Using Isothermal Titration Microcalorimetry. *Biomacromolecules, 10*(6), 1490-1499.

Le chapitre 5 présente une nouvelle approche que nous avons développée pour la quantification directe du chitosane libre après l'avoir séparé des complexes ADN/chitosane. Nous avons utilisé la technique de fractionnement par flux-force avec flux asymétrique (AF4). Le couplage en ligne de cette technique avec un spectrophotomètre UV-visible, un détecteur de diffusion de lumière multi-angles (MALS) et un détecteur de diffusion dynamique de lumière

(DLS) nous a permis de déterminer en une seule expérience trois paramètres importants des complexes ADN/chitosane: la taille et la distribution de la taille des particules ainsi que la concentration du chitosane libre dans une dispersion. La quantification du chitosane libre nous a ensuite permis de calculer la composition des complexes ADN/chitosane. La taille hydrodynamique des complexes mesurée par le système AF4/UV-Vis/MALS/DLS a été confirmée par des techniques traditionnelles comme le DLS en mode batch et la microscopie électronique à balayage (SEM). Cet article est paru : Ma, P. L., Buschmann, M. D. et Winnik, F. M. (2010). One-Step Analysis of DNA/Chitosan Complexes by Field-Flow Fractionation Reveals Particle Size and Free Chitosan Content. *Biomacromolecules, 11*(3), 549-554.

Le chapitre 6 présente l'étude de caractérisation des complexes d'ADN formés avec des chitosanes de masses molaires et de DDA différents par le système AF4/UV-Vis/MALS/DLS. Nous avons déterminé précisément l'effet de ces paramètres moléculaires et des conditions de préparation sur la fraction du chitosane libre et la structure des complexes, telle que la taille, la distribution de taille, la composition et la conformation des particules. La concentration du chitosane et de l'ADN utilisées lors de la préparation des complexes ont été également testées. Nous avons validé les fractions du chitosane libre obtenues avec le système AF4 couplé avec des détecteurs multiples par une méthode alternative combinant l'ultracentrifugation des échantillons et l'analyse des surnageants par colorimétrie. Cette étude a été soumis pour publication dans la revue *Analytical Chemistry* : Ma, P. L., Buschmann, M. D. et Winnik, F. M. Simultaneous Determination of Unbound Polycation and Particle Size of DNA/Chitosan Complexes by Asymmetrical Flow Field-Flow Fractionation.

La stabilité des complexes ADN/chitosane en présence de différents biopolymères anioniques a été également étudiée. Cette étude est présentée dans l'annexe 2 sous la forme d'un article en vue de soumission dans le journal *Langmuir*. La capacité des polyanions compétiteurs

à dissocier les complexes ADN/chitosane et à interagir électrostatiquement avec le chitosane a été évaluée en fonction de plusieurs paramètres : la densité de charge du polyanion compétiteur, la masse molaire, le DDA et la concentration du chitosane. La spectroscopie de fluorescence a été utilisée pour détecter et quantifier l'ADN dissocié du chitosane en utilisant le Picogreen comme marqueur fluorescent qui se lie sélectivement à l'ADN. De plus, la constante d'interaction de chaque système binaire chitosane-polyanion compétiteur a été déterminée par ITC et comparé avec celle du couple chitosane-ADN.

CHAPITRE 4 NEW INSIGHTS INTO CHITOSAN-DNA INTERACTIONS USING ISOTHERMAL TITRATION MICROCALORIMETRY

Pei Lian Ma, Marc Lavertu, Françoise M. Winnik, and Michael D. Buschmann

Department of Chemical and Biomedical Engineering, Ecole Polytechnique de Montréal, P.O. 6079 Succ. Centre-Ville, Montreal, Quebec, H3C 3A7, Canada, and Department of Chemistry and Faculty of Pharmacy, Université de Montréal, P.O. 6128 Succ. Centre-Ville, Montreal, Quebec, H3C 3J7, Canada.

4.1 Abstract

The interaction of chitosan with plasmid DNA was investigated as a function of pH, buffer composition, degree of deacetylation (DDA) and molecular weight (M_n) of chitosan, using isothermal titration microcalorimetry (ITC). The Single Set of Identical Sites model was used to obtain the enthalpy of interaction, the binding constant, and the stoichiometry of binding. The chitosan-DNA interaction was shown to be coupled with proton transfer from the buffer to chitosan, as revealed by the dependence of the measured heat release on the ionization enthalpy of the buffer. The measured enthalpy of binding was almost entirely due to proton transfer, since it was accounted for by the enthalpy of ionization of the buffer and of chitosan once the number of protons transferred was calculated. This proton transfer during binding resulted in the protonation an additional 17, 37, and 58% of total glucosamine units at pH 5.5, 6.5 and 7.4, respectively. The strong polyanionic nature of DNA facilitates the ionization of glucosamines of chitosan upon complexation and is responsible for proton transfer. Interestingly, using the

chitosan-DNA stoichiometry provided by ITC and the calculated degree of ionization of chitosan in the complex, the charge ratio of protonated amines to negative phosphate groups in the complex was nearly constant at 0.50-0.75 after saturation and was independent of the pH, buffer type and chitosan molecular characteristics. The chitosan-DNA binding constant was in the range of 10^{9}-10^{10} M^{-1}. The binding constant was pH-dependent and was greater at lower pH due to increased electrostatic attraction to DNA when chitosan is highly charged. Furthermore, the DDA and molecular weight of chitosan exerted a great influence on binding affinity which increased by almost an order of magnitude with an increase of the latter from 7 to 153 kDa. The binding affinity did not change significantly with DDA from 72 to 80% when the M_n was kept constant near 80 kDa, but it increased substantially with DDA from 80 to 93% to reach a value similar to that obtained with chitosan of M_n = 153 kDa and 80% DDA. These results provide insight into the previously reported dependence of the transfection efficiency of DNA/chitosan complexes on chitosan DDA and molecular weight, where complex stability and chitosan-DNA binding strength play a critical role.

4.2 Keywords

Chitosan, DNA, electrostatics, proton transfer, binding affinity, enthalpy of binding, stoichiometry of binding, degree of deacetylation, molecular weight.

4.3 Introduction

Chitosan is a biodegradable and biocompatible polysaccharide prepared by alkaline deacetylation of chitin found in the shells of crustaceans. It is a linear cationic polyelectrolyte composed of D-glucosamine and *N*-acetyl-D-glucosamine linked by β(1,4)-glycosidic bonds. The glucosamine monomer fractional content is defined as the degree of deacetylation or DDA. First investigated as a carrier for plasmid DNA by Mumper et al. (1995), chitosan has shown great potential for gene delivery. Chitosan forms complexes with DNA primarily through electrostatic interactions between the protonated glucosamine units of chitosan and the negatively charged phosphate groups of DNA. Interactions that involve a weak polybase, such as chitosan, are influenced by the solution pH, due to the low intrinsic pK_a (~6.7) (Filion et al., 2007) of the amine group in the glucosamine units. Typically, DNA/chitosan complexes are prepared in acidic aqueous solutions (Mao, H.Q. et al., 2001; Liu, W. et al., 2005; Strand et al., 2005; Maurstad et al., 2007), where chitosan is highly ionized. However, in some studies, the complexation process was carried out in aqueous solutions of pH 7.0-7.4 (Danielsen et al., 2004; Strand et al., 2005; Maurstad et al., 2007), where chitosan is only partially ionized. In addition to solution pH, the DDA and molecular weight of chitosan influence the physicochemical and biological properties of chitosans and the transfection efficiencies of DNA/chitosan complexes (MacLaughlin et al., 1998; Ishii et al., 2001; Koping-Hoggard et al., 2001; Lavertu et al., 2006). Recently, high levels of transgene expression of plasmid DNA/chitosan complexes were reported using chitosans with specific DDA and molecular weight, whose optimal values depend on the ratio of chitosan amine to DNA phosphate groups (Lavertu et al., 2006). High transgene expression levels were achieved by simultaneously lowering the chitosan molecular weight and increasing the DDA, or by lowering the DDA and increasing the molecular weight. This

coupling between the DDA and the molecular weight of chitosan suggests that an optimal binding strength of chitosan to DNA is required for maximum transgene expression, namely, it should be strong enough to condense and protect DNA, but weak enough to permit intracellular disassembly. The dependence of transfection efficiciency on the structure of the polycation and on the balance between complex stability and dissociation emphasizes the need to obtain quantitative information on the binding properties of DNA with polycations such as chitosan.

Several techniques have been applied to characterize DNA/polycation complexes, including electrophoretic analysis, zeta potential measurements, dynamic light scattering, ethidium bromide displacement assay, and microscopy (Rungsardthong et al., 2003; Strand et al., 2005). Recently, isothermal titration calorimetry (ITC) has been used to determine the binding constant, enthalpy of complex formation and the stoichiometry of binding of DNA with cationic polymers, such as polyethyleneimine (PEI), poly-L-lysine (PLL), poly(2-(dimethylamino)ethyl methacrylate) (PDMAEMA), poly(2-(diethylamino)ethyl methacrylate) (PDEAEMA), and poly(glycoamidoamine) (Bronich et al., 2001; Ehtezazi et al., 2003; Rungsardthong et al., 2003; Kim, W. et al., 2006; Tan et al., 2006; Prevette et al., 2007; Huang, D. et al., 2008; Prevette et al., 2008; Yin et al., 2008). ITC has also been used to study the effect of solution pH on the DNA-polycation complexation (Choosakoonkriang et al., 2003; Rungsardthong et al., 2003). For example, higher binding constants between DNA and PDMAEMA at low pH were reported due to higher degrees of ionization of the polycation (Rungsardthong et al., 2003). However, there are no studies reporting quantitatively the thermodynamic parameters that characterize the chitosan-DNA interaction and examining how this interaction is influenced by solution pH, buffer type, and chitosan molecular characteristics. In general, ITC has been particularly useful to investigate binding events where protonation changes occur, as in protein-DNA interactions (Lundback et Hard, 1996). However, there is a lack of systematic studies exploiting this proton

transfer effect in polycation-DNA interactions. By using buffers with different protonation enthalpies and at a single solution pH, Ehtezazi *et al.* demonstrated that the interaction of DNA with poly(bis-acryloylpiperazine-2-methyl-piperazine induces a proton transfer from the buffer to the polycation, resulting in a change of the ionization degree of the buffer and of the polymer upon interaction with DNA in a stoichiometric charge-charge fashion (Ehtezazi et al., 2003). Similar findings exploiting this protonation effect were reported by Choosakoonkiang *et al.* for the DNA/PEI system at variable pH (Choosakoonkriang et al., 2003), although no clear relationship was derived between the solution pH and the number of protons transferred to PEI. These studies benefited from the fact that protonation or deprotonation of the interacting species will contribute to the total enthalpy change in proportion to the number of protons exchanged with the buffering system (Hinz et al., 1971). Recently, the interaction of DNA with poly(glycoamidoamine)s was found to be exothermic after eliminating the energy of buffer ionization from the observed binding enthalpy (Prevette et al., 2007; 2008). The negative enthalpies were attributed tentatively to the formation of hydrogen bonds in the complexes (Prevette et al., 2007). These studies all point to the fact that the heat associated with the protonation changes of the polycation, in addition to that of the buffer, can contribute significantly to the observed total enthalpy of binding but has often been omitted. This can lead to possible misinterpretation of the intrinsic binding enthalpy, and consequently, of the nature of the interactions, after only subtracting the ionization enthalpy of the buffer.

In the study reported here, we hypothesized that chitosan binding to DNA would induce proton transfer from the buffer to chitosan and increase the degree of ionization of chitosan in the bound state, compared to its free and soluble state. A detailed analysis of the different protonation events allowed us to assess the contribution of the buffer ionization and the protonation of chitosan to the observed total enthalpy of binding. We calculated the ionization

state of free and bound chitosan in the different buffer systems and at different solution pH (below and above the pK_a of chitosan). In addition, the chitosan-DNA binding constant and the number of chitosan chains bound per plasmid DNA were determined by fitting ITC data to a standard model. The stoichiometry of binding together with the degree of ionization of bound chitosan enabled the calculation of the charge ratio of the complexes at saturation of the binding sites. Furthermore, a series of chitosans previously investigated for their potential as gene delivery vectors was assessed in order to understand the effect of the DDA and molecular weight of chitosan on the chitosan-DNA interaction.

4.4 Materials and Methods

4.4.1 Materials

The 6.4 kb plasmid EGFPLuc (Clontech Laboratories) encodes for a fusion of enhanced green fluorescent protein and luciferase from the firefly *Photinus pyralis*, driven by a human cytomegalovirus (CMV) promoter. This plasmid was amplified in DH5α bacteria and purified using the Qiagen Plasmid Mega Kit. The plasmid purity and concentration were determined by UV spectrophotometry as previously reported (Lavertu et al., 2006). A stock solution of DNA (0.33 mg/mL) was prepared in deionized water and stored at –20°C before use. Ultrapure heterogeneously deacetylated chitosans (Ultrasan™) with DDA of 72, 80, 93, and 98% were provided by Biosyntech Inc. (Laval, Qc, Canada) and were previously depolymerized by Lavertu et al. (2006) using nitrous acid to achieve specific number-average molecular weight (M_n) of about 7, 80, and 153 kDa. Table 1 summarizes the M_n and polydispersity index of chitosans measured by analytical SEC (Lavertu et al., 2006) as well as the DDA determined by ^{1}H NMR (Lavertu et al., 2003) and the calculated number of glucosamine units per chain of chitosan. For

the binding study between DNA and chitosan, a chitosan stock solution of 5 mg/mL was prepared by dissolving the sample overnight on a rotary mixer in hydrochloric acid/deionized water using an HCl/glucosamine ratio of 1. Since chitosan powder is hygroscopic, the water content was determined by drying it at 60°C for two days using a heated centrifugal vaccuum concentrator (Savant Speedvac, model SS110). Taking into account the water content that varied from 8 to 14% (wt/wt), the corrected concentration of chitosan stock solution was between 4.3 to 4.6 mg/mL. For tests characterizing the enthalpy of protonation of chitosan without any DNA present, a chitosan stock solution of 0.88 mg/mL (after correction for water content) was similarly prepared using an HCl/glucosamine ratio of 0.85.

Table 4.1. Molecular Characteristics of the Chitosans Studied.

DDA	M_n (kDa)	M_w/M_n	Glucosamine units/Chitosan[a]
72%	86	3.5	358
80%	7.4	1.3	35
80%	94	2.1	443
80%	153	1.6	721
93%	80	1.5	455
98%	79	1.6	479

[a] The number of glucosamine units per chain of chitosan was calculated by $M_n \div M_{monomer} \times$ DDA. $M_{monomer}$ is the average molar mass of the chitosan monomer and was calculated by 161.2 DDA + 203.2 (1 - DDA), where 161.2 and 203.2 are the molar mass (g) of the glucosamine unit and *N*-acetylglucosamine unit respectively.

4.4.2 pH and Ionic Strength Adjustment of Solutions

For ITC analysis of chitosan binding to DNA, the chitosan stock solution was diluted with a buffer to reach a concentration of glucosamine units between 0.708 to 0.758 mM, corresponding to 1.01-20.6 μM of chitosan depending on M_n or 123-176 μg/mL of chitosan depending on the DDA. The DNA stock solution was diluted with the same buffer to a constant concentration of 0.120 mM in phosphate or nucleotide units (9.42 nM or 39.6 μg/mL of DNA), using an average molar mass of 330 g/mol per nucleotide. The following buffers were used: 10 mM sodium acetate buffer at pH 5.5, 5 mM sodium phosphate buffer at pH 6.5 and 7.4, 25 mM MES buffer at pH 5.5, 6.5, and 7.4, 25 mM MOPS buffer at pH 6.5 and 7.4, 5 mM piperazine buffer at pH 5.5, and 10 mM Tris-HCl buffer at pH 7.4. They were used at a pH close to their pK_a and buffer concentrations were selected to maintain buffering capacity and reduce specific ion effects. The total ionic strength of the buffers was kept constant at 25 mM by adding NaCl. This ionic strength was chosen to obtain an ITC profile without excessive salt screening, particularly when the heat of interaction is low. Table 4.2 summarizes the composition and the enthalpies of ionization of the buffers. The absence of phase separation in these dilute chitosan solutions (80% DDA, 94 kDa) even at pH 7.4 was confirmed by subjecting the samples to ultracentrifugation (65,000 rpm, 30 min) and measuring the concentration of chitosan in the supernatant by the Orange II depletion method (Drogoz et al., 2007). The concentration of soluble chitosan in the supernatant was unchanged in the pH range of 5.5 to 7.4.

Table 4.2. Buffer Characteristics at the pH of Titrations.

Buffer	ΔH_{buffer} [a] (kcal/mol)	pK_a [b]	pH	I_{buffer} [d] (mM)
10 mM Acetate	-0.10	4.76	5.5	8
5 mM Phosphate	0.86	6.82[c]	6.5 7.4	8 13
25 mM MES	3.54	6.15	5.5 6.5 7.4	5 18 24
25 mM MOPS	5.05	7.20	6.5 7.4	4 15
5 mM Piperazine	7.44	5.33	5.5	9
10 mM Tris-HCl	11.35	8.08	7.4	8

[a] Enthalpy of ionization taken from reference (Goldberg et al., 2002). [b] pK_a values taken from reference Dean (1999) (except where indicated). [c] pK_a value from reference (Kumler et Eiler, 1943). [d] Buffer ionic strength prior to adding NaCl to achieve a total ionic strength of 25 mM.

4.4.3 Degree of Ionization of Chitosan

The ionization state of chitosan in each buffering system was obtained numerically using a mathematical model of solution electroneutrality and acid-base equilibria, implemented with Mathematica (Wolfram Research, Champaign, IL). The proton dissociation of the buffer ($HA^z \rightleftharpoons A^{z-1} + H^+$) is given by

$$pK_a^{buffer} = pH + \log_{10}\frac{[HA^z]}{[A^{z-1}]} \qquad \textbf{(4.1)}$$

Based on a model previously developed (Filion et al., 2007; Lavertu et al., 2008), the proton dissociation equilibrium of the glucosamine monomer of chitosan in the mean field approximation is given by

$$\mathrm{p}K_{\mathrm{ap}} = \mathrm{pH} + \log_{10}\left(\frac{\alpha}{1-\alpha}\right) \approx \mathrm{p}K_0 - \frac{e\psi\big|_{r=a}}{kT\ln 10} \qquad \textbf{(4.2)}$$

where $\mathrm{p}K_{\mathrm{ap}}$ is the apparent proton dissociation constant of chitosan, α is the degree of ionization of chitosan, $\mathrm{p}K_0$ the intrinsic dissociation constant of the glucosamine unit (i.e. $\mathrm{p}K_{\mathrm{ap}}$ when $\alpha = 0$), and $\psi|_{r=a}$ is the electrostatic potential at the surface of the polyelectrolyte in the Poisson-Boltzmann cylindrical cell model. It has been demonstrated previously that the rightmost term in Equation 4.2 is approximately linear with α, such that the $\mathrm{p}K_{\mathrm{ap}}$ of chitosan can be expressed as (Filion et al., 2007; Lavertu et al., 2008)

$$\mathrm{p}K_{\mathrm{ap}} = \mathrm{pH} + \log_{10}\left(\frac{\alpha}{1-\alpha}\right) \approx \mathrm{p}K_0 - m\alpha \qquad \textbf{(4.3)}$$

where m depends on the ionic strength. We solved the Poisson-Boltzmann equation for chitosan (DDA = 80%) in the acetate buffer (see Table 4.2) and obtained $m = 0.8$. This value was used for all other chitosan solutions since it is almost invariant in the range of DDA investigated here, and all solutions had an ionic strength of 25 mM. The chitosan $\mathrm{p}K_0$ in Equation 4.3 is 6.63, 6.57, 6.48 and 6.48 for 72, 80, 93 and 98% DDA, respectively (Filion et al., 2007). The condition of electroneutrality, neglecting protons (H^+) and hydroxyl ions (OH^-), is given by

$$[\mathrm{GlucNH_3^+}] + [\mathrm{Na^+}] + z[\mathrm{HA^z}] = [\mathrm{Cl^-}] + (1-z)[\mathrm{A^{1-z}}] \qquad \textbf{(4.4)}$$

where $[\mathrm{GlucNH_3^+}]$ is the concentration of protonated glucosamine units. The degree of ionization of chitosan, α, and the pH of each solution were calculated numerically from Equations 4.1, 4.3, and 4.4 using the known total concentrations of buffer and of glucosamine units on chitosan. The calculated pH was consistent with the measured pH.

4.4.4 Isothermal Titration Calorimetry

Binding studies were performed using a VP-ITC microcalorimeter from MicroCal (Northampton, MA) with a cell volume of 1.428 mL at 25^{o}C. Samples were degassed in a ThermoVac system (MicroCal) prior to use. The sample cell was filled with the DNA solution and the reference cell with buffer solution only. The chitosan solution was introduced into the thermostatted cell by means of a syringe which also stirred at 250 rpm. Each titration consisted of an initial 2 μL injection (neglected in the analysis) followed by 28 subsequent 10 μL injections each of which were 20 s in duration and were programmed to occur at 400 s intervals. The heats of dilution from titrations of chitosan solution into buffer only (without DNA) were subtracted from the heats obtained from titrations of chitosan solution into DNA solution to obtain net binding heats. All experiments were carried out in duplicate.

In the ITC experiments of protonation of chitosan (80% DDA, 94 kDa) in the absence of DNA, titrations of HCl into chitosan were performed in a manner similar to that described above except that the sample cell was filled with chitosan and the syringe with 5 mM HCl. The chitosan solution was prepared by diluting the stock solution of 0.88 mg/mL (HCl/glucosamine ratio of 0.85) to a final concentration of 5.97 μM of chitosan (2.64 mM of glucosamine units) with deionized water. Appropriate amounts of 500 mM NaCl were added to achieve a final NaCl concentration of 25 mM in both chitosan and HCl solutions. The heats of dilution of 5 mM HCl into 25 mM NaCl (without chitosan) were subtracted from the heats obtained from titrations of HCl into chitosan solution to obtain net binding heats.

4.4.5 Analysis of Binding Isotherms

Raw ITC data of chitosan binding to DNA was processed with the Origin software provided by the manufacturer and the isotherms were fit using the Single Set of Identical Sites (SSIS) model by a nonlinear least-squares analysis (Wiseman et al., 1989; MicroCal LLC., 2004). The equilibrium binding constant, K, between a free molecule of chitosan and a free binding site on DNA is represented by Equation 4.5, assuming independent binding sites. The relationship between total and free chitosan concentrations (L_T and L) is given by Equation 4.6.

$$\text{Free binding site on polyanion} + \text{Free chitosan} \underset{}{\overset{K}{\rightleftharpoons}} \text{Bound chitosan}$$

$$K = \frac{[\text{Bound chitosan}]}{[\text{Free binding sites}][\text{Free chitosan}]} = \frac{\Theta}{(1-\Theta)[L]} \qquad \textbf{(4.5)}$$

$$[L] = [L_T] - n\Theta[M_T] \qquad \textbf{(4.6)}$$

where Θ = [Bound chitosan]/(n[M_T]) is the fraction of plasmid DNA binding sites occupied by chitosan, [M_T] is the total DNA molar concentration and n the number binding sites on plasmid DNA for chitosan (the number of moles of chitosan chains bound to each mole of plasmid DNA at saturation of the binding sites). Combining Equations 4.5 and 4.6 gives the quadratic Equation 4.7, which is solved to obtain Θ in Equation 4.8.

$$\Theta^2 - \Theta\left(1 + \frac{1}{nK[M_T]} + \frac{[L_T]}{n[M_T]}\right) + \frac{[L_T]}{n[M_T]} = 0 \qquad \textbf{(4.7)}$$

$$\Theta = \frac{1}{2}\left(1 + \frac{1}{nK[M_T]} + \frac{[L_T]}{n[M_T]} - \sqrt{\left(1 + \frac{1}{nK[M_T]} + \frac{[L_T]}{n[M_T]}\right)^2 - \frac{4[L_T]}{n[M_T]}}\right) \qquad \textbf{(4.8)}$$

The total heat content Q of the solution in the sample cell of volume V_o at fractional saturation Θ is

$$Q = n[M_T]V_o\Delta H\Theta \quad \textbf{(4.9)}$$

where ΔH is the enthalpy of binding per mole of bound chitosan. Since the instrument senses the change of heat content at the ith injection, ΔQ_i, it is this parameter of interest that is fit to experimental data, after taking into account displaced volume effects as

$$\Delta Q_i = Q_i - Q_{i-1} + \frac{\Delta V_i}{V_o}\left[\frac{Q_i + Q_{i-1}}{2}\right] \quad \textbf{(4.10)}$$

where ΔV_i is the injection volume at the ith injection. Equations 4.8, 4.9 and 4.10 are simultaneously fit to the experimental values of ΔQ_i to obtain best fit values of n, K, and ΔH. The entropy change was calculated from $\Delta S = (\Delta H - \Delta G)/T$, where $\Delta G = -RT\ln K$. Note that K is written in its ideal form where activities have been replaced with concentrations (Equation 4.5). These parameters are reported as the mean of two measurements with errors representing their minimum and maximum. For the titrations of HCl into chitosan (in the absence of DNA), the isotherms were fit using Mathematica 6.0 (Wolfram Research) and similarly applying the SSIS model, except the cell already contained 2.25 mM of HCl prior to titrations.

4.4.6 Zeta Potential

The zeta potential of DNA/chitosan complexes was measured with a Malvern Zetasizer Nano ZS (Worcestershire, UK). Prior to mixing with plasmid DNA, a chitosan stock solution (80% DDA, 94 kDa) was diluted to 6 and 8 μg/mL with 25 mM MES buffer at pH 6.5 and 25 mM of ionic strength (adjusted with NaCl). DNA/chitosan complexes were then prepared by fast mixing 625 μL of diluted chitosan solution with an equal volume of DNA solution (13.2 μg/mL by diluting the DNA stock solution in the same buffer) to reach desired N/P ratios of 0.70 and 1.0

in the final dispersion. The zeta potential of the complexes was calculated from the electrophoretic mobility values using the Smoluchowski equation.

4.5 Results and Discussion

4.5.1 Chitosan-DNA ITC Isotherms

The ITC profiles recorded for the titration of chitosan (80% DDA, 94 kDa) into a plasmid DNA solution, both in 25 mM MES buffer at pH 6.5, and the titration of chitosan into MES buffer providing the heat of dilution of chitosan are shown in Figure 4.1. Panel A shows the heat rate during the titration as a function of time. Each injection of chitosan into DNA produces a sharp negative peak indicating an exothermic interaction. As the chitosan content in the cell increases, the heat released decreases indicating progressive neutralization of DNA. Figure 4.1B shows the integrated heats of binding obtained from the heat rate normalized to the moles of chitosan titrated, prior to subtracting the blank, and are represented as a function of both the molar ratio of chitosan to DNA and the corresponding N/P molar ratio (the number of glucosamine units in chitosan to the number of negative phosphate units in DNA). The heat of dilution of chitosan in the buffer is negligible compared to the heat of chitosan-DNA interaction, except near the end of the titration where chitosan-DNA interactions had ceased. In order to compare results of the different conditions studied, the isotherms presented in the course of this study will be as a function of N/P ratio only.

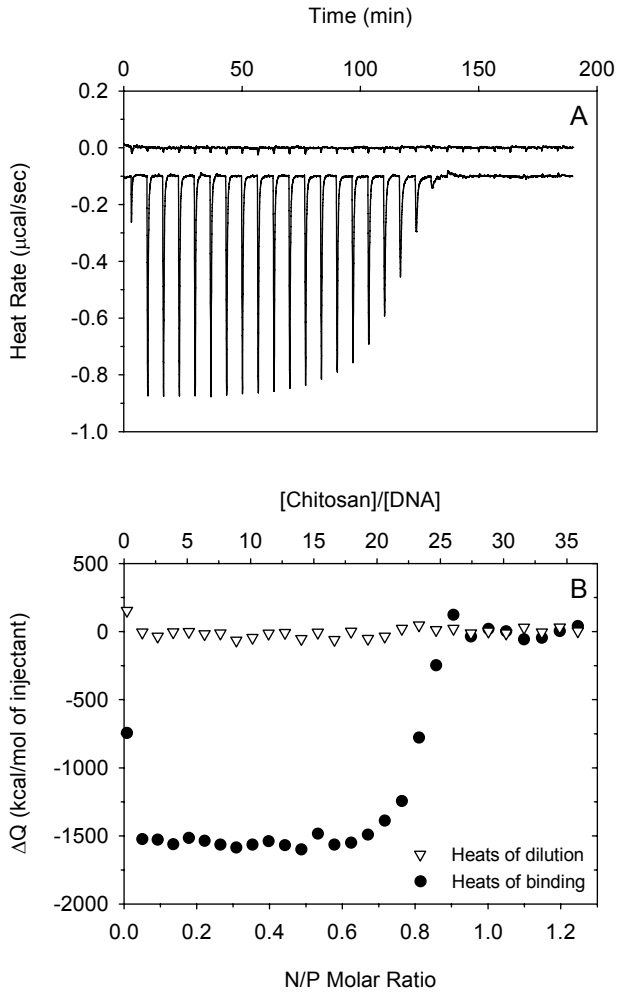

Figure 4.1. ITC raw data (panel A) for the interaction between DNA and chitosan (80% DDA, 94 kDa) in 25 mM MES buffer at pH 6.5 with I=25 mM. The upper curve shows the blank titration of chitosan into buffer resulting in heats of dilution, and the lower curve shows the binding heats from the titration of chitosan into DNA solution. In panel B, the corresponding integrated heats of dilution and of binding are shown versus the ratio of chitosan amine to DNA phosphate groups and versus molar ratios of chitosan to DNA.

4.5.2 Buffer and pH-Dependence of the Measured Enthalpy of Chitosan-DNA Binding

DNA has a constant negative charge over the pH range studied here, since the pK_a of its phosphate group is about 1 (Bloomfield et al., 2000). Therefore, varying the solution pH will only influence the degree of ionization of chitosan and of the buffer. The calorimetric responses of the binding of DNA with chitosan (80% DDA, 94 kDa) in different buffers at pH 5.5, 6.5 and 7.4 are shown in Figure 4.2. At pH 5.5, the amplitude of binding heat of chitosan to DNA was buffer dependent (top panel in Figure 4.2). This buffer-dependence became more apparent at pH 6.5, displaying greater exothermic amplitudes (middle panel in Figure 4.2). Interestingly, however, the interaction between DNA and chitosan was not always exothermic. For example, complex formation at pH 7.4 was exothermic in sodium phosphate buffer but endothermic in Tris buffer.

The dependence of the heat of interaction of chitosan with DNA on the nature of the buffer is an indication that the buffer is ionized or neutralized in the process of chitosan binding to DNA, and therefore, that protons are transferred between chitosan and the buffer. This effect is taken into account in the observed enthalpy of binding, ΔH_{obs}, by a term proportional to the molar ionization enthalpy of the buffer, ΔH_{buffer} (Hinz et al., 1971):

$$\Delta H_{obs} = \Delta H_{o} + \Delta n_{H^+} \Delta H_{buffer} \qquad \textbf{(4.11)}$$

where Δn_{H^+} is the number of moles of protons taken up or released by the buffer, and ΔH_o is the chitosan-DNA molar binding enthalpy that would be measured if ΔH_{buffer} was zero. ΔH_{obs} was obtained from the fit of the SSIS model to the ITC binding isotherms. The dependence of ΔH_{obs} on the buffer type is illustrated in Figure 4.3, where ΔH_{obs} is plotted as a function of buffer ionization enthalpy, ΔH_{buffer}, at pH of 5.5, 6.5 and 7.4. As expected from Equation 4.11, the

linear dependence and positive slope confirm the release of protons from the buffer and their uptake by chitosan, implying that initially neutral glucosamines are protonated during complex formation. The linear regression indicates that 74 (±7) moles of protons per mole of chitosan (80% DDA, 94 kDa) were transferred from the buffer to chitosan bound to DNA at pH 5.5. At pH 6.5 and 7.4, the binding was associated with an uptake of approximately 165 (±40) and 256 (±41) moles of protons per mole of chitosan bound to DNA, respectively. More protons were transferred when complexation occurred at higher pH, since in this case chitosan was less charged initially than at lower pH (see calculated α in Table 4.3). These results are consistent with previous studies of the interaction of DNA with cationic lipids (Lobo et al., 2003) and with small ligands (Nguyen, B. et al., 2006). For chitosan with a DDA of 80% and M_n of 94 kDa, we calculated 443 glucosamine units per chain, which results in proton transfer from the buffer to chitosan during binding that protonated an additional 17, 37, and 58% of total glucosamine units at pH 5.5, 6.5, and 7.4, respectively.

The strong polyanionic nature of DNA increases the ionization of a polycation such as chitosan by reducing its surface potential (rightmost term in Equation 4.2) and thereby increasing the polycation pK_a. The binding of anionic phosphate groups of DNA to cationic amine groups on chitosan can be seen as a means to reduce the electrostatic repulsion between the protons in solution and the chitosan chain, due to charge neutralization after binding to DNA phosphate groups (Zelikin et al., 2003). These mechanisms are discussed in Tsuchida et al. (1974), where the complexation of polyammonium polymers with weak polyelectrolytes such as polycarboxylic acids was found to decrease the pK_a of the polyanions. pK_a shifts were also reported in studies involving DNA binding to small ligands and proteins (Misra, V. K. et Honig, 1995; Misra, Vinod K. et al., 1998). In the latter studies, pK_a shifts were determined by the change of electrostatic free energy produced by the ionization of a residue of the ligand bound to DNA when all other

residues of this ligand are neutral (low dielectric cavity in water) relative to the ionization of the same residue free in water prior to binding to DNA. The change of electrostatic free energy was calculated using a nonlinear Poisson-Boltzmann model.

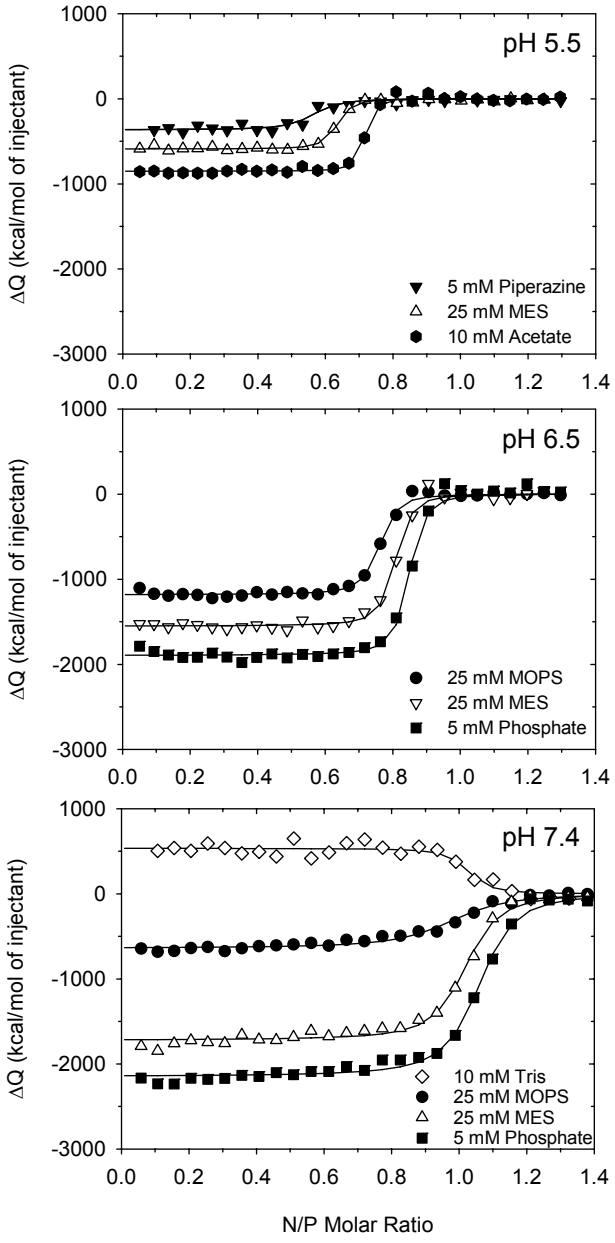

Figure 4.2. Integrated heats of interaction from calorimetric titrations of chitosan (80% DDA, 94 kDa) into DNA in different buffers at pH 5.5, 6.5 and 7.4 with a total ionic strength of 25 mM (adjusted with NaCl). Solid lines represent best-fits generated from the SSIS model.

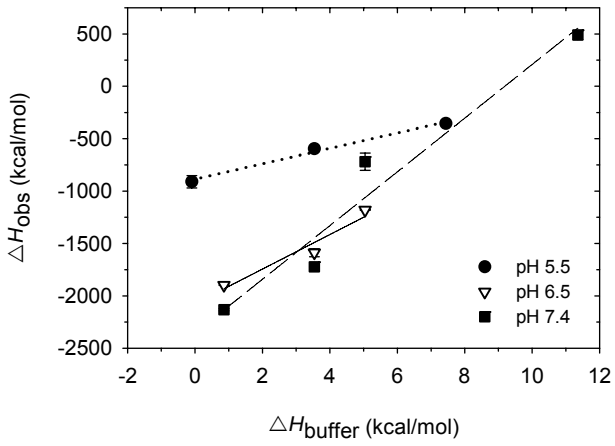

Figure 4.3. Variation of the apparent enthalpy of binding, ΔH_{obs} (obtained from fitting SSIS model to ITC isotherms), for the interaction between DNA and chitosan (80% DDA, 94 kDa) as a function of buffer ionization enthalpy, ΔH_{buffer}, (Table 4.2) at pH 5.5, 6.5 and 7.4 with a total ionic strength of 25 mM (adjusted with NaCl). The lines represent linear regressions of the data to Equation 4.11 resulting in : i) Δn_{H+}= 74 ± 7 moles of protons per mole of bound chitosan and ΔH_o= -887 ± 34 kcal/mol (dotted line, coefficient r^2= 0.9905) at pH 5.5 , ii) Δn_{H+}= 165 ± 40 moles of protons per mole of bound chitosan and ΔH_o= -2074 ± 145 kcal/mol (full line, coefficient r^2= 0.9434) at pH 6.5, and iii) Δn_{H+}= 256 ± 41 moles of protons per mole of bound chitosan and ΔH_o= -2355 ± 263 kcal/mol (dashed line, coefficient r^2= 0.9521) at pH 7.4. Means are shown with error bars representing minimum and maximum of duplicates.

Table 4.3. Parameters of Interaction of Chitosan (80% DDA, 94 kDa) with Plasmid DNA (6.4 kb) in Buffers with Different Protonation Enthalpies and at Constant Ionic Strength of 25 mM Obtained by Fitting ITC Isotherms to the SSIS model.

Buffer	α[a]	β[b]	n[c]	$n_{N/P}$[d]	$n_{N+/P-}$[e]	ΔH_{obs} (kcal/mol)	K_{obs} (x 10^9 M^{-1})	ΔS_{obs} (kcal/(mol.K))
A. pH 5.5								
Piperazine	0.77	0.94	15.6 ± 0.1	0.54 ± 0.01	0.51	-355 ± 9	---[f]	---
MES	0.76	0.93	16.9 ± 0.8	0.59 ± 0.03	0.54	-596 ± 6	5.3 ± 0.2	-2.0 ± 0.0
Acetate	0.77	0.94	18.8 ± 1.2	0.65 ± 0.04	0.61	-911 ± 59	13.8 ± 3.2	-3.0 ± 0.2
B. pH 6.5								
Phosphate	0.46	0.83	23.8 ± 0.0	0.83 ± 0.00	0.69	-1897 ± 3	6.7 ± 0.6	-6.3 ± 0.0
MES	0.39	0.76	23.1 ± 0.4	0.80 ± 0.02	0.61	-1588 ± 38	4.7 ± 1.5	-5.3 ± 0.1
MOPS	0.40	0.77	20.2 ± 1.1	0.70 ± 0.04	0.54	-1180 ± 1	3.8 ± 1.1	-3.9 ± 0.0
C. pH 7.4								
Phosphate	0.18	0.76	28.2 ± 1.7	0.98 ± 0.06	0.74	-2133 ± 11	1.5 ± 0.0	-7.1 ± 0.0
MES	0.15	0.73	28.0 ± 0.7	0.97 ± 0.03	0.71	-1723 ± 4	1.5 ± 0.1	-5.7 ± 0.0
MOPS	0.12	0.70	30.3 ± 2.6	1.05 ± 0.09	0.74	-720 ± 83	---[f]	---
Tris	0.17	0.75	27.4 ± 1.4	0.95 ± 0.05	0.71	490 ± 44	---[f]	---

[a] Degree of ionization of chitosan in the titrant buffer prior to complexation (calculated from Equations 4.1, 4.3 and 4.4). [b] Degree of ionization of chitosan in the complex after accounting for proton transfer from buffer to chitosan, using Equation 4.11. [c] The number of moles of binding sites for chitosan on each mole of plasmid DNA. [d] The ratio of chitosan amine to DNA phosphate groups in the complex when all binding sites are occupied at saturation (calculated from n). [e] The charge ratio (protonated chitosan amine to DNA phosphate groups) in the complex when all binding sites are occupied at saturation (calculated by multiplying $n_{N/P}$ by β). [f] The determination of K_{obs} was not precise since the interaction was strong and almost athermal. The parameters n, ΔH_{obs}, and K_{obs} were determined from the SSIS model fit using the molar concentration of chitosan and DNA as the binding entities and not their glucosamine and phosphate groups. Means are shown with error representing minimum and maximum of duplicates.

4.5.3 Stoichiometry of Binding and Composition of the Complexes at Saturation

Table 4.3 summarizes the calculated degree of ionization of chitosan (80% DDA, 94 kDa) in the solution state, α, and the parameters obtained from fitting the SSIS model to the ITC isotherms in the different buffers at different solution pH. The degree of ionization of chitosan after proton transfer (β) was also calculated taking into account the transfer of protons from the buffer to chitosan during complex formation (the Δn_{H^+} from Figure 4.3 and Equation 4.11). Chitosan-DNA binding increased the degree of ionization of chitosan i) from 77% in the unbound state to 94% in the complex when buffered at pH 5.5, ii) from about 42% in the unbound state to 79% in the complex when buffered at pH 6.5, and iii) from about 16% in the unbound state to 74% in the complex when buffered at pH 7.4. It is interesting to note from these results that DNA/chitosan (80% DDA, 94 kDa) complexes formed at pH 7.4 with about 74% of their glucosamine residues being protonated in the complex achieve a nearly 1:1 amine-phosphate ratio at saturation of the binding sites ($n_{N/P}$). While those formed at lower pH of 5.5 that are 94% protonated in the complex reach $n_{N/P}$ of only about 60%. The larger amount of chitosan in the complexes formed at higher pH than at low pH therefore suggests a less extended conformation of bound chitosan. However, in all cases, the ratio of protonated amine to negative phosphate groups in the complex ($n_{N+/P-} = n_{N/P} \times \beta$) when all the binding sites are occupied, is about 50-75% and is seen to be an experimentally conserved quantity, largely independent of the buffer and of the solution pH used to form the complexes. The fact that the measured ratio of 0.50-0.75 charged amines per charged phosphate in the complex is different from the 1:1 stoichiometry may be attributed to differences in the linear charge density between DNA and chitosan. The average intercharge spacing between phosphates on double stranded DNA is 0.17 nm for the B-

conformation (0.33 nm of rise per base pair along the helix axis) (Dickerson et al., 1982) compared to an average intercharge spacing between charged amine groups on chitosan that is slightly higher than the 0.52 nm monomer length of chitosan, depending on DDA and the degree of ionization. Therefore, if one chitosan chain binds to a particular section of a DNA strand in a fully extended conformation, this would result in a ratio of charged glucosamines to phosphate groups of approximately 0.63 (= 0.33 nm ÷ 0.52 nm) that is quite similar to $n_{N+/P-}$ of 0.50-0.75 obtained in our analyses. Such deviations from a 1:1 stoichiometric charge ratio have been previously observed when there was a large mismatch in linear charge density between the oppositely charged polyelectrolytes (Koetz et al., 1986; Philipp et al., 1989; Schwarz et al., 2006).

The above analysis predicts anionic complexes near the point of saturation. We obtained zeta potentials of -36 mV and -13 mV for the complexes prepared at N/P ratios of 0.70 and 1.0, respectively, confirming that the resulting complexes are negatively charged for these conditions, which correspond to the region of saturation in ITC isotherms at pH 6.5 (Figure 4.2). For successful transfection, complexes are usually prepared by one-shot fast mixing to get positively charged complexes. However, this method cannot provide information about the interaction parameters. In ITC, precipitation of the complexes will occur after saturation and further addition of chitosan will not bind to the precipitates. Whether the complexes are prepared by titration or by fast mixing, they should not differ significantly in structure and properties as long as the N/P ratio of the complexes is lower or equal to $n_{N/P}$.

4.5.4 The Enthalpy of Binding without the Buffer Contribution

The heat sensed by the microcalorimeter is the net contribution of all thermal events involved in the complexation between DNA and chitosan. At a specific solution pH, the plot of the observed total enthalpy change, ΔH_{obs}, versus the enthalpy of ionization of the buffer, ΔH_{buffer}, yields an intercept corresponding to the enthalpy of binding with no contribution from changing ionization state of the buffer, ΔH_o (Figure 4.3). For the binding of chitosan (80%DDA, 94 kDa) to DNA, ΔH_o was found from this extrapolation to be -887 (± 34), -2074 (± 145), and -2355 (± 263) kcal/mol at pH 5.5, 6.5, and 7.4, respectively. From these values, the binding of chitosan to DNA is seen to be exothermic and becomes more exothermic with increasing pH. However, the term ΔH_o is not the intrinsic enthalpy of binding, as is commonly stated, since it still contains the contribution from the enthalpy of protonation of the glucosamine units of chitosan. Two ionization events are involved since protons are transferred from the buffer to chitosan. Thus, it is important to recall that ΔH_{buffer} provides the enthalpy of ionization associated with the buffer but not the enthalpy of ionization associated with protonation of chitosan in this proton transfer process. This latter contribution of ligand ionization toward the enthalpy of binding has not been taken into consideration in previous studies of the complexation of cationic polymers with DNA (Choosakoonkriang et al., 2003; Ehtezazi et al., 2003; Prevette et al., 2007; Prevette et al., 2008). Therefore, we estimated the enthalpy of protonation of chitosan (80% DDA, 94 kDa) by calorimetric titration of HCl into chitosan to generate the ITC binding isotherms shown in Figure 4.4. The fit of the data using the SSIS model resulted in an enthalpy of binding of -9.37 (± 0.02) kcal/mol of protons (ΔH_{gluc}) bound to the glucosamine units. We used this value of the enthalpy of binding of protons to chitosan, along with the calculated number of moles of protons bound to chitosan during complex formation (Caption of Figure 4.4), at a specific solution pH, to obtain

the total enthalpy of protonation of chitosan during complex formation. This analysis resulted in a total enthalpy of protonation of chitosan of -693 (± 66), -1546 (± 376), and -2398 (± 385) kcal/mol of chitosan (80% DDA, 94 kDa) bound to DNA, corresponding to 78, 75, and 102% of ΔH_o at pH 5.5, 6.5, and 7.4, respectively. These analyses lead to the interesting conclusion that heat effects seen upon binding of a protonable polycation to DNA in the presence of a buffer are almost entirely due to ionization changes of the polycation and buffer, $\Delta H_{obs} \approx \Delta n_{H+}(\Delta H_{buffer} + \Delta H_{gluc})$. This finding is in agreement with a previous study where negligible heat was detected under conditions of full ionization of oppositely charged polyelectrolytes.(Rungsardthong et al., 2003) From this approximation, it is possible to predict whether the chitosan-DNA interaction in a specific buffer will be endothermic or exothermic. Among the buffers used in this study, only in Tris-HCl buffer the observed enthalpy of interaction was found to be positive because the enthalpy of ionization of the buffer is higher than the enthalpy of protonation of the glucosamine unit. In comparison to the heat arising from changes in buffer ionization and chitosan ionization, heat effects associated with changes in polymer conformation, counterion release, hydrogen bonding, solvation, and hydrophobic effects only contribute in a relatively minor fashion to the enthalpy of binding.

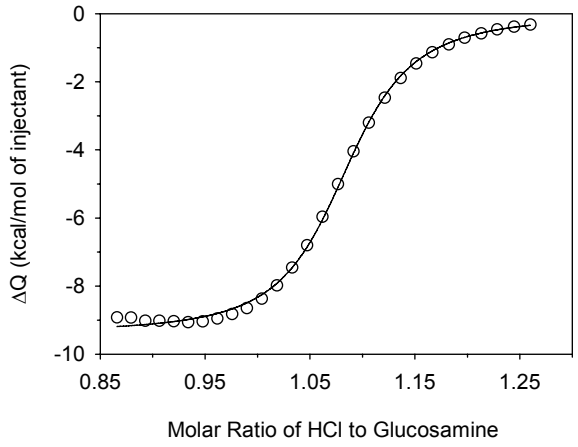

Figure 4.4. Integrated heats of binding from calorimetric titrations of 5 mM HCl into 5.97 μM of chitosan (80% DDA, 94 kDa) at an initial ratio of HCl/glucosamine of 0.85. The NaCl concentration was 25 mM. The solid line represents the best-fit generated from the SSIS model which gave a binding enthalpy of -9.39 ± 0.01 kcal/mol of bound protons, 483 ± 3 HCl binding sites per chitosan (corresponding to a molar ratio of HCl/glucosamine at saturation of 1.09 ± 0.01), and a binding constant of $(3.78 \pm 0.11)\text{x}10^5$ M^{-1}.

4.5.5 pH-Dependence of the Binding Constant

We found a reduced binding affinity at the higher pH of 7.4 versus 6.5 and 5.5 (Table 4.3), consistent with a lower level of ionization of chitosan at the higher pH and therefore reduced electrostatic attraction toward DNA. More specifically when the pH is increased from 5.5 to 6.5, α, the initial ionization state of chitosan is reduced by a factor of 1.8 and the averaged binding constant K_{obs} decreases only slightly by a factor of about 1.9. However, further increasing of the pH from 6.5 to 7.4 reduces α by a factor of 2.7 and is associated with a 3.3 fold reduction in K_{obs} (Table 4.3). In contrast to ΔH_{obs}, K_{obs} does not appear to depend on the choice of buffer, since it is similar for different buffer systems at pH 6.5 and 7.4. Similar results were

reported for the interaction between DNA and poly(bis-acryloylpiperazine-2-methyl-piperazine (Ehtezazi et al., 2003). It is important to note that, due to the tight binding between DNA and chitosan, it is necessary to work at low concentrations of DNA and chitosan to avoid a step function character of the binding isotherms that would be difficult to fit accurately to the SSIS model. This requires the high sensitivity of the ITC system since lower heat rates are generated, relative to the heat of dilution, and noise can result in reaching the detection limit of the ITC. Some experiments therefore resulted in a lack of precision in determining the binding constant K_{obs}. For example, the binding in piperazine buffer at pH 5.5 resulted in low signal since its enthalpy of ionization (7.44 kcal/mol of protons) almost canceled out that of chitosan (-9.37 kcal/mol of protons), generating low levels of detected heat from proton transfer.

4.5.6 The Entropy of Binding

The entropy change in Table 4.3 was directly calculated from $\Delta S_{obs} = (\Delta H_{obs} - \Delta G_{obs})/T$, where $\Delta G_{obs} = -RT\ln K_{obs}$. As a result, ΔS_{obs} is buffer dependent since it contains the contribution from the ionization changes of the buffer. The interpretation of these values has, therefore, limited significance. In addition to the protonation changes of the buffer and chitosan, ΔS_{obs} also reflects the net contributions of other events, including counterion release, release of water molecules, changes in water structure, and changes in ion distribution, as a consequence of the complexation process primarily driven by electrostatic interactions. Our results cannot provide quantitative information about their relative contribution to the entropy of binding. It is worth mentioning here that K_{obs} was calculated using concentrations with the assumption that the solution containing plasmid DNA, chitosan and complexes is ideal. Therefore, ΔS_{obs} calculated in this manner is an approximation and does not take into account activity coefficients of the

complexes and the polyelectrolytes. The behaviour of polyelectrolytes can be far from ideal, as reported previously (Ise et Okubo, 1966, 1968).

Table 4.4. Parameters of Interaction of Chitosan with Plasmid DNA as a Function of Chitosan DDA and Molecular Weight (M_n) in 25 mM MES Buffer at pH 6.5 (Without NaCl) Using the SSIS Model.

DDA	α^a	β^b	n^c	$n_{N/P}{}^d$	$n_{N+/P-}{}^e$	ΔH_{obs} (kcal/mol)	K_{obs} (x 10^9 M^{-1})
A. M_n = 7 kDa							
80%	0.39	0.76	286 ± 20	0.79 ± 0.06	0.60	-135 ± 3	1.4 ± 0.6
B. M_n ≈ 80 kDa							
72%	0.41	0.78	25.4 ± 1.0	0.71 ± 0.03	0.56	-1334 ± 1	5.8 ± 0.1
80%	0.39	0.76	21.8 ± 0.4	0.76 ± 0.01	0.58	-1638 ± 4	5.5 ± 0.4
93%	0.35	0.72	20.1 ± 0.4	0.72 ± 0.01	0.52	-1768 ± 18	11.2 ± 0.7
98%	0.35	0.72	19.4 ± 0.1	0.73 ± 0.00	0.53	-1816 ± 15	14.4 ± 0.4
C. M_n = 153 kDa							
80%	0.39	0.76	12.1 ± 0.0	0.69 ± 0.00	0.52	-2559 ± 8	11.6 ± 0.6

[a, c, d, e] Refer to the footnotes of Table 4.3. [b] The degree of ionization of chitosan in the complex after accounting for proton transfer from buffer to chitosan. Using a chitosan with DDA of 80% carrying approximately 443 glucosamine units per chain, proton transfer resulted in the protonation of 37% of the total glucosamine units at pH 6.5 (Figure 4.3 and Equation 4.11). Assuming that this percentage of proton transfer does not vary significantly with DDA and M_n at pH 6.5, β was calculated by adding 0.37 to α. The parameters n, ΔH_{obs} and K_{obs} were determined from the SSIS model fit using the molar concentration of chitosan and DNA as the binding entities and not their glucosamine and phosphate groups. Means are shown with error representing minimum and maximum of duplicates.

4.5.7 Influence of Chitosan Molecular Weight on Binding to DNA

The influence of chitosan molecular weight, or chain length, on chitosan-DNA binding at pH 6.5 was analyzed by comparing three chitosans with M_n of about 7, 80, and 153 kDa, all with a similar DDA of 80% (Table 4.4, Figure 4.5). The number of chitosan chains bound to DNA at saturation of the binding sites was inversely proportional to the chitosan molecular weight.

Indeed this result is simply a consequence of the above mentioned conserved quantity of the ratio of the number of ionized glucosamine to phosphate groups in the complex, $n_{N+/P-}$, which was always in the range 0.50-0.75. The number of chitosan chains bound to plasmid DNA appears to be primarily driven by this requirement along with a slight modification by the pH at the time of complexation. The binding constant increases significantly from 1.4×10^9 to 11.6×10^9 M^{-1} as the chitosan molecular weight increases from 7 to 153 kDa due to the increasing number of ionic linkages per chain (Figure 4.5A). Increasing chitosan molecular weight also resulted in increased exothermic values of ΔH_{obs}, from -135 kcal/mol of bound chitosan at 7 kDa to -2559 kcal/mol of bound chitosan at 153 kDa that was entirely accounted for by the increasing number of protons transferred from the buffer to chitosan due to a greater number of glucosamines per chitosan at higher molecular weight (Figure 4.5B). To our knowledge, magnitudes of ΔH_{obs} higher than 200 kcal/mol of bound chains have not been previously reported for other DNA-polycation systems where absolute values of ΔH_{obs} typically ranged from 30 to 200 kcal/mol (Ehtezazi et al., 2003; Rungsardthong et al., 2003; Tan et al., 2006). However, these previous studies investigated relatively short polycations carrying less than 50 protonable monomeric units per chain. Similarly, the magnitude of the binding constants found in our study ($K_{obs} \approx 10^9$-10^{10} M^{-1}) is higher than previous experimentally measured values of $K_{obs} \approx 10^5$-10^7 M^{-1} for the interaction of DNA with shorter polycations (Ehtezazi et al., 2003; Rungsardthong et al., 2003; Tan et al., 2006; Prevette et al., 2007), but similar to values obtained with dendritic star polycations (Yin et al., 2008) and to calculated binding constants between DNA and poly-L-histidine (Zelikin et al., 2003).

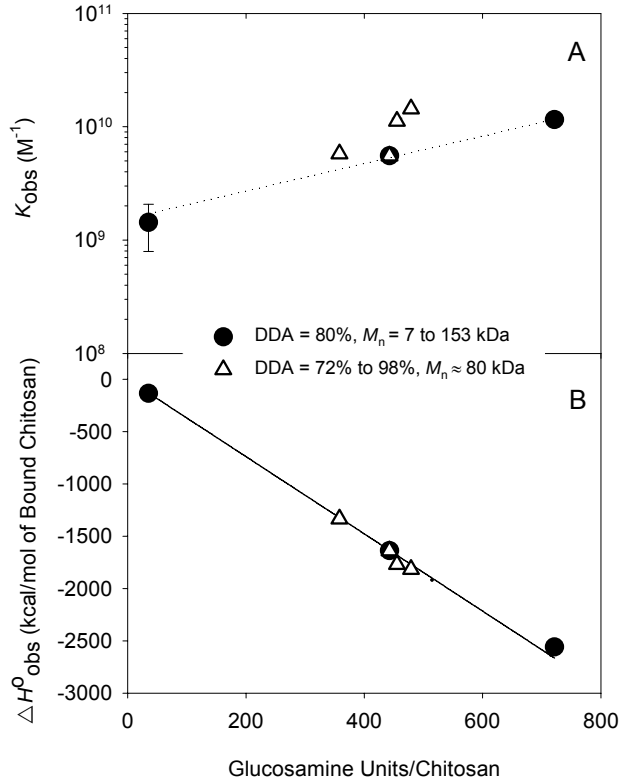

Figure 4.5. The binding constant of chitosan to DNA, K_{obs} (A), and the enthalpy of interaction per mole of bound chitosan, ΔH_{obs} (B), for chitosans with different molecular weight and DDA as a function of the number of glucosamine units per chain of chitosan (in 25 mM MES buffer at pH 6.5, found by fitting ITC isotherms to the SSIS model). (●) Chitosans of different M_n varying from 7 kDa to 153 kDa for DDA= 80%, and (△) chitosans of different DDA ranging from 72% to 98% for $M_n \approx$ 80 kDa. Linear regression in B results in ΔH_{obs}= -3.69 ± 0.04 kcal/mol of glucosamine (r^2 = 0.995).

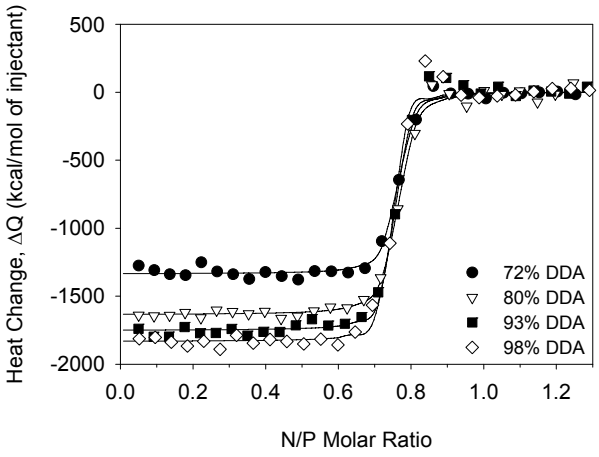

Figure 4.6. Integrated heats of interaction of DNA with chitosans of different DDA for $M_n \approx 80$ kDa (in 25 mM MES buffer at pH 6.5). Solid lines represent best-fits generated from the SSIS model.

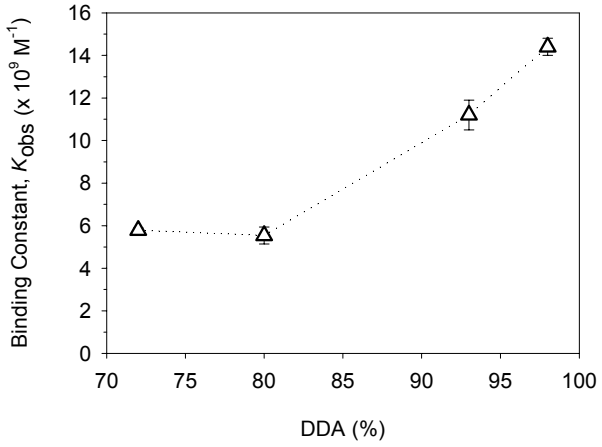

Figure 4.7. The influence of DDA on the binding constant, K_{obs}, between DNA and chitosans of different DDA for $M_n \approx 80$ kDa (in 25 MES buffer at pH 6.5, found by fitting ITC isotherms to the SSIS model).

4.5.8 Influence of Chitosan DDA on Binding to DNA

The binding isotherms between DNA and chitosans with similar molecular weights ($M_n \approx$ 80 kDa) but different DDA are shown in Figure 4.6. Increasing the DDA of chitosans increases the charge density along the molecular chain of chitosan. As a result fewer chitosan chains were bound to DNA at saturation of the binding sites, as reflected by a decrease in the value of *n* from 25.4 at 72% DDA to 19.4 at 98% DDA (Table 4.4). This is once again simply a consequence of the fact that the charge ratio in the complex, $n_{N+/P-}$, is preserved at about 0.50-0.75, such that more chains at lower DDA are required to provide the same number of ionized glucosamine residues. The enthalpy of binding, ΔH_{obs}, gained in amplitude with increasing DDA from -1334 kcal/mol at 72% DDA to -1816 kcal/mol at 98% DDA due to the greater number of ionizable glucosamines at higher DDA requiring proportionally more proton transfer as described above (Figure 4.5B). The binding constant did not change significantly when increasing DDA from 72% to 80%. However, further increasing DDA resulted in a greater binding affinity since K_{obs} increased from 5.5 x 10^9 M^{-1} at 80% DDA to 11.2 x 10^9 M^{-1} at 93% DDA and to 14.4 x 10^9 M^{-1} at 98% DDA (Figure 4.7). Increasing the content of acetyl groups by lowering DDA was found previously to inhibit precipitation of chitosan solutions probably through steric hindrance from bulky acetyl groups (Filion et al., 2007). Herein, a possible indication of reduced precipitation of DNA/chitosan complexes at lower DDA can be observed in the isotherms of Figure 4.6 where the positive overshoots occurring close to saturation, probably due to precipitation, are reduced with the lowest DDA of 72%. These observations along with the greater binding affinity found with increasing DDA are therefore consistent with both reduced steric hindrance and increased linear charge density along the chitosan chain. We also analyzed ITC isotherms with the noncooperative version of the McGhee and von Hippel (McGhee et von Hippel, 1974; Velázquez-Campoy, 2006) model that accounts for the statistical configurations of a large ligand

(chitosan) binding to multiple sites (consecutive free phosphate groups) on a lattice. Most isotherms were fit well by this model and gave similar binding parameters as the SSIS model. However, the McGhee and von Hippel model was highly sensitive to the positive overshoots of some ITC isotherms resulting in large fluctuations of the binding constant which are not reported here.

The above results concerning the influence of chitosan molecular weight and DDA on binding affinity to DNA are compatible with previous studies where these two parameters were found to be determining factors for the structure and stability of DNA/chitosan complexes (Strand et al., 2005; Maurstad et al., 2007). Short chitosans bind more strongly to DNA at high charge density, whereas low DDA chitosans bind more strongly with longer chain length (Maurstad et al., 2007). In another study, a minimum of 6 to 9 glucosamine units on fully deacetylated chitosan oligomers was required to provide chitosan-DNA apparent binding strength comparable to that of a fully deacetylated chitosans of 900 glucosamine units at pH 5.0-6.5 as judged by the ethidium bromide displacement assay (Strand et al., 2005). Moreover, the latter study did not find any increased apparent binding affinity with increasing chain length of fully deacetylated chitosans from 9 to 900 glucosamine units. In contrast, we found an 8-fold increase of the binding constant for chitosans with M_n ranging from 7 to 153 kDa at a constant DDA of 80%, corresponding to 35 to 721 glucosamine units (Table 4.4, Figure 4.5A), suggesting that the binding affinities between DNA and chitosan evaluated by the ethidium displacement assay are qualitative. Our results also provide evidence for a previously characterized coupling between the DDA and molecular weight of chitosan in determining complex stability which in turn has great influence on transfection efficiency of DNA/chitosan complexes (Lavertu et al., 2006). For example, we found in the current study that similar binding affinities were obtained with the high M_n chitosan of intermediate DDA (153 kDa, 80% DDA) and the intermediate M_n chitosan of high

DDA (80 kDa, 93% DDA) that are consistent with the dependence of transfection efficiency on M_n and DDA reported in the previous study (Lavertu et al., 2006). It is interesting to note that only a 1.2-fold increase of the DDA from 80% to 93% at constant M_n of ~80 kDa, corresponding to a small increase of glucosamine units from 443 to 455 (3% increase) resulted in the doubling of the binding constant (Table 4.4, Figure 4.5A). To achieve a similar increase in binding strength by changing molecular weight without changing DDA (80%), a 1.6-fold increase of molecular weight was required, corresponding to a substantial increase of glucosamine units from 443 to 721 (63% increase). Thus, chitosan DDA or charge density was demonstrated here to play a more important role in binding affinity compared to chain length or total charge.

4.5.9 Biological Significance

The process of gene delivery involves DNA compaction, DNA protection, cell targeting, cellular uptake, and intracellular trafficking to the nucleus to produce the desired therapeutic effect. Intracellular DNA unpackaging from its vector after nuclear localization has been demonstrated to be a limiting factor for efficient gene expression in nonviral systems (Schaffer et al., 2000). This ability of DNA/polycation complexes to dissociate inside the nucleus is dependent upon the complex stability, and hence on the polycation-DNA binding strength. If the DNA/polycation complexes are not sufficiently stable, they will be dissolved in the medium by competing polyanions or enzymatically degraded prior to reaching the target cell. On the other hand, highly stable complexes will be readily endocytosed but may not disassemble intracellularly to permit DNA trafficking to the nucleus and transgene expression. To achieve a balance between complex stability and the ability to dissociate inside the cell, it is critical to know how tightly the polycation is bound to DNA. Gel retardation and ethidium bromide

displacement assays are fast and descriptive methods but do not provide quantitative binding affinity. As demonstrated here by ITC, the chain length and DDA or charge density of chitosan can be modulated to achieve different binding affinities which can also be adjusted by chemical modification of the structure such as pegylation (Mao, S. et al., 2005), quaternization (Mao, S. et al., 2005) and phosphorylcholine substitution (Tiera et al., 2006). These strategies were used to optimize transfection efficiencies by improving the solubility of chitosan and other polycations, and decreasing aggregation. However, substantial modification of the polycation structure can impede proton transfer from the buffer upon binding with DNA or influence significantly the binding affinity to compromise the balance between complex stability and DNA unpackaging. Interactions other than electrostatics could also be identified by ITC if their contributions to the heat of interaction are significant after subtracting the heat associated with the ionization changes of the buffer and of the polycation. In addition, in the emerging field of gene silencing, formulations developed for plasmid DNA need to be adjusted for the delivery of siRNA in part to account for different binding properties. Quantitative information on the binding of siRNA with its carrier and deciphering the mechanism of interaction would be beneficial toward understanding the structure-property-activity relationships of the delivery systems.

4.6 Conclusion

We have used isothermal titration microcalorimetry to characterize the heat changes associated with the formation of plasmid DNA/chitosan complexes in dilute aqueous solutions. The observed enthalpy of chitosan-DNA interaction is buffer dependent, due to proton transfer from the buffer to chitosan during binding. We found that the heat associated with the protonation changes of the buffer and chitosan mainly accounts for the observed enthalpy of

binding. The proton transfer mechanism allows DNA/chitosan complexes to be formed at a pH above the pK_a of chitosan where chitosan is only slightly ionized in the unbound state, for example, in the pH range of 7.0-7.4. By performing ITC using a library of chitosans of different chain lengths and DDA, electrostatic effects were found to dictate the binding of chitosan to DNA resulting in a conserved ratio of ionized glucosamine to phosphate groups in the complex of 0.50-0.75. The binding constant between chitosan and plasmid DNA was significantly influenced by molecular weight and by DDA. These findings reveal important relationships between chitosan-DNA binding affinity and complex stability and in turn, the efficiency of chitosan-DNA complexes for gene transfection, providing important guidelines in the design of effective gene delivery systems.

4.7 Acknowledgments

This work was supported by the Canadian Institutes of Health Research (CIHR) and by the Natural Sciences and Engineering Research Council of Canada (NSERC). Pei Lian Ma received a doctoral fellowship from the Fonds québécois de la recherche sur la nature et les technologies. Marc Lavertu received a doctoral fellowship from the CIHR. We would like to thank Isabelle Richard for fitting the isotherms using the McGhee and von Hippel model.

CHAPITRE 5 ONE-STEP ANALYSIS OF DNA/CHITOSAN COMPLEXES BY FIELD-FLOW FRACTIONATION REVEALS PARTICLE SIZE AND FREE CHITOSAN CONTENT

Pei Lian Ma, Marc Lavertu, Françoise M. Winnik, and Michael D. Buschmann

Department of Chemical and Biomedical Engineering, Ecole Polytechnique de Montréal, PO 6079 Succ. Centre-Ville, Montreal, Quebec, H3C 3A7, Canada, and Department of Chemistry and Faculty of Pharmacy, Université de Montréal, PO 6128 Succ. Centre-Ville, Montreal, Quebec, H3C 3J7, Canada.

5.1 Abstract

The composition of samples obtained upon complexation of DNA with chitosan was analyzed by asymmetrical flow field flow fractionation (AF4) with on-line UV-visible, multi-angle light scattering (MALS), and dynamic light scattering (DLS) detectors. A chitosan labelled with rhodamine B to facilitate UV-Vis detection of the polycation was complexed with DNA under conditions commonly used for transfection (chitosan glucosamine to DNA phosphate molar ratio of 5). AF4 analysis revealed that 73% of the chitosan-rhodamine remained free in the dispersion and that the DNA/chitosan complexes had a broad size distribution ranging from 20 to 160 nm in hydrodynamic radius. The accuracy of the data was assessed by comparison with data from batch-mode DLS and scanning electron microscopy. The AF4 combined with DLS allowed the characterization of small particles that were not detected by conventional batch-mode DLS. The AF4 analysis will prove to be an important tool in the field of gene therapy since it readily provides, in a single measurement, three important physicochemical parameters of the

complexes: the amount of unbound polycation, the hydrodynamic size of the complexes, and their size distribution.

5.2 Keywords

Chitosan, DNA, asymmetrical flow field-flow fractionation, free polycation content.

5.3 Introduction

A variety of non-viral gene delivery vectors are being investigated intensively in chemical laboratories and in clinical settings (Mintzer et Simanek, 2009). The high level of interest in these systems is motivated by the greater safety of synthetic DNA vectors compared to viral vectors, and by the ease of their preparation. Indeed, condensation of DNA into positively-charged nanoparticles spontaneously occurs upon mixing DNA and a polycation as a result of electrostatic attraction. The resulting dispersion may be used directly in transfection experiments or subjected to physicochemical analysis. The size distribution of DNA/polycation complexes is accessible via conventional techniques, including dynamic light scattering (DLS), microscopy, and analytical ultracentrifugation (AUC). DLS measures the time-dependent fluctuations of the light scattered by the particles to derive their hydrodynamic sizes. For samples having a broad polydispersity in size, DLS may not be able to detect small changes in the size distributions. The presence of large particles and small amounts of aggregates can mask the light scattered by the smaller particles, limiting their detection. Microscopic techniques such as AFM, SEM, and TEM have been very useful in visualizing the particles and characterizing their size and morphology but they often require sample drying and the use of contrast staining agents that can influence the

properties of the particles. The hydrodynamic size and size distribution can be obtained with AUC but this technique requires the knowledge of the specific volume of the hydrated particles (Bootz et al., 2004). Asymmetrical flow field-flow fractionation (AF4), an analytical separation technique in which the retention of macromolecules and particles is governed by their diffusivities, is rarely used for the size determination of gene delivery systems, despite its wide applicability in colloidal science. Comparatively few studies have been published to date on the AF4 analysis of gene and drug delivery systems, including polyelectrolytes complexes (Yohannes et al., 2005; Le Cerf et al., 2007), DNA/cationic lipid complexes (Lee, H. et al., 2001), virus-like particles (Citkowicz et al., 2008), and other types of nanoparticle drug carrier systems (Fraunhofer et al., 2004; Jahn et al., 2007; Zillies et al., 2007; Augsten et al., 2008; Kang et al., 2008). This technique was used alone or combined with other detectors to obtain the particle size, the size distribution, and the molar mass distribution of monodisperse and polydisperse samples.

It is generally accepted that optimal transfection is achieved when the DNA condensation is performed in the presence of a large excess of amine groups (N/P $\geq$ 5, the molar ratio of polycation protonable amine groups to DNA phosphate groups) (Boeckle et al., 2004; Lavertu et al., 2006; Strand et al., 2008). Under these conditions, it can be expected that a significant amount of unbound polycation coexists in the dispersion with the DNA/polycation complexes. Recent experimental data from fluorescence correlation spectroscopy (FCS) (Clamme et al., 2003) and size exclusion chromatography (SEC) (Boeckle et al., 2004) confirmed that in DNA/poly(ethyleneimine) (PEI) complexes prepared at N/P ratios above 6, the majority of the PEI molecules are not bound to DNA. The free PEI was nonetheless seen to be important since it was found to increase substantially the level of gene expression and was suggested to contribute to the proton sponge effect leading to greater endosomal release of the complexes (Boeckle et al.,

2004). In another study, a large excess of free chitosan was detected, but not quantified, by FCS in preparations of DNA/chitosan complexes (Reitan et al., 2009). These findings highlight the importance for the quantification of the amount of uncomplexed free polycation which still remains an analytical challenge. The FCS technique can provide quantitative data on the free polycation content, but it relies on the use of mathematical models to fit the autocorrelation data of the dispersion assuming the presence of two different species (free and bound polycation) (Clamme et al., 2003). The separation method with SEC for these polydisperse samples is fraught with technical difficulties, such as loss of material, column blockages, and shearing of large particles. Moreover, it is necessary to perform a colorimetric assay on isolated fractions in order to determine the concentration of free polycation in each fraction.

We report here a new approach to characterize DNA/polycation complexes using asymmetrical flow field-flow fractionation (AF4) coupled online with UV/Vis spectroscopy, multi-angle light scattering, and dynamic light scattering. In addition to the determination of size and size distribution, this multimodal AF4 system was optimized for the direct quantification of the free polycation content. Chitosan was selected as the polycation since it is a prominent natural polymer used in gene delivery, due to its biocompatibility and biodegradability. The relationship between transfection efficiency and physicochemical factors including the molecular weight, the degree of deacetylation, the N/P ratio, and the solution pH have been extensively studied (MacLaughlin et al., 1998; Ishii et al., 2001; Koping-Hoggard et al., 2001; Lavertu et al., 2006; Ma, P.L. et al., 2009). These parameters were found to influence the physicochemical and biological properties of DNA/chitosan complexes. The resulting surface charge, particle size and colloidal stability of DNA/polycation complexes are interrelated properties which, in turn, have a strong impact on transfection efficiency. A complete characterization of the physicochemical properties of DNA complexes with polycations, such as chitosan, is therefore essential to define

the structure-activity relationship for the optimization of gene delivery systems. The aim of this study was to demonstrate the feasibility of this combined AF4 system to separate free chitosan from DNA/chitosan complexes and to determine directly the particle size, the size distribution, and the free chitosan content in a single run. We describe briefly the principle of the AF4 method in the experimental section. The design of the separation protocol is then presented followed by the description of the outcome of the analysis in terms of size and size distribution of the complexes, and of the content of unbound polycation. Results of the AF4 analysis are then directly compared with data gathered by DLS and ESEM analysis of the same samples.

5.4 Materials and Methods

5.4.1 Materials

The 6.4 kb plasmid EGFPLuc (Clontech Laboratories) was amplified in DH5α bacteria and purified using the Qiagen Plasmid Mega Kit. A stock solution of EGFPLuc (0.33 mg/mL) was prepared in deionized water and stored at –20 ^{o}C before use. Ultrapure chitosan (150,000 g/mol, degree of deacetylation (DDA): 80%) was provided by Biosyntech Inc. It was degraded according to Lavertu et al.(2006) using nitrous acid to achieve a number-average molecular weight (M_n) of 42,000 g/mol and a polydispersity index of 1.35 (determined by GPC (Nguyen, S. et al., 2009)). Rhodamine B-labelled chitosan (Ch-rho, M_n= 42,000 g/mol, DDA= 80%, 1.2% mole of rhodamine/mole of glucosamine) was prepared following a previously reported procedure (Ma, O. et al., 2008) (see supporting information (SI) for details).

5.4.2 Preparation of DNA/Chitosan Complexes

Unlabelled and labelled chitosan stock solutions of 5 mg/mL were prepared by dissolving the samples overnight in deionized water containing hydrochloric acid (from 1M aqueous HCl solution), such as to reach an HCl/glucosamine ratio of 1. DNA and chitosan stock solutions were diluted with deionized water to concentrations of 82.5 μg/mL and 283 μg/mL, respectively. The DNA/chitosan complexes were prepared by adding 100 μL of the diluted chitosan solution to an equal volume of the diluted DNA solution to reach a glucosamine to phosphate groups (N/P) ratio of 5 in the final dispersion. The mixing was done quickly by up and down pipetting of the solutions. Samples were allowed to incubate at room temperature 30 min before analysis.

5.4.3 AF4/UV/MALS/DLS System

5.4.3.1 Instrumentation

An asymmetrical flow field-flow fractionation (AF4) system (AF 2000 MT, Postnova Analytics) with a channel thickness of 350 μm fitted with a regenerated cellulose membrane (10 kDa cut-off, Z-MEM-AQU-631, RC amphiphilic, Postnova Analytics) suitable for analysis of amphiphilic or cationic polymers was used. The AF4 was connected on-line to an UV/Vis detector (SPD-20A, Postnova Analytics), a multi-angle light scattering (MALS, Dawn 8+, Wyatt Technology), and a dynamic light scattering (DLS) detector (WyattQELS, Wyatt Technology) connected to the 108^{o} angle of the MALS Dawn 8+ detector. The MALS was equipped with a K5 cell and a GaAs laser operating at 658 nm. The samples were measured at 1 s intervals for the MALS and 3 s intervals for the DLS. The UV, MALS and DLS signals were simultaneously recorded as fractograms, plots of detector signal versus time. Data collection and analysis were done using ASTRA version 5.3.4.14 (Wyatt Technology). The online DLS detector equipped

with an avanlanche photodiode measures the auto-correlation function for every slice of 3 seconds eluting from the AF4. Each fractionated slice of 3 sec contains a narrow distribution of sizes, so that the auto-correlated function for a dilute and monodisperse population can be analyzed leading to the diffusion coefficient of the corresponding slice (Chu, 1991). The hydrodynamic radius (R_H) of the assumed sphere is then calculated according to the Stokes-Einstein equation. Each curve shown is representative of triplicate samples.

5.4.3.2 Separation Principle

The theory of asymmetrical flow field-flow fractionation (AF4) has been discussed in detail elsewhere (Wahlund et Giddings, 1987; Schimpf et al., 2000). The fractionation of a sample containing different species occurs in a thin and open trapezoidal channel as illustrated in Figure 5.1. After focusing and relaxation of the sample species, the flow along the channel drives the sample to the outlet. This channel flow is laminar with a parabolic flow profile having layers of different velocities. The highest flow rate is in the center of the channel and the lowest flow rate along the wall. An external field generated by the cross flow and applied perpendicularly to the channel flow drives the sample toward the accumulation wall. However, diffusion opposes this field, causing migration of the sample species away from the wall. The cross flow leaves the channel through an ultrafiltration membrane covering the accumulation wall. The molecular cut-off of the membrane is chosen such that the analysed species cannot penetrate the membrane. Since small particles have higher diffusion coefficients, they achieve equilibrium positions which on the average lie within the channel flow layers of higher velocity, while larger particles reach equilibrium in flow layers of lower velocity. Consequently, in the

normal mode of separation, small species are transported faster and are eluted prior to larger species, the latter being closer to the membrane.

5.4.3.3 Separation Conditions

A prefiltered 50 mM acetic acid/sodium acetate buffer at pH 4.0 was used as the eluent. The total ionic strength was adjusted to 20 mM by addition of NaCl. After flow equilibration, the sample (21 µL) was injected with a flow rate of 0.2 ml/min, followed by a 9 min-focusing with a cross flow rate and a detector flow rate of 1 mL/min each. Following a 1 min-transition, a four-step cross flow rate gradient was initiated for the elution mode. The starting flow rate (1 ml/min) was decreased exponentially first with an exponent factor of 0.4 to 0.4 ml/min within 10 min, then with an exponent factor of 0.8 from 0.4 to 0.15 ml/min within 20 min, and finally it was decreased linearly from 0.15 to 0.05 mL/min within 15 min. The cross flow rate was then kept constant at 0.05 mL/min for 15 min. The detector flow rate was kept at 1 ml/min throughout. All the flow rates were controlled by the AF2000 Control software (Postnova Analytics). The cross flow was generated by Kloehn syringe pumps (Postnova Analytics) while the axial and focusing flows were delivered by isocratic pumps (PN1130, Postnova Analytics).

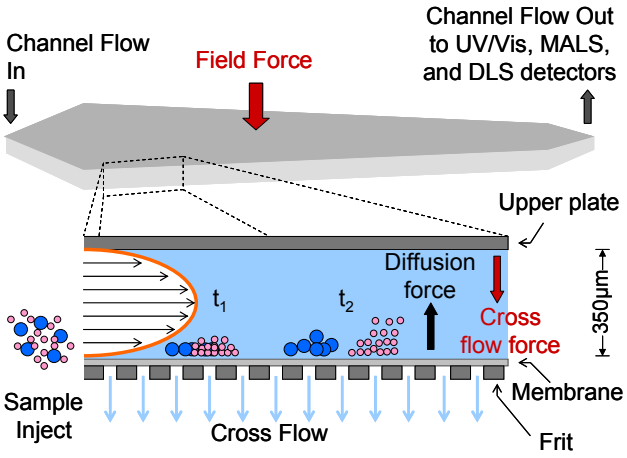

Figure 5.1. Schematic representation of the separation process at different elution times ($t_2 > t_1$) in an AF4 channel.

5.4.4 Mass Recovery and Quantification of Free Chitosan

The mass recovery of pure Ch-rho solutions was determined from the AF4 fractograms monitored by UV/Vis detection at 556 nm. The eluted mass was calculated from the integrated peak area and the extinction coefficient of Ch-rho determined prior to conducting the AF4 experiments. The extinction coefficient of Ch-rho was 3.477 mL/(mg.cm) at 556 nm, calculated based on a calibration curve. The mass recovery was determined by comparing the calculated mass of Ch-rho with the injected mass. The mass recovery of Ch-rho was constant for at least 60 injections. For the quantification of unbound free Ch-rho in a DNA/Ch-rho dispersion, the integrated areas under the curve of the corresponding peak before and after complexation were compared. The results reported are the average (± standard deviation) of three independent measurements.

5.4.5 Scanning Electron Microscopy

An Environmental Scanning Electron Microscope (Quanta 200 ESEM FEG, FEI) was used to image fractions of DNA/chitosan complexes collected from AF4 separations. The fractions were collected from the outlet flow of the detectors for various elution times. A drop (10 μL) of a fraction was deposited on freshly cleaved mica, left to dry for 30 minutes, and then sputter-coated with gold (Agar Manual Sputter Coater, Marivac Inc.). Observations were performed at 20 kV in the high vacuum mode of the ESEM microscope. The average particle size (± standard deviation) was determined by measuring the diameter of more than 150 particles from at least 6 different fields for each fraction using the microscope XT Docu software.

5.4.6 Batch Mode Dynamic Light Scattering

Size measurements of the DNA/chitosan complexes before fractionation were carried out using an ALV/CGS-3 Compact Goniometer System equipped with a 22 mW HeNe laser operating at a wavelength of 632.8 nm. The complexes were diluted 4 times in the running buffer prior to analysis. The correlation functions were measured at 25°C over an angular range between $\theta = 40^{o}$ and 150^{o}. For each scattering angle, a second-order cumulant fit was then applied to the data to obtain the first cumulant (Γ),which is related to the diffusion coefficient (D) by $\Gamma = D\,q^2$ where $q = (4\pi n/\lambda_0)\sin(\theta/2)$ with n, λ_0, and θ being the solvent refractive index, the wavelength of the incident light in vacuum, and the scattering angle, respectively. The diffusion coefficient of the particles was determined by extrapolation to zero scattering angle from a plot of Γ/q^2 versus q^2. The z-average hydrodynamic radius was calculated from the diffusion coefficient and the Stokes-Einstein equation. The data were also analyzed using the CONTIN regularized fit to determine the particle size distribution.

5.5 Results and Discussion

5.5.1 Optimization of the Analytical Conditions

To obtain reliable and reproducible separations, it is critical to ensure that the eluting species do not interact with the membrane or permanently adhere to it. We found that a special regenerated cellulose membrane designed for the separation of amphiphilic or cationic polymers was well-suited for the analysis of positively charged DNA/chitosan complexes in an acetic acid/acetate running buffer of pH 4 and low ionic strength. The running buffer does not alter the physical properties of the DNA/chitosan complexes initially prepared in a solution pH of 4.8. At pH 4, the residual unbound chitosan is fully ionized and can be detected and quantified, since it does not adhere onto the membrane. The experimentally determined Ch-rho mass recovery (87% ± 2%) upon injection of a Ch-rho solution confirmed that the loss of chitosan and cationic DNA/chitosan nanoparticles by adsorption was indeed negligible. The detection of unbound negatively-charged DNA is not possible under these conditions, due to irreversible adsorption of DNA on the membrane observed in control studies involving injections of DNA solutions. A complete lack of UV and LS signals was observed during the AF4 separation as well as during the flushing at zero cross flow. Since an excess of chitosan was used to prepare the complexes (N/P ratio of 5), all the DNA was bound to chitosan, as confirmed by ethidium bromide gel electrophoresis experiments (Strand et al., 2005). The mass recovery of DNA in the complexes was estimated to be about 95% from the integrated peak area of the complexes under the curve of the UV signal at 260 nm and using the extinction coefficient of DNA. We tested other membranes, such as the commonly used and regular regenerated cellulose membrane, but the results were erratic, presumably as a consequence of massive eluate adsorption.

The four-step field gradient was optimized for the separation of free chitosan from DNA/chitosan complexes. The first exponential decrease of the cross flow from 1.0 to 0.4 mL/min within 10 min was applied to allow the elution of free chitosan. The cross flow was then decreased slowly in the following steps to obtain a good resolution for the fractionation of the complexes without inducing particle-particle interactions in an extent that would affect the elution times and peak shape of the fractograms. The elution of the species was complete in less than 60 min after which the cross flow was reduced to zero and no signal was observed. The sample concentration and injected volume were chosen to obtain a high signal-to-noise ratio. The elution times and peak shape of the fractograms did not change when the sample concentration was decreased, confirming the appropriateness of the separation conditions and the absence of undesirable sample overloading effects.

5.5.2 Free Chitosan Content in a Dispersion of DNA/Ch-rho Nanoparticles of N/P=5

The AF4 separation of free chitosan from DNA/Ch-rho complexes was monitored via UV detection of the eluting fractions. Since the UV absorbance of chitosan occurs at wavelengths < 210 nm, a spectral region where DNA also absorbs light, it was necessary to use a chitosan labelled with a small fraction of a dye that absorbs light at wavelengths for which DNA is transparent. We selected a Ch-rho sample with a labelling level of 1.2% mole of rhodamine/mole of glucosamine and a maximum absorbance at 556 nm. Prior to the fractionation, we have verified that the size of the DNA/chitosan complexes is not affected by the labelling (see below). Elution profiles recorded at 556 nm and 260 nm for a solution of Ch-rho (dashed line) and for a dispersion of DNA/Ch-rho nanoparticles (full line) are presented in Figure 5.2. Ch-rho elutes

between 1 and 9 min (dashed lines in Figure 5.2A (556 nm) and Figure 5.2B (260 nm)). Profiles recorded for DNA/Ch-rho complexes (full line) present a band at longer elution times, between 8 and 32 min, attributed to the elution of the complexes, in addition to the band due to Ch-rho. Focussing on the profiles recorded at 556 nm (Figure 5.2A), we note that the intensity of the faster eluting band is significantly lower for the dispersion of DNA/Ch-rho complexes, compared to the Ch-rho solution. Moreover, there is a weak band eluting from about 10 to 25 min (Figure 5.2A), which can be attributed to the absorbance at 556 nm of Ch-rho entrapped in the complexes. Rhodamines in aqueous media are well-known to undergo spectroscopic changes due to aggregation, mainly by dimerization (Selwyn et Steinfeld, 1972; Ilich et al., 1996). This may be induced upon the compaction of DNA by Ch-rho since rhodamine moieties are brought closer together. Rhodamine aggregation is usually accompanied by a significant hypochromic effect of the absorbance centered around 556 nm (Selwyn et Steinfeld, 1972) and could account for the lack of signal of the nanoparticles at this wavelength. This observation is in agreement with the decrease of the absorption band of Ch-rho around 556 nm when comparing the absorption spectra of Ch-rho and DNA/Ch-rho prior to the separation (see the SI, Figure 5.SI-1). Further evidence for the formation of nanoparticles was obtained by monitoring the elution with a MALS detector (see below).

Comparison of the areas of the elution bands of Ch-rho before and after complexation (Figure 5.2A, 556 nm) revealed that 73% (± 2%) of Ch-rho is in the free form. The remainder of Ch-rho that is not free is bound to DNA. It follows that the N/P ratio in the complexes themselves is 1.4 (± 0.1), although the nominal N/P ratio is 5, based on the Ch-rho and DNA amounts used to prepare the complexes. This finding is in good agreement with previous reports on DNA/PEI complexes prepared at a N/P ratio of 6 for which fluorescence correlation spectroscopy analysis indicated that 86% of the PEI is free in solution (Clamme et al., 2003). A

lower value (58% of free PEI) was reported in the case of DNA/PEI complexes analysed by a colorimetric assay following purification of the complexes by SEC (Boeckle et al., 2004).

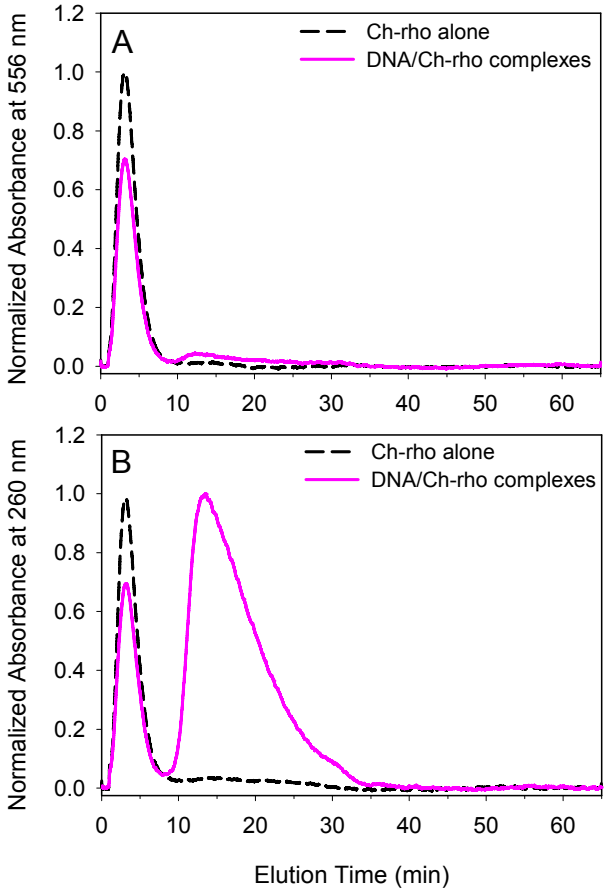

Figure 5.2. AF4 fractograms of chitosan-rhodamine and DNA/chitosan-rhodamine monitored by UV/Vis showing A) normalized absorbance at 556 nm, and B) normalized absorbance at 260 nm as a function of the elution time.

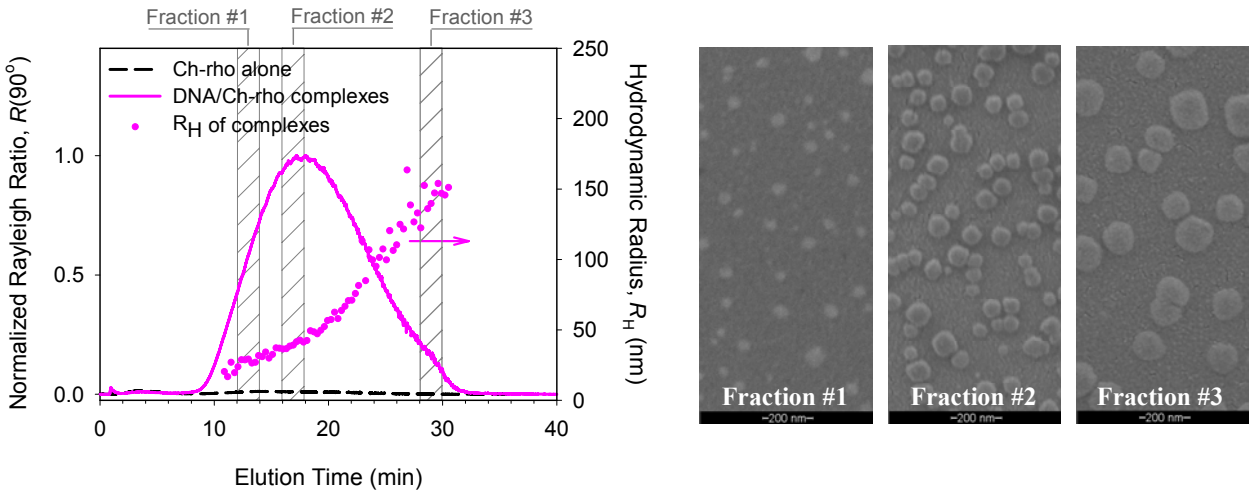

Figure 5.3. AF4 fractograms of chitosan-rhodamine and DNA/chitosan-rhodamine complexes with the lines and the dots representing the normalized Rayleigh ratio at 90° and the hydrodynamic radius (from online DLS) as functions of the elution time, respectively. The micrographs are ESEM images of the collected fractions of DNA/chitosan-rhodamine complexes eluted between: fraction #1) 12 – 14 min, fraction #2) 16 – 18 min, and fraction #3) 28 – 30 min.

5.5.3 Size and Size Distribution of DNA/Ch-rho Nanoparticles

The elution of the DNA/Ch-rho complexes was monitored on-line using for each injection, not only a UV/Vis detector, but also MALS and DLS detectors. Elution profiles of a Ch-rho solution and of a DNA/Ch-rho dispersion monitored by light scattering detectors are presented in Figure 5.3 which shows the normalized Rayleigh ratio at 90° (left-hand axis) and the hydrodynamic radius (R_H) of the nanoparticles (right-hand axis). The intense light scattering signal from 9 to 32 min is attributed to the complexes. The elution time of the complexes detected by MALS corresponds exactly to the elution time recorded by UV at 260 nm (Figure 5.2B). The chitosan molecules are too small to scatter light significantly at the concentration

used. Hence they were not detected by MALS and DLS under our experimental conditions. If the characterization of chitosan is desired, the use of concentrated chitosan solutions will enable such detection, as shown in previous reports combining AF4 with MALS to determine molar masses of chitosan and its derivatives (Mao, S. et al., 2007; Augsten et Maeder, 2008).

Generally, the hydrodynamic radius can be calculated from the elution time based on the theory of field flow fractionation (Schimpf et al., 2000). However, the retention time of the sample could be affected by interactions of charged particles with the membrane or between charged particles. Thus we chose to calculate absolute values of the hydrodynamic size of the nanoparticles directly from data gathered via the on-line DLS detector. For each eluted fraction, the auto-correlated function from DLS leads to the diffusion coefficient of the particles, from which the hydrodynamic radius was calculated. From the DLS fractograms (Figure 5.3), it can be seen that the DNA/Ch-rho nanoparticles are polydisperse in size with a hydrodynamic radius ranging from 20 to 160 nm. It should be noted that the profile of the hydrodynamic radius with the elution time is not linear because of the cross flow exponential decays used for the AF4 separation. As mentioned above, the separation conditions were appropriately optimized to avoid effects caused by particle interactions. The different elution times demonstrate the ability of AF4 to separate different species based on their hydrodynamic size. Smaller particles having higher diffusion coefficients are less retained by the cross flow in the channel and elute prior to the larger particles. The validity of the on-line DLS data was confirmed by ESEM imaging of several AF4 fractions collected after different elution times. Micrographs of three fractions are presented in Figure 5.3 showing nanoparticles having a spherical shape. The mean radii of the particles measured on ESEM images collected at the time intervals from 12 to 14 min, 16 to 18 min, and 28 to 30 min are, respectively, 27 ± 5, 41 ± 8, and 74 ± 12 nm. The radii of the first and second collected fractions are similar to the values obtained from the on-line DLS detection.

However, smaller particle sizes are obtained from image analysis of the fraction collected last. Such discrepancy is attributed, in part, to the fact that DLS measures the hydrodynamic size of the charged particles assumed to be hydrated spheres whereas dried particles are characterized by ESEM. Drying and imaging in high vacuum of the samples can also change the particle properties and cause shrinking of the particles, as reported in previous studies (Lee, S. et al., 1996; Bootz et al., 2004). Since the sample is polydisperse in size, the nanoparticles may have different properties and be subjected differently to drying and high vacuum conditions. Further analysis of collected fractions within the same sample by other means can provide information about the difference in their physical properties other than size (zeta potential, composition, density...). We did not succeed to measure the zeta potential of collected fractions because the particles recovered were too diluted.

The fact that the majority of the DNA/chitosan complexes have an elution time in the 11 to 20 min range and hydrodynamic radii of about 30 to 50 nm can also be inferred from the fractograms monitored by UV absorbance at 260 nm (Figure 5.2B) and on line DLS (Figure 5.3). Focussing on the elution of the nanoparticles, data from these fractograms were converted to a size distribution shown in Figure 5.4, presented by plots of the cumulative and differential weight fraction as a function of the particle hydrodynamic radius. The concentration of nanoparticles was assumed to be proportional to the absorbance at 260 nm. To ascertain the validity of this assumption, we verified that the shape of the curves does not change with the sample concentration (at constant N/P ratio of 5, injected DNA concentration from 21 to 41 μg/mL) and that the corresponding peak areas of the eluting nanoparticles follow the Beer-Lambert relation (see SI, Figure 5.SI-2a and b). Since the nanoparticles are highly diluted in the flowing eluent, turbidity at this wavelength should be negligible compared to the absorption of DNA. The predominant range of particle hydrodynamic radius was 30 to 55 nm with about 10% of the

particles having an R_H above 90 nm and about 10% with R_H less than 25 nm. The ability to provide size distribution and to fractionate particles according to size using AF4 with these combined detectors will be useful to correlate complex size with transfection efficiency.

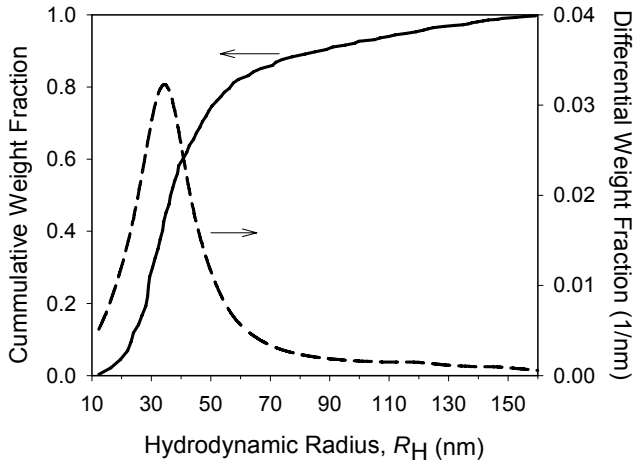

Figure 5.4. Cumulative and differential weight fraction from on-line DLS and absorbance (260 nm) measurements of AF4 fractionated DNA/Ch-rho nanoparticles.

It is common practice to assess the average size of DNA/polycation nanoparticles from DLS data (batch mode) of the dispersion obtained upon mixing polycations and DNA solutions. We carried out this measurement for a DNA/Ch-rho sample prior to AF4 analysis. Figure 5.5 shows the intensity distributions of hydrodynamic radii of this sample determined at three different angles. The angular dependence of the corresponding apparent diffusion coefficient is a consequence of the sample polydispersity. The z-averaged hydrodynamic radius was 130 nm, calculated from the Stokes-Einstein equation and the zero-angle extrapolated diffusion coefficient (see the SI, Figure 5.SI-3). The ranges of R_H values (about 40 to 300 nm) measured at several angles by batch DLS are larger than the range of R_H values extracted from the AF4 on-line DLS

detection and confirmed via ESEM imaging of fractions collected throughout the elution. Both the on-line and batch mode DLS measurements yield the overall range of hydrodynamic radii but the contribution of the large particles to the scattered light detected by the batch mode DLS is significant, yet larger particles were found to represent only a small fraction of the sample by the combined AF4 system. Since the nanoparticles are separated by AF4 on the basis of their size *prior to DLS measurement*, the data analysis does not suffer from interference from the scattering of trace amounts of larger particles or aggregates, contrary to the situation for DLS in batch mode, for which particle size distribution is always biased towards larger particles. Also presented in Figure 5.5, is the size distribution of DNA/Ch nanoparticles obtained upon mixing DNA and unlabelled chitosan. It is identical to the size distribution recorded for DNA/Ch-rho nanoparticles, confirming that the labelling of chitosan did not alter the size distribution of the complexes. Moreover, we also confirmed that the AF4 separation was not affected by the labelling of chitosan by recording fractograms of DNA/Ch complexes monitored by the absorbance at 260 nm, MALS, and DLS. These fractograms were almost identical to those recorded for DNA/Ch-rho (Figure 5.6).

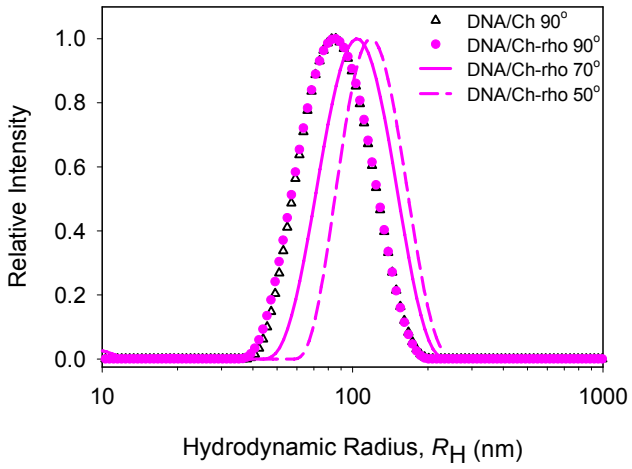

Figure 5.5. Intensity distributions of the hydrodynamic radius of unfractionated complexes of DNA with unlabelled chitosan (Ch) and chitosan-rhodamine (Ch-rho). The DLS measurements were carried out in batch mode at different scattering angles.

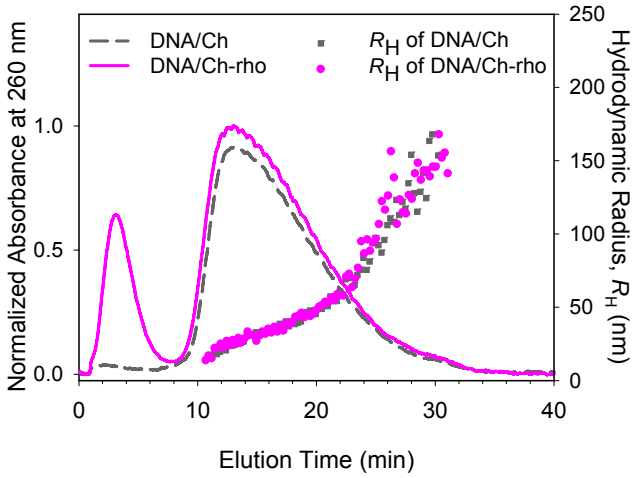

Figure 6. AF4 fractograms of DNA complexes prepared with unlabelled chitosan and chitosan-rhodamine monitored by the absorbance at 260 nm and by online DLS.

5.6 Conclusion

Investigations by AF4 with on-line UV/Vis, MALS, and DLS detectors of DNA/chitosan complexes formed upon mixing of DNA and chitosan solutions have demonstrated that it is possible to obtain in a single measurement the size and the size distribution of the complexes together with the content of unbound polycation. This combination of techniques provides the particle hydrodynamic size and size distribution with high resolution since a fractionation step takes place prior to size measurement by DLS, eliminating the difficulty of detecting size in polydisperse samples in batch-mode DLS. The separation and the size measurement were confirmed by ESEM visualization of eluate fractions. Accurate quantification of unbound polycation can provide insight into the contribution of the free polycation in the process of gene delivery. An excess of positive charges is required for full DNA compaction and nuclease protection but this constraint implies that a substantial amount of free polycation coexists with the complexes, as demonstrated in this study. The presence of free polycation is a factor to be accounted for since on the one hand, it may improve transfection efficiency, while on the other hand, it may also hinder cellular uptake of complexes and increase cytotoxicity and non-specific effects, depending on the polycation type. Future studies include the characterization of DNA complexes formed with chitosans having different molecular features and with polycations other than chitosan. AF4 can also be used to separate the eluting complexes into fractions with narrow size distribution and devoid of free polycation. Analysis of the physical and biological activity of such fractions will provide new understanding of structure-activity relationships and allow optimization of the physical properties of DNA/polycation complexes for enhanced transfection efficiency.

5.7 Acknowledgments

We would like to thank Monica Nelea for ESEM imaging of the collected fractions of complexes. This work was supported by the Canadian Institutes of Health Research (CIHR) and by the Natural Sciences and Engineering Research Council of Canada (NSERC). Pei Lian Ma received a doctoral fellowship from the Fonds québécois de la recherche sur la nature et les technologies.

5.8 Supporting Information

Description of the labelling of chitosan with rhodamine B isothiocyanate. Absorption spectra of DNA, Ch-rho, Ch, DNA/Ch-rho and DNA/Ch complexes. AF4 fractograms of DNA/Ch-rho complexes at a constant N/P ratio of 5 and different sample concentrations monitored by the UV absorbance at 260 nm. Plot of the integrated peak areas of the nanoparticles versus the DNA concentration in the samples. Extrapolation of the batch DLS data to zero scattering angle from a plot of Γ/q^2 against q^2 to determine the diffusion coefficient. This material is available free of charge via the Internet at http://pubs.acs.org.

Labelling of Chitosan with Rhodamine B-Isothiocyanate. A chitosan solution (10 mg/mL, 47 mM of glucosamine units) was prepared by dissolving overnight 89 mg of sample in a solution of acetic acid (33 mM). An equal volume of methanol as the chitosan solution was then added under stirring. After 3 hours, the solution was degassed and kept under N_2 atmosphere. Rhodamine-B isothiocyanate was dissolved in methanol at a concentration of 4 mM and 2.64 mL was injected into the chitosan solution under stirring. The reaction mixture was protected from light and left to proceed for 17 hours. The unreacted rhodamine B-isothiocyanate was removed

by precipitation of chitosan with drop-wise addition of 0.2 M NaOH to the mixture until the pH is above 10. After 5 washes with deionized water and centrifugations (3500 rpm, 5 min), the chitosan precipitate was recovered for freeze-drying. To determine the degree of substitution, the labelled chitosan was dissolved overnight at a concentration of 1 mg/mL in deionized water and hydrochloric acid (HCl/glucosamine ratio of 0.9) and further diluted to 0.1 mg/mL with deionized water. The absorbance was measured at 556 nm and a calibration curve was prepared using solutions of rhodamine B-isothiocyanate dissolved in deionized water.

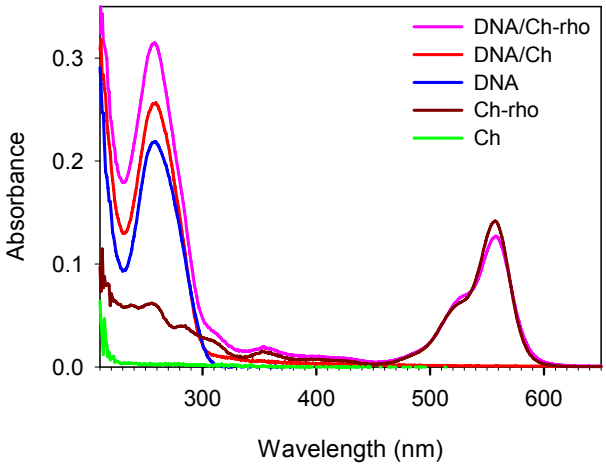

Figure 5.SI-1. Absorption spectra of DNA, Ch-rho, Ch, DNA/Ch-rho, and DNA/Ch complexes (N/P = 5) obtained with a batch UV/Vis spectrophotometer (Beckman DU-600) prior to the AF4 separation. C_{DNA} = 11.4 µg/mL, $C_{Ch\text{-}rho}$ = C_{Ch} = 39 µg/mL in the eluent (50 mM acetic acid/sodium acetate buffer, pH 4.0, total ionic strength of 20 mM ajusted with NaCl).

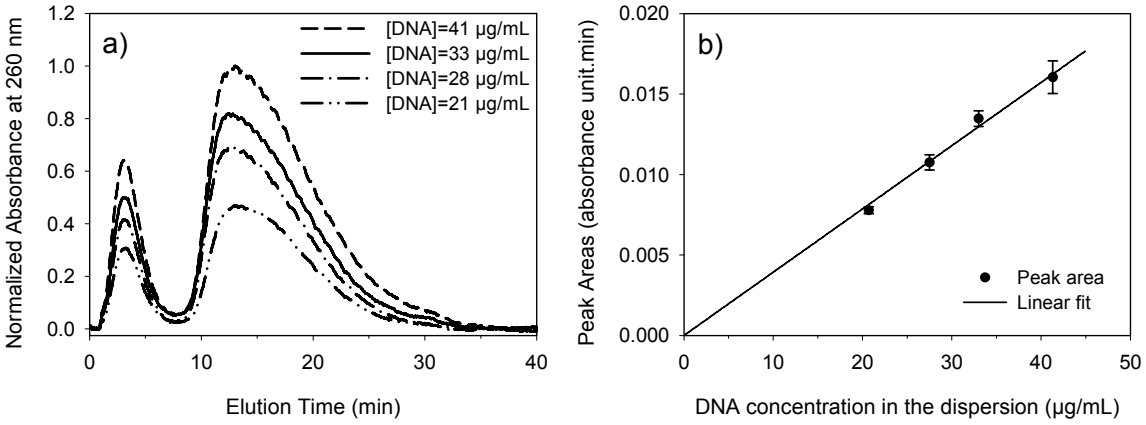

Figure 5.SI-2. a) AF4 fractograms monitored at 260 nm of DNA/Ch-rho complexes at a constant N/P ratio of 5 and different sample concentrations. b) A plot of the integrated peak areas of the nanoparticles versus the DNA concentration in the samples. The full line represents the linear regression of the data (coefficient $r^2 = 0.989$).

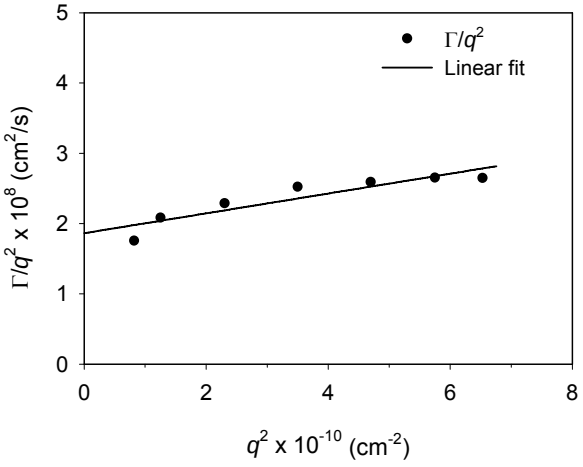

Figure 5.SI-3. Angular dependence of Γ/q^2 of the DNA/chitosan complexes determined by a Cumulant fit of the auto-correlation function at several angles. Linear extrapolation to zero scattering angle yields a diffusion coefficient of 1.86×10^{-8} cm^2/s which was then converted to a hydrodynamic radius of 130 nm by the Stokes-Einstein equation.

CHAPITRE 6 SIMULTANEOUS DETERMINATION OF UNBOUND POLYCATION AND PARTICLE SIZE OF DNA/CHITOSAN COMPLEXES BY ASYMMETRICAL FLOW FIELD-FLOW FRACTIONATION

Pei Lian Ma, Marc Lavertu, Françoise M. Winnik, and Michael D. Buschmann

Department of Chemical and Biomedical Engineering, Ecole Polytechnique de Montréal, PO 6079 Succ. Centre-Ville, Montreal, Quebec, H3C 3A7, Canada, and Department of Chemistry and Faculty of Pharmacy, Université de Montréal, PO 6128 Succ. Centre-Ville, Montreal, Quebec, H3C 3J7, Canada.

6.1 Abstract

Different preparations of DNA/chitosan complexes were characterized by asymmetrical flow field-flow fractionation (AF4) coupled with online UV, multiangle light scattering (MALS), and dynamic light scattering (DLS). Parameters known to influence the transfection efficiency of DNA/chitosan complexes were investigated, including the DNA concentration at mixing, the ratio of chitosan amine to DNA phosphate (N/P) used in the preparations, the chitosan molecular weight, and its degree of deacetylation. The AF4 combined system provided, in one experiment, five important physicochemical parameters of the complexes: the particle size, the size distribution, the structural conformation, the free chitosan content, and the composition of the nanoparticles. All preparations yielded similar ranges of particle hydrodynamic radii ($15 \leq R_H \leq 160$ nm) but that differed in size distribution. Either an increase of the DNA concentration at mixing or an increase of chitosan molecular weight generated the formation of a higher fraction

of larger particles (R_H > 60 nm) in the dispersions. The dispersions contained a majority of free chitosan in solution that was separated from the nanoparticles and quantified by the AF4 combined system. The free chitosan content was 53 to 92% in dispersions prepared with N/P ratios from 3 to 15, respectively, corresponding to an N/P ratio in the particles that was relatively constant in the range 1.3 to 1.6. The accuracy of the free chitosan determination by AF4 was confirmed by ultracentrifugation of the dispersion and analysis of the supernatant by the Orange II dye depletion method. This study reveals the utility of AF4 in the analysis of DNA/polycation dispersions and the importance of quantifying and understanding the role of the free polycation component in these non-viral gene delivery systems.

6.2 Introduction

Cationic polymers have been extensively investigated as vectors for gene delivery due to their low immunogenicity, their enhanced safety compared to their viral counterparts, and the ease of their preparation. Cationic polymers can condense DNA through electrostatic interactions to form nanoparticles that can be internalized by cells. It has been observed that for efficient *in vitro* and *in vivo* transfection to occur, the DNA/polycation complexes should be prepared by mixing DNA with an excess of polycation, such that the molar ratio of polycation protonable amines to DNA phosphates, known as the N/P ratio, is about 3 or higher (Boeckle et al., 2004; Koping-Hoggard et al., 2004; Jean et al., 2009; Strand et al., 2010). These conditions generate positively charged nanoparticles which resist aggregation as a consequence of repulsive electrostatic forces. Typically, not all of the polycation binds to the DNA, leaving the excess polycation dissolved and soluble in the aqueous medium. This free and soluble polycation component appears to play a critical role in the transfection process, possibly by triggering the

endosomal escape of the complexes through the proton sponge effect (Clamme et al., 2003; Boeckle et al., 2004; Saul et al., 2008; Ma, P.L. et al., 2010a). According to this hypothesis, polycations act as buffers in the endosome by absorbing a large amount of protons that generate an influx of Cl^- ions to maintain electroneutrality (Boussif et al., 1995; Behr, 1997). The resulting increase of osmotic pressure causes the rupture of the endosomes and the release of the complexes in the cytoplasm. Calculations based on the Poisson-Boltzmann theory have predicted that the endosome must contain a sufficiently large amount of free polycation for the proton sponge effect to take place (Yang et May, 2008). The DNA/polycation complexes alone are unable to induce the rupture of the endosomal membrane. The proton sponge hypothesis has been invoked frequently, but it remains a somewhat controversial issue and contradictory evidence has been reported (Funhoff et al., 2004; Gabrielson et Pack, 2006). The general consensus among researchers in this field is that the unbound polycation is a significant, yet only partly understood, factor in gene delivery. In order to further understand the role of the free polycation fraction and in view of the inherent toxicity of several polycations used for transfection (Godbey et al., 2001), it is important to determine accurately and reliably the physicochemical state of transfection formulations in terms of concentrations of unbound polycation and of DNA/polycation ratio in the complexes, in particular cases where high N/P ratios (between 20 and 60 for DNA formulations (Koping-Hoggard et al., 2004; Germershaus et al., 2008; Strand et al., 2008; Strand et al., 2010) and up to 150 for siRNA vectors (Liu, X. et al., 2007; Howard et al., 2008)) appear to be effective.

The free polycation present in gene delivery dispersions has been detected by gel electrophoresis coupled with selective staining of the migrating DNA and polycation by ethidium bromide and coomassie blue, respectively (Zhao et al., 2007; 2008). This technique provides qualitative information on the presence of free and bound components in the mixture. Isothermal

titration calorimetry (ITC) yields the stoichiometry of binding along with the binding affinity by analysing thermal events involved in the DNA-polycation interaction (Ma, P.L. et al., 2009). Once electrostatic neutralisation is achieved in a titration, the neutral complexes precipitate and the polycation added beyond this point will merely be subjected to dilution without binding to the precipitated complexes. The stepwise addition of the titrant (polycation) to a DNA solution carried out in an ITC measurement is indeed different from the standard one-shot fast mixing of DNA with a large excess of polycation, employed to prepare nonviral gene delivery vehicles. Ultrafiltration (Erbacher et al., 2004) and SEC (Boeckle et al., 2004; Storkle et al., 2007; Saul et al., 2008) have been used to separate the free polycation from DNA complexes. Further analysis of the filtrate or the collected fractions, respectively, by fluorescence or colorimetric assays is necessary to determine the concentration of free polycation. These methods are not without technical difficulties. For example, ultrafiltration can be hindered by the build-up of material on the membrane surface, while common problems encountered in SEC are loss of material, interaction with the packing, and column blockages. Fluorescence correlation spectroscopy (FCS) provides quantitative data on the free polycation content by analysis of a dispersion, without involving an additional separation step. The unbound polycation concentration is derived from fits of the autocorrelation data collected from the dispersion to mathematical models assuming the presence of two species diffusing with different rates (Clamme et al., 2003; Reitan et al., 2009). Data from different studies have not always been consistent. For instance, different amounts of free PEI were reported for DNA/PEI dispersions prepared at the same N/P ratios, depending on the method employed (Clamme et al., 2003; Boeckle et al., 2004). Data gathered by SEC showed a marked increase of the unbound PEI concentration with the N/P ratio (Boeckle et al., 2004), while data recovered from FCS analysis displayed no dependence on this parameter

(Clamme et al., 2003). Such discrepancies need to be resolved, preferably by the use of alternative methods.

Other analytical techniques are needed to characterize the DNA/polycation complexes themselves. The size and size distribution of the nanoparticles are obtained usually by dynamic light scattering (DLS), which yields the hydrodynamic radius of the complexes, and via microscopic imaging techniques such as transmission electron microscopy (TEM), scanning electron microscopy (SEM), and atomic force microscopy (AFM). The surface charge of the complexes can be approximated from zeta potential measurements. We reported recently the application of AF4 coupled with online UV/visible, multi-angle light scattering (MALS), and DLS detectors for the characterization of a DNA/polycation dispersion used in gene delivery (Ma, P.L. et al., 2010a). The principles of AF4 separation are based on the diffusion properties of the analytes. The method, which has been well described elsewhere (Wahlund et Giddings, 1987; Schimpf et al., 2000), has been used to determine the size and size distributions of colloidal suspensions (Lee, S. et al., 1996; Pauck et Colfen, 1998; Prestel et al., 2006), various delivery systems (Lee, H. et al., 2001; Fraunhofer et al., 2004; Yohannes et al., 2006; Jahn et al., 2007; Augsten et al., 2008; Hupfeld et al., 2010; Smith et al., 2010), and polymers (Liu, M.K. et Giddings, 1993; Viebke et Williams, 2000; Andersson et al., 2001; Takahashi et al., 2003; Augsten et Maeder, 2008). Our work has demonstrated that AF4 can yield, from a single analysis of a transfection mixture, the size and size distribution of the DNA/polycation nanoparticles as well as the concentration of free polycation, from which the composition of the nanoparticles was calculated. The sample analyzed was a gene delivery system formed by interaction of DNA with chitosan, a naturally-derived cationic polysaccharide extensively used for DNA transfection for recombinant protein expression and in the emerging field of gene

silencing using RNA interference, due to its biocompatibility, biodegradability, and versatility towards chemical modification (Tiera et al., 2006; Strand et al., 2008).

In this study, we applied the AF4 combined system to investigate the effects of key experimental parameters on the free polycation content, the size, and the size distribution of DNA/chitosan complexes. Parameters known to affect the transfection efficiency of DNA/chitosan complexes (MacLaughlin et al., 1998; Ishii et al., 2001; Koping-Hoggard et al., 2001; Lavertu et al., 2006) were assessed, including the N/P ratio, the DNA concentration at mixing, the chitosan molecular weight and degree of deacetylation (DDA). In addition, the validity of the free polycation concentration determined by this combined AF4 system was assessed by comparison with data obtained by standard ultracentrifugation and subsequent quantitative analysis of the free polycation in the supernatant by the Orange II dye depletion method.

6.3 Materials and Methods

6.3.1 Materials

The 6.4 kb plasmid EGFPLuc (Clontech Laboratories) was amplified in DH5α bacteria and purified using the Qiagen Plasmid Mega Kit. A stock solution of this plasmid (0.33 mg/mL) was prepared in deionized water and stored at –20 ^{o}C before use. Ultrapure heterogeneously deacetylated chitosans (Ultrasan^{TM}) with a DDA of 72%, 80%, and 92% were provided by Biosyntech Inc. (Laval, Qc, Canada) and were depolymerized according to Lavertu et al (Lavertu et al., 2006) using nitrous acid to achieve specific number-average molecular weight (M_n) of 10, 40, and 76 kDa. For UV/Vis detection, the chitosans were labelled with rhodamine B-isothiocyanate as previously reported (Ma, P.L. et al., 2010a). Table 6.1 summarizes the M_n and

polydispersity index of chitosans measured by analytical SEC (Darras et al., 2010), the DDA determined by ^{1}H NMR, (Lavertu et al., 2003) as well as the level of rhodamine B. Orange II was from Sigma-Aldrich (product no 195235).

6.3.2 Preparation of DNA/Chitosan Complexes

Unlabelled and labelled chitosan stock solutions of 5 mg/mL were prepared by dissolving the samples overnight in deionized water and hydrochloric acid (from 1 M HCl solution), such as to reach an HCl/glucosamine ratio of 1. Prior to mixing, chitosan solutions were diluted with deionized water to reach the desired amine to phosphate N/P ratio when 100 µL of chitosan would be mixed with 100 µL of DNA solution which was initially at a fixed concentration of 82 µg/mL in deionized water. This concentration of DNA solution was used in all preparations, except in one at 164 µg/mL to examine the effect of concentration. The mixing was done quickly by up and down pipetting of the dispersions. Samples were allowed to incubate at room temperature 30 min before analysis.

Table 6.1. Molecular Characteristics of the Chitosans.

DDA	M_n (kDa)	M_w/M_n	Level of Rhodamine B Labelling (mol % rho/NH_2)
72%	35	1.3	1.7
80%	42	1.4	1.2
80%	76	1.6	1.2
92%	10	1.3	1.3
92%	41	1.4	1.4

6.3.3 AF4/UV/MALS/DLS System

An asymmetrical flow field-flow fractionation (AF4) system (AF 2000 MT, Postnova Analytics) with a channel thickness of 350 μm fitted with a special regenerated cellulose membrane (10 kDa cut-off, RC amphiphilic, Z-MEM-AQU-631, Postnova Analytics) suitable for analysis of amphiphilic or cationic polymers was used. The AF4 was connected on-line to an UV/Vis detector (SPD-20A, Postnova Analytics), a multi-angle light scattering (MALS, Dawn 8+, Wyatt Technology), and a dynamic light scattering (DLS) detector (WyattQELS, Wyatt Technology) connected to the 108^{o} angle of the MALS Dawn 8+ detector. The MALS equipped with a K5 cell and a GaAs laser operating at 658 nm takes measurements at 1 s intervals. Data collection and analysis were done using ASTRA version 5.3.4.15 (Wyatt Technology).

6.3.4 AF4 Separation Conditions

The carrier medium was a prefiltered 50 mM acetic acid/sodium acetate buffer at pH 4.0 with a total ionic strength of 20 mM (adjusted by addition of NaCl). After flow equilibration, the sample was injected with a flow rate of 0.2 ml/min (injection loop volume: 21 μL), followed by a 9 min-focusing with a cross flow rate and a detector flow rate of 1 mL/min each. Following a 1 min-transition, a four-step cross flow rate gradient was initiated for the elution mode. The starting flow rate (1 ml/min) was decreased exponentially first with an exponent factor of 0.4 to 0.4 ml/min within 10 min, then with an exponent factor of 0.8 from 0.4 to 0.15 ml/min within 20 min, and finally it was decreased linearly from 0.15 to 0.05 mL/min within 15 min. The cross flow rate was then kept constant at 0.05 mL/min for 15 min. The detector flow rate was kept at 1 ml/min throughout. All the flow rates were controlled by the AF2000 Control software (Postnova Analytics). The cross flow was generated by Kloehn syringe pumps (Postnova

Analytics) while the axial and focusing flows were delivered by isocratic pumps (PN1130, Postnova Analytics).

6.3.5 Quantification of Free Chitosan and Monitoring of DNA/Chitosan Particles

The free polycation separated by AF4 from the DNA/chitosan complexes was monitored using rhodamine B labeled chitosan (Ch-rho) and by UV/Vis detection at 556 nm. The free Ch-rho content was quantified by comparing the integrated areas under the curves of the corresponding peak in the fractograms before and after complexation with DNA. The detection of the eluting fractionated DNA/chitosan nanoparticles was performed sequentially by UV absorbance at 260 nm, MALS and DLS. Each fractogram presented is representative of triplicate samples. For every slice eluting from the AF4, the MALS data in the angular range of 35-90^{o} were analysed according to Andersson et al. (2003) by constructing the Debye plot using the Berry method (Berry, 1966). The extrapolation to zero scattering angle yields the slope from which the radius of gyration was calculated. The online DLS measures the autocorrelated function leading to the diffusion coefficient from which the hydrodynamic radius was calculated using the Stokes-Einstein equation. The reported values are the average (± standard deviation) of three independent measurements.

6.3.6 Ultracentrifugation and Orange II Colorimetric Assay

The free chitosan content in a dispersion of DNA/chitosan complexes was confirmed by subjecting the samples to ultracentrifugation and measuring the concentration of chitosan in the supernatant by the Orange II depletion method (Drogoz et al., 2007). The samples (600 µL of

dispersion) were ultracentrifuged at 65,000 rpm for 30 min (Beckman, Optima MAX-E, TLA-110 fixed rotor). The supernatant (100μL) was collected and diluted 10 to 20 fold with 50 mM acetic acid/sodium acetate buffer at pH 4.0 such that the concentration of Orange II is always in excess compared to the amine groups of chitosan to be assayed. To 1 mL of diluted supernatant, 100 μL of 1 mM Orange II (in the acetic acid/sodium acetate buffer) was added and mixed. After 15 min of incubation, the suspension of chitosan/Orange II was centrifuged (20,000g for 30 min) to precipitate the complexes and recover the supernatant containing the unbound dye. The absorbance of the supernatant was then measured at 484 nm. The free chitosan content in DNA/chitosan dispersions was calculated from calibration curves obtained with solutions of chitosan of identical molar mass and DDA. The reported values are the average (± standard deviation) of triplicates.

6.3.7 Zeta Potential

The complexes were diluted 4 times in the running buffer prior to analysis with a Malvern Zetasizer Nano ZS (Worcestershire, UK). The zeta potential of the complexes was calculated from the electrophoretic mobility values using the Smoluchowski equation.

6.4 Results and Discussion

The optimized AF4 operating conditions for the separation of DNA/chitosan dispersions into unbound chitosan and nanoparticles according to their sizes were described previously (Ma, P.L. et al., 2010a). These conditions were used in this study without further modifications. They allow high sample mass recoveries (87-92% for chitosan injected alone and at least 95% for DNA/chitosan complexes). The complete elution of the separated species was monitored by

online UV-vis, MALS, and DLS detectors in series. The accuracy of the particle hydrodynamic sizes measured by online DLS was confirmed by batch DLS measurements of the same samples prior to AF4 separation and by SEM observations of collected fractions at different elution times (Ma, P.L. et al., 2010a) .

6.4.1 Effect of DNA Concentration at Mixing on the Particle Size

Previous studies using batch-mode DLS measurements have shown that the hydrodynamic radius of a dispersion of DNA/chitosan complexes increases with the concentration of DNA in the solutions used to prepare the nanoparticles (MacLaughlin et al., 1998; Koping-Hoggard et al., 2004). To assess the ability of the AF4 system to detect this change in particle size, we prepared two batches of DNA/chitosan complexes starting from DNA solutions of concentrations of 82 and 164 μg/mL. The N/P ratio was set at 5 by adjusting the concentration of the chitosan solution prior to mixing with DNA. Since chitosan absorbs only at wavelength < 210 nm, a rhodamine-B labeled chitosan (Ch-rho) was used, so that a single dispersion of DNA/polycation can be used to detect both the complexes and the unbound polycation in the dispersion by UV detection at 260 nm. The dispersion with the highest DNA concentration was diluted twice with deionized water prior to injection, so that the DNA concentration was the same in both injected dispersions allowing direct comparison of their elution profiles. The AF4 fractograms of the two dispersions of DNA/Ch-rho (80%DDA, 42 kDa) complexes monitored by the absorbance at 260 nm are shown in Figure 6.1A, together with a fractogram of a solution of Ch-rho used as control (corresponding to a DNA concentration of 0 μg/mL). The injection of the Ch-rho solution resulted in a single peak eluting between 1 and 9

min. The intensity of this signal is lower in the fractograms of the DNA/Ch-rho dispersions as a result of the complexation, but its elution time is the same.

The UV fractogram of each DNA/Ch-rho dispersion presents an additional band at longer elution times, between 9 and 34 min, attributed to the elution of the DNA/Ch-rho nanoparticles that was also confirmed by light scattering detection (see below). The complexation between DNA and chitosan is characterized by a high association constant in the range of 10^9-10^{10} M^{-1} (Ma, P.L. et al., 2009). Therefore, in an excess of chitosan, all the DNA is expected to be in the complexed form, as confirmed by gel electrophoresis (Strand et al., 2005). Note that injections of DNA alone in AF4 resulted previously in no signal due to interaction with the membrane (Ma, P.L. et al., 2010a). The nanoparticles eluted in the same time interval in both dispersions, but their elution profiles differ in intensity and shape. The profile recorded for the dispersion prepared with the higher DNA concentration features an important shoulder around 30 min, which cannot be seen in the profile of the dispersion obtained starting with a solution of lower DNA concentration. The shape of the signals detected by UV was validated by injecting various dilutions of the same sample (see the Supporting Information, Figure 6.SI-1; and in Ma, P.L. et al., 2010a). The integrated areas under the curve of the peaks for various dilutions correspond linearly to the injected DNA concentration. The concentration of eluting DNA/chitosan complexes was therefore proportional to the absorbance at 260 nm. The shoulder observed around 30 min in the UV fractogram of the concentrated preparation is an indication of a significant amount of large particles eluting from the AF4.

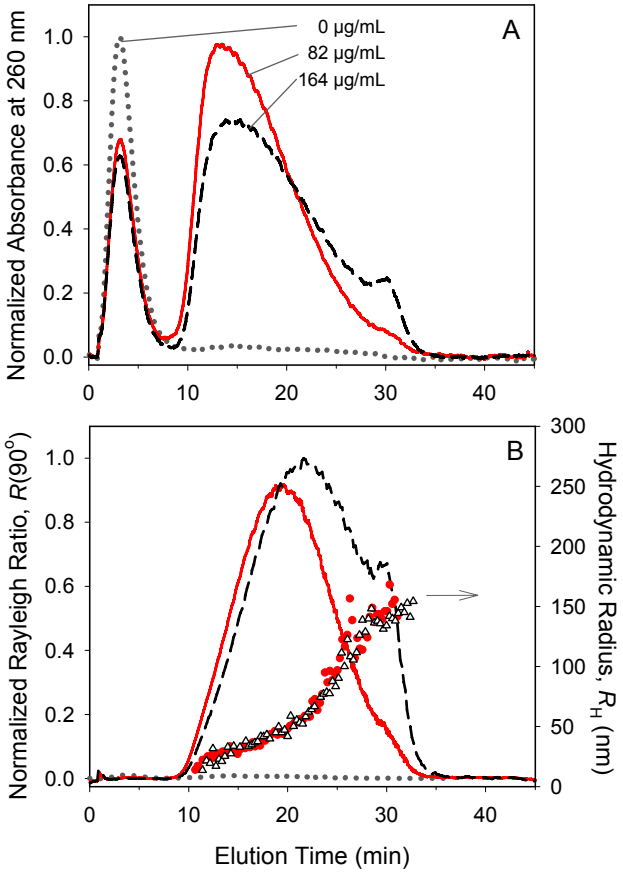

Figure 6.1. AF4 fractograms of DNA/Ch-rho (80% DDA, 42 kDa) complexes prepared at initial DNA concentrations of 82 µg/mL (—, ●) and 164 µg/mL(----, Δ) (N/P = 5). Also shown are the signals of Ch-rho alone, corresponding to DNA concentration of 0 µg/mL (….). A) UV detection at 260 nm, B) Rayleigh ratio at 90° (lines) and hydrodynamic radius (symbols).

The elution profiles of the DNA/chitosan complexes monitored online by MALS and DLS detectors are presented in Figure 6.1B. Within the concentration ranges studied here, the light scattered by the free chitosan in solution (the leftmost peak in Figure 1A) was not significant compared to the intensity of the light scattered by the much larger nanoparticles which have hydrodynamic radii (R_H) ranging from 15 to 160 nm, as calculated from the DLS signals.

Smaller particles eluted prior to larger ones because they have a higher diffusion constant and, consequently, were less retained by the cross-flow in the AF4 channel. A qualitative comparison of the elution profiles monitored by UV and DLS for each dispersion (Figure 6.1 A and B) reveals that the majority of the nanoparticles elute before 22 min and have an $R_H < 60$ nm. The UV and DLS data were used to obtain the size distributions of the DNA/chitosan nanoparticles that are presented in Figure 6.2 as plots of the cumulative and differential weight fractions as functions of the hydrodynamic radius. Although both preparations produced nanoparticles within the same size ranges, it is interesting to note that the fraction of nanoparticles having an $R_H > 60$ nm represents only 20% of the sample prepared with the lower DNA concentration while this fraction increased to 40% in the more concentrated preparation. The doubling of this fraction of large particles, although in minor proportion in the sample, contributed to the intense light scattered detected by the MALS in the 20 to 34 minutes elution range (Figure 6.1B). In batch DLS measurements, this fraction of large and intensely scattering particles can mask the presence of the smaller particles. It can be predominant in intensity-averaged hydrodynamic radii distributions, as demonstrated in a previous report (Ma, P.L. et al., 2010a). In such a case, the data must be interpreted with care particularly in the characterization of polydisperse samples, a situation that is resolved here using the AF4 combined system where a fractionation step takes place *prior* to measurement by the online DLS. Since the formation of the complexes using an initial DNA concentration of 82 μg/mL yielded in majority smaller particles sizes, this concentration was chosen throughout the study.

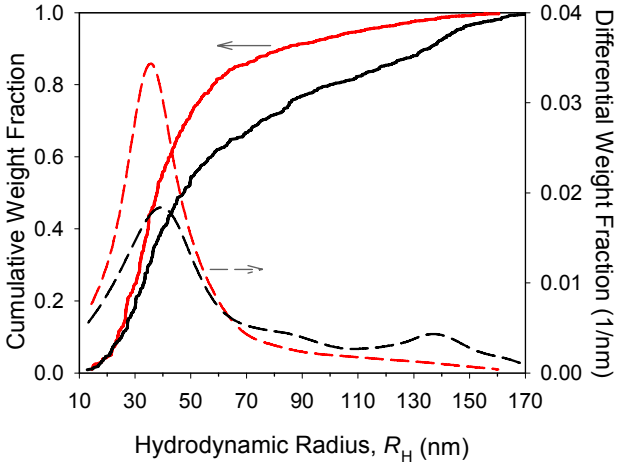

Figure 6.2. Cumulative (full lines) and differential (dashed lines) weight fractions of AF4 fractionated DNA/Ch-rho (80% DDA, 42 kDa) nanoparticles prepared at initial DNA concentrations of 82 µg/mL (—) and 164 µg/mL (—) (N/P = 5).

6.4.2 Effect of the N/P Ratio on the Free Chitosan Content and Particle Size

Dispersions with N/P ratios in the range of 3 to 15 were prepared by mixing increasing concentrations of Ch-rho (80%DDA, 42 kDa) solutions with a DNA solution of fixed concentration (82 µg/mL). They were subjected to AF4 separation and the elution was monitored by UV/Vis detection, MALS, and DLS. The amount of unbound Ch-rho was determined quantitatively on the basis of fractograms monitored by the UV/Vis signal at 556 nm, the wavelength of maximum absorbance of Ch-rho. DNA does not absorb light at this wavelength, and consequently, does not interfere in the quantification of Ch-rho. These fractograms at 556 nm yield the free chitosan content with the highest precision, compared to the ones monitored at 260 nm, and without interference of the DNA/chitosan complexes. The elution profiles of free Ch-rho separated from the complexes prepared at different N/P ratios are presented in Figure 6.3

(full lines), together with the controls corresponding to Ch-rho injections (dashed lines) at the same concentration as in each dispersion but without DNA. From the integrated areas under the curves, the free chitosan content was determined in each dispersion and the values are listed in Table 6.2. The free chitosan content increases from 53 to 92% as the N/P ratio used in the preparations increases from 3 to 15. These values were then used to calculate the composition of the DNA/Ch-rho nanoparticles. They are listed in Table 6.2 expressed as N/P values. The composition of the nanoparticles was nearly the same in all samples, with an average N/P value of 1.3-1.5, even in dispersions containing a large excess of chitosan initially added to the DNA solution. This finding confirmed that the one-shot fast mixing of DNA with an excess of chitosan generates positively charged nanoparticles that cannot be formed by slow titrations of chitosan into DNA, as in isothermal titration microcalorimetry (ITC) where the complexes precipitated once the DNA binding sites were saturated close to charge neutrality (Ma, P.L. et al., 2009). The chitosan amine content in nanoparticles formed by fast mixing and determined by the AF4 combined system is almost 2-3 fold higher than the amount of amine bound to DNA by the slow titration mixing in ITC.

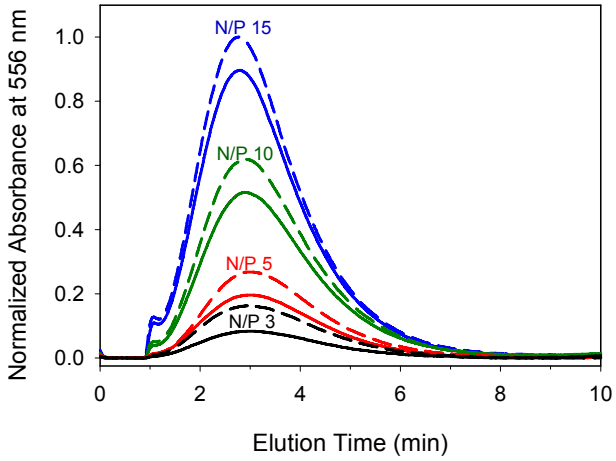

Figure 6.3. AF4 fractograms of Ch-rho (80% DDA, 42 kDa) before and after complexation with DNA at different N/P ratios monitored by the absorbance at 556 nm. The elution sections between 0 and 10 min shows Ch-rho alone as the control (dashed lines) and unbound Ch-rho separated from DNA/Ch-rho complexes (full lines).

Table 6.2. Free Chitosan Content in Dispersions of DNA/Chitosan Complexes Prepared at Different N/P Ratios.

	AF4[b]		Ultracentrifuge[c]	
N/P[a]	Free Ch-rho (%)	Particles N/P	Free Ch (%)	Particles N/P
3	53 ± 1	1.4 ± 0.1	61 ± 2	1.2 ± 0.1
5	73 ± 2	1.4 ± 0.1	75 ± 1	1.3 ± 0.1
10	85 ± 1	1.5 ± 0.1	87 ± 1	1.4 ± 0.1
15	92 ± 1	1.3 ± 0.1	92 ± 1	1.3 ± 0.1

[a] Used to prepare the complexes with chitosan (80% DDA, 42 kDa). [b] UV/Vis detection at 556 nm. [c] Analysis of the supernatant with Orange II.

The accuracy of the fraction of unbound Ch-rho data obtained by the AF4 combined system was assessed by subjecting the dispersions of DNA/chitosan complexes to the depletion method with the Orange II dye employed by Drogoz et al. (2007) for the characterization of polyelectrolyte complexes. The dispersions were prepared under identical conditions as the samples analyzed by AF4, except that unlabelled chitosan (Ch) was used rather than Ch-rho. Because of material build-up and inefficient removal of the DNA/chitosan complexes by the filtration step suggested by Drogoz et al. (2007), we separated the complexes from soluble chitosan by ultracentrifugation instead of filtration and recovered the supernatant containing free chitosan. The sulfonated Orange II dye was then added to the supernatant to interact with the protonated amine groups of chitosan. The ultracentrifugation step was necessary since the positively charged complexes also bind to the dye, resulting in an overestimation of the fraction of free chitosan. The values of free chitosan content determined by ultracentrifugation combined with the depletion method are listed in Table 6.2. An excellent agreement between the two analytical methods exists throughout the series of samples, confirming the validity of both methods to determine the free chitosan content in DNA/chitosan dispersions.

A number of previous studies aimed at determining the fraction of free polycation in DNA/polycation dispersions have been reported. Clamme et al. (2003) using FCS obtained a constant value of 86% of free PEI in preparations of DNA/PEI complexes formed at N/P ratios of 6 and 10 (corresponding to an N/P ratio of 0.84 and 1.3 in the nanoparticles, respectively). FCS combined with dual-labeling of the components for colocalized signals was used to characterize a dispersion of DNA/chitosan oligomers with an N/P ratio of 10. The fraction of free chitosan calculated from the autocorrelation functions was 49% in that sample (Reitan et al., 2009). In these two latter studies, FCS does not provide a direct quantitative measurement of free polycation because it relies on fitting autocorrelation functions to the contributions of two

assumed components, i.e. the free polycation and the complex, each idealized as having one diffusion coefficient, versus the continuum of particle sizes observed by AF4 (Figure 6.1B). The separation by SEC of DNA/PEI complexes prepared with initial N/P ratios of 6 and 12 yielded an almost constant N/P ratio of 2.5 for the composition of the nanoparticles (Boeckle et al., 2004). This value was calculated from the concentration of unbound PEI determined by analysis of collected fractions eluting from the SEC system. The fact that the composition of the DNA/PEI nanoparticles was constant in these dispersions prepared with different initial N/P ratios is in agreement with our data, although the value in that report is higher. This discrepancy may reflect differences in the composition of complexes of DNA with different polycations. The shorter intercharge spacing on PEI compared to chitosan may be a factor contributing to the increased amine content in the DNA/PEI complexes. The discrepancy may also be related to a loss of material adsorbed to the SEC column packing, a problem often encountered with this technique.

The combined use of the online DLS and UV detectors coupled to AF4 also provided the size distribution of the fractionated particles in dispersions obtained at different mixing N/P ratios, shown in Figure 6.4. Remarkably, the size distribution was nearly the same in all samples, regardless of the initial N/P ratio under the conditions of excess chitosan, compared to DNA, selected in this study. This observation together with the constant composition of the nanoparticles indicate that the DNA binding sites are saturated under these conditions and that most of the chitosan in excess is dissolved, unbound, in the aqueous medium. In view of the observed enhanced transfection efficiency of DNA/chitosan dispersions prepared with N/P ratios up to 20 or 60 (Koping-Hoggard et al., 2004; Germershaus et al., 2008; Strand et al., 2008; Strand et al., 2010), our data suggest that the free chitosan fraction plays an important role in the gene delivery pathways. This conclusion merits further mechanistic analysis, since it is at odds

with suggestions made in other studies that such high N/P ratios are necessary for chitosan to fully condense DNA (Danielsen et al., 2004; Strand et al., 2008).

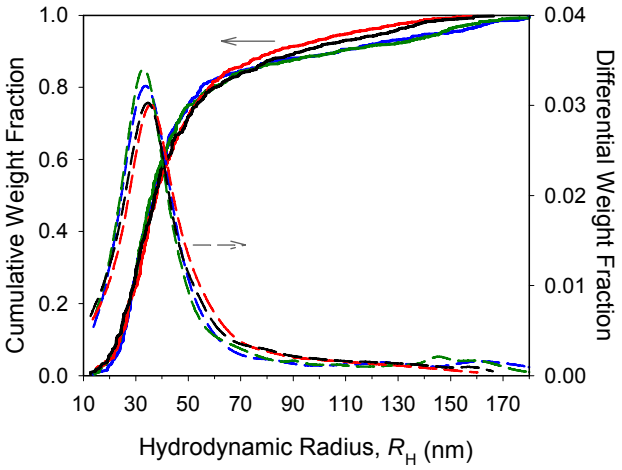

Figure 6.4. Cumulative (full lines) and differential (dashed lines) weight fractions of AF4 fractionated DNA/Ch-rho (80% DDA, 42 kDa) nanoparticles prepared at N/P ratios of 3 (black), 5 (red), 10 (green), and 15 (blue).

6.4.3 Effect of Chitosan Molecular Weight and Degree of Deacetylation

Previous studies have indicated that both parameters affect the DNA-chitosan binding affinity, which itself is related to the ability of the complexes to dissociate inside the cell nucleus for gene expression (Lavertu et al., 2006; Ma, P.L. et al., 2009; Strand et al., 2010). The charge density of chitosan can be modulated by its degree of deacetylation (DDA) defined as the glucosamine monomer fractional content. Increasing the DDA of chitosan increases the charge density along the molecular chain of chitosan. Dispersions of DNA/Ch-rho of constant initial N/P ratio of 5 were prepared with chitosans of different DDA and M_n values (see Table 6.1). The AF4 fractograms of these complexes monitored by the absorbance at 260 nm and by light

scattering are presented in Figure 6.5 A and B, respectively. If we consider first dispersions prepared with chitosans of comparable mass (M_n ~ 42 kDa and 35 kDa) but different DDA, we note that their fractograms are very similar, independently of the detection mode (absorbance, Rayleigh ratios at 90^o and hydrodynamic radii). The only differences are a more intense peak for the eluting free chitosan and a slightly higher absorbance of the complexes with Ch-rho of 72% DDA, compared to the complexes with Ch-rho of 80% DDA. Since the number of glucosamines per chain of Ch-rho of 72 % DDA is lower than that of Ch-rho of 80% DDA, a higher amount of Ch-rho of 72% DDA was required to reach the same mixing N/P ratio of 5. Hence the observed relative intensity of the two bands reflects the higher chitosan concentration in the 72% DDA versus 80% DDA dispersions. In addition, the slightly higher level of rhodamine B labeling on the chitosan with a DDA of 72% (Table 6.1) is a factor which also contributes to these increased intensities observed. The fraction of free chitosan calculated from the AF4 fractograms was in the order of 71-73% in both samples, resulting in a nanoparticle N/P ratio of about 1.4.

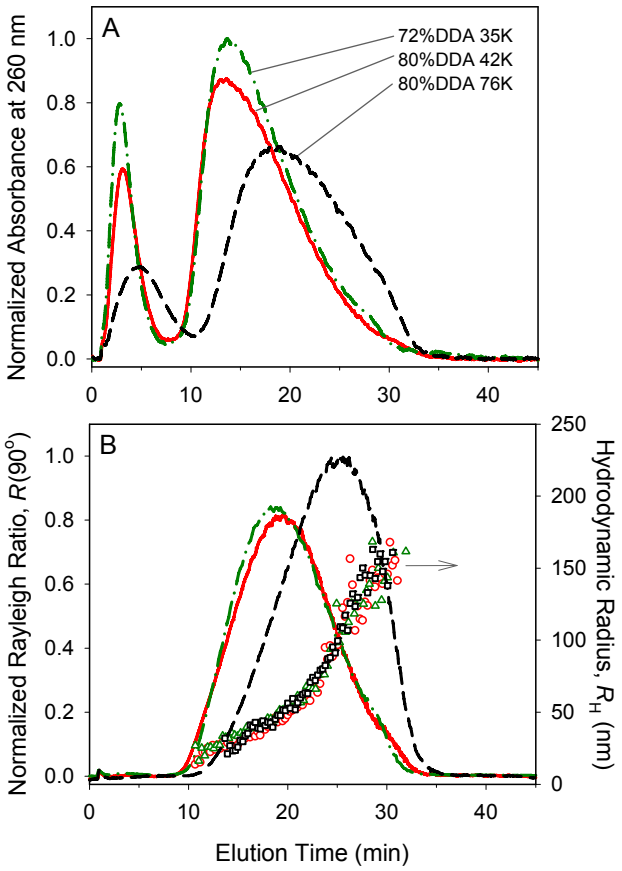

Figure 6.5. AF4 fractograms of DNA complexed with Ch-rho having different values of DDA and M_n (N/P = 5) showing (A) the absorbance at 260 nm, (B) the Rayleigh ratio at 90° (lines) and the hydrodynamic radius (symbols).

We compare next the elution profiles of DNA complexed with Ch-rho samples of identical DDA (80%) but significantly different M_n values (42 and 76 kDa) which are also presented in Figure 6.5 A and B. The unbound chitosan fraction of the sample obtained with the chitosan of higher M_n has a longer retention time, as expected on the basis of the mechanism of AF4 separation, while the nanoparticles elute from about 10 min to 34 min ($15 \leq R_H \leq 160$ nm) for both dispersions (Figure 6.5 A and B). The shape and intensity of the nanoparticles elution bands are different for the two samples, whether monitored by UV at 260 nm or by MALS. It

appears that the sample formed with the longer chitosan had a greater proportion of large particles (R_H > 60 nm). This trend is reflected by significant changes in the size distributions of the DNA/Ch-rho complexes prepared with chitosans of DDA 80 % and different M_n (42 and 76 kDa) (Figure 6.6). To test the generality of this observation, we carried out AF4 separations of DNA complexes formed with two additional chitosans having a similar DDA (92%) and different M_n (10 and 41 kDa) (Figure 6.7). For this pair of samples, we also observed a greater proportion of large particles in the sample obtained with the longer chitosan. In these samples too, the unbound chitosan content exhibited no dependence on chitosan DDA or M_n. The calculated N/P value for the nanoparticles composition was once more 1.4-1.6, the range of values recorded in all samples described in this study (Table 6.3). We also confirmed that the nanoparticles were always positively charged, in conditions of excess chitosan, by carrying out zeta potential measurements of all samples (25-29 mV; Table 6.3) prior to the AF4 separation.

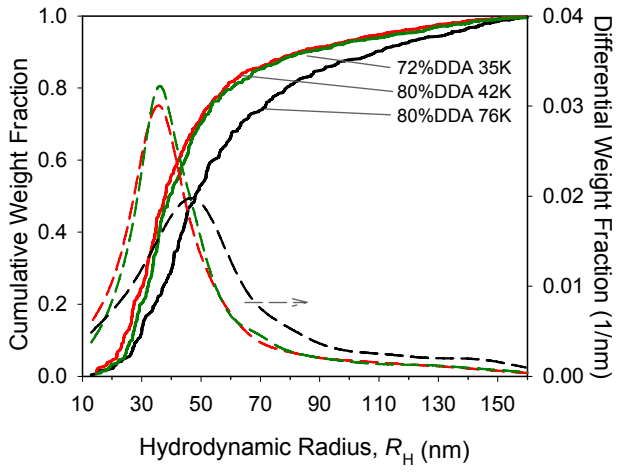

Figure 6.6. Cumulative (full lines) and differential weight (dashed lines) fraction as a function of the hydrodynamic radius of nanoparticles of DNA complexed with Ch-rho having different values of DDA and M_n (N/P = 5).

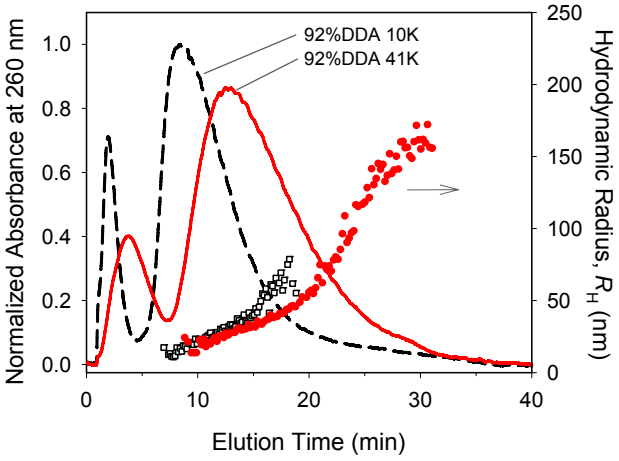

Figure 6.7. AF4 fractograms of DNA complexed with Ch-rho having a DDA = 92% but different M_n of 10 and 41 kDa (N/P = 5), monitored by the UV signal at 260 nm (lines) and the DLS (symbols).

Table 6.3. Free Ch-rho Content Determined by AF4 and Other Properties of Dispersions of DNA/Ch-rho Complexes Prepared with Different Chitosans (N/P = 5).

DDA	M_n (kDa)	Free Ch-rho (%)	Particles N/P	Zeta Potential (mV)
72%	35	71 ± 2	1.5 ± 0.1	28 ± 1
80%	42	73 ± 2	1.4 ± 0.1	29 ± 2
80%	76	70 ± 4	1.5 ± 0.2	29 ± 2
92%	10	70 ± 2	1.6 ± 0.1	25 ± 2
92%	41	73 ± 2	1.4 ± 0.1	29 ± 2

[a] By Zetasizer prior to AF4 separation.

6.4.4 Conformation of the Complexes: R_g/R_H

The AF4 separation is based on the diffusion coefficient of the particles but it does not have the ability to differentiate the shape and density of the particles (Pauck et Colfen, 1998).

Nonetheless, information on the shape of the eluting nanoparticles can be extracted from light scattering data provided by the online MALS and DLS detectors. DLS data yields the hydrodynamic radius of the eluting particles while the radius of gyration can be obtained by analysis of the MALS data. The characteristic ratio of R_g to R_H provides information on the shape of nanoparticles (Burchard, W., 1983; Burchard, Walther, 1996). The values of R_g/R_H derived from AF4 fractograms of the nanoparticles (N/P = 5, $[DNA]_{initial}$ = 82 μg/mL) prepared with four different chitosans are plotted in Figure 6.8 as a function of the measured hydrodynamic radius. The values of R_g/R_H ranged from 1.1 to 1.5, suggesting a conformation similar to that of polymeric stars and clusters rather than hard non-draining spheres (R_g/R_H = 0.78) or rods ($R_g/R_H > 2$) (Burchard, W., 1983; Burchard, Walther, 1996). This range of R_g/R_H values determined for DNA/chitosan complexes suggest a spherical shape with dangling unbound chitosan loops or tails on their surfaces. This conformation is in agreement with the spherical shape of nanoparticles observed previously by SEM imaging of collected fractions from the AF4 (Ma, P.L. et al., 2010a). Similar values of R_g/R_H were reported previously for DNA/polycation complexes using conventional static light scattering (Tan et al., 2006; Storkle et al., 2007). The R_g/R_H ratio decreased slightly with increasing size of DNA/chitosan nanoparticles and reached an almost constant value of about 1.1-1.2 for $R_H > 80$ nm. It is interesting to note that the smallest R_g/R_H values (1.1-1.2) throughout the size range was recorded for the DNA/chitosan complexes formed with the chitosan of highest molecular weight (80% DDA, 76 kDa). It appears that nanoparticles with a $R_H < 80$ nm formed with this chitosan had a tendency towards a more compact structure (Burchard, Walther, 1996).

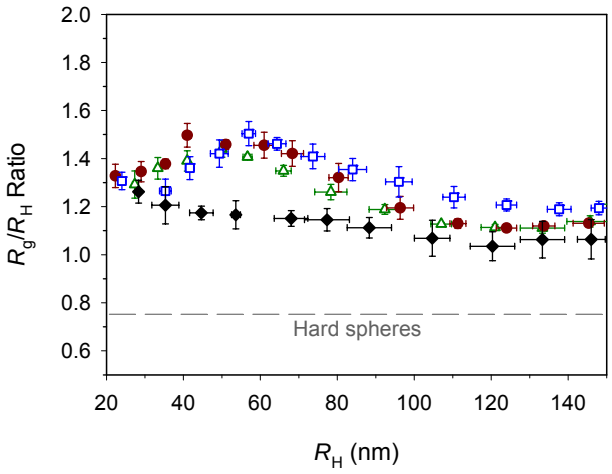

Figure 6.8. Ratio of the radius of gyration (R_g) to the hydrodynamic radius (R_H) of DNA/chitosan complexes (N/P = 5) with Ch-rho DDA 72% and 35 kDa (□); Ch-rho DDA 80% and 42 kDa (●); Ch-rho DDA 80% and 76 kDa (♦); and Ch-rho DDA 92% and 41 kDa (Δ). The broken line represent hard spheres (R_g/R_H = 0.77).

6.5 Conclusions

AF4 was applied for the first time to investigate different transfection formulations of DNA/polycation complexes that were prepared by varying the mixing conditions between DNA and chitosan as well as the molecular features of chitosan. The ability of AF4 combined with online UV, MALS, and DLS detection to provide an overall characterization of DNA/polycation complexes was demonstrated. Five important parameters were obtained simultaneously: the particle size, the size distribution, the composition and conformation of the complexes as well as the free chitosan content. The understanding of the influence of physicochemical factors on gene expression relies on the accurate determination of these parameters. Because of the fractionation step, the AF4 combined system was able to detect small changes between the differently prepared

complexes. For the size distribution of polydisperse samples, this precision exceeds that of conventional DLS where the light scattered by large particles dominates the measurement, masking the majority of the population. The assessment of free polycation content determined by the AF4 combined system was confirmed by ultracentrifugation of the dispersions and subsequent analysis of the recovered supernatant. The composition of the complexes was always about 1.4 in terms of N/P ratio, regardless of the amount of excess chitosan added compared to DNA. This finding emphasizes the important role of the free chitosan in gene delivery. Our findings also provide important insights in the understanding of the structure-activity relationships and the elaboration of strategies to improve the efficiency of gene delivery systems.

6.6 Acknowledgments

This work was supported by the Canadian Institutes of Health Research (CIHR) and by the Natural Sciences and Engineering Research Council of Canada (NSERC). Pei Lian Ma received a doctoral fellowship from the Fonds québécois de la recherche sur la nature et les technologies.

6.7 Supporting Information

UV fractograms at 260 nm of a DNA/chitosan dispersion at different dilutions (with Ch-rho 80% DDA and 42 kDa; N/P = 5; initial mixing DNA concentration of 164 µg/mL) and plot of the corresponding integrated peak areas of the nanoparticles versus DNA concentration. This material is available free of charge via the Internet at http://pubs.acs.org.

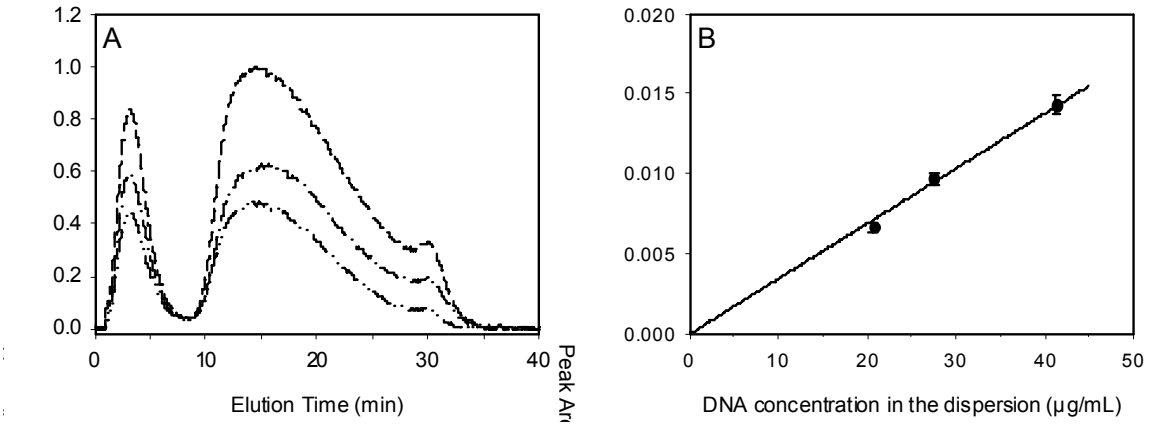

Figure 6.SI-1. UV fractograms at 260 nm of DNA/chitosan complexes (with Ch-rho 80% DDA and 42 kDa; N/P = 5; initial mixing DNA concentration of 164 µg/mL) at various dilutions (A): [DNA] = 41 µg/mL (—), 28 µg/mL (— ·), and 21 µg/mL (— ··). Plot of the corresponding integrated peak areas of the nanoparticles versus the DNA concentration in the samples (B). The full line represents a linear regression of the data (r^2 = 0.99).

CHAPITRE 7 DISCUSSION GÉNÉRALE

Notre première étude (chapitre 4) avait pour objectif d'étudier les interactions chitosane-ADN par calorimétrie de titrage isotherme (ITC). Cette technique a été choisie car elle permet de quantifier l'affinité du chitosane pour l'ADN en solution comparativement aux autres techniques qui requièrent soit la fixation d'une des composantes (résonance plasmonique de surface) ou donnent des informations plutôt qualitatives (déplacement du bromure d'éthidium). Cette étude nous a permis de déterminer la constante thermodynamique d'interaction, l'enthalpie d'interaction et la stœchiométrie des complexes à partir des isothermes obtenues. Tout d'abord, nous avons étudié l'effet du pH sur l'affinité du chitosane pour l'ADN car c'est un facteur qui influence le degré d'ionisation du chitosane. Nous avons effectué les titrages par ITC avec plusieurs types de solutions tamponnées à des valeurs de pH différentes. La constante d'affinité augmente lorsque le pH diminue, due aux interactions électrostatiques plus fortes avec un chitosane plus ionisé. L'association chitosane-ADN dépendait également de la nature des solutions tampon et était soit exothermique, soit endothermique. Cette dépendance indique un échange de protons entre le chitosane et le système tampon (l'ADN était entièrement ionisé aux conditions étudiées) lors de la complexation chitosane-ADN. En effet, le caractère fortement anionique de l'ADN induit un transfert de protons du système tampon au chitosane au cours de l'interaction. Le degré d'ionisation du chitosane complexé est donc plus élevé qu'à l'état libre en solution. Nous avons également analysé la contribution des changements d'ionisation de chaque composante à l'enthalpie d'interaction mesurée. Nous étions surpris que l'enthalpie d'interaction chitosane-ADN mesurée par ITC est entièrement due aux changements d'ionisation du chitosane et du système tampon.

Cette étude nous a permis également de déterminer la stœchiométrie des complexes ADN/chitosane formés par titrage. Une fois les sites d'interaction de l'ADN saturés et proche de la neutralité des charges, les complexes précipitent et le chitosane ajouté reste en solution. Le titrage ne permet donc pas de former des complexes chargés positivement contrairement à un mélange rapide avec un excès de polycation. À partir des valeurs de stœchiométrie des complexes et de l'état d'ionisation du chitosane complexé, nous avons trouvé que le ratio de charges amine protonée du chitosane par rapport aux charges négatives de l'ADN dans les complexes se situe entre 0.5 et 0.7 et n'est pas significativement affectée par le pH, le système tampon et les caractéristiques moléculaires du chitosane.

Une série de chitosanes de masses molaires (M_n) et de degrés de désacétylation (DDA) différents, préalablement bien caractérisés, ont été testés afin de déterminer leurs influences sur les paramètres d'association car le DDA est également un facteur qui permet de moduler la densité de charge du chitosane. En général, l'affinité du chitosane pour l'ADN augmente avec la masse molaire et le DDA. Pour un DDA de 80%, la constante d'affinité augmente d'environ 1 x 10^9 à 12 x 10^9 M^{-1}, soit un ordre de grandeur, lorsque M_n varie de 7 à 153 kDa. Cet effet sur l'affinité chitosane-ADN a été quantifié pour la première fois alors qu'il n'a pas été observé dans une étude récente employant la technique du déplacement du bromure d'éthidium (Strand et al., 2005). Pour une masse molaire constante d'environ 80 kDa, un DDA variant de 72 à 80% ne semble pas affecter l'affinité du chitosane pour l'ADN (environ 6 x 10^9 M^{-1}). Cependant, un DDA de 80% à 98% augmente de façon significative la constante d'affinité jusqu'à 14 x 10^9 M^{-1}. Si on compare les constantes d'affinité selon le nombre de monomères glucosamine sur les chaînes de chitosane, on remarque que l'augmentation du DDA de 80% à 98% (environ 80 kDa) a un effet plus important sur l'affinité du chitosane pour l'ADN qu'une augmentation de la masse molaire de 7 à 153 kDa (80% DDA). Ces résultats suggèrent que la densité de charge du

chitosane a un effet plus important sur l'affinité que sur la longueur de la chaîne ou le nombre total de charges. Cette étude a montré que les interactions électrostatiques gouvernent la complexation entre le chitosane et l'ADN.

La deuxième étude de mon projet de thèse (chapitre 5) était de développer une approche pour caractériser de façon précise les paramètres physico-chimiques des complexes ADN/chitosane. La quantification du chitosane libre et la mesure de la taille des particules dans une dispersion de complexes ADN/chitosane étaient les objectifs principaux de cette étude. C'était jusqu'à présent un défi à cause des difficultés techniques que présentent les méthodes conventionnelles. Dans l'approche que nous avons développée, nous avons combiné la technique de fractionnement par flux-force avec flux asymétrique (AF4) avec un spectrophotomètre UV-visible, un détecteur de diffusion de lumière multi-angles (MALS) et un détecteur de diffusion dynamique de lumière (DLS). La combinaison de ces détecteurs en ligne nous a permis de déterminer, en une seule étape, trois paramètres importants des complexes ADN/chitosane: la taille, la distribution de la taille des particules ainsi que la concentration du chitosane libre dans une dispersion. La technique AF4 sépare le chitosane libre des complexes dans une dispersion et le détecteur UV-vis en ligne permet de quantifier cette fraction. Nous avons trouvé que dans une dispersion ADN/chitosane préparé par mélange rapide avec un ratio N/P de 5 (ratio des groupements amine du chitosane par rapport aux groupements phosphate de l'ADN), 73% du chitosane était libre en solution, c'est à dire non complexé à l'ADN. Avec une seule injection, la technique AF4 a permis de fractionner les particules selon leur taille avant de mesurer avec précision le rayon hydrodynamique des particules et leur distribution en taille grâce au détecteur DLS. Pour un tel échantillon avec une polydispersité élevée, le DLS conventionnel en mode batch ne permettrait pas de mesurer la taille des petites particules qui diffusent moins de lumière que les grosses. Ainsi, nous avons pu déterminer le rayon hydrodynamique des complexes

ADN/chitosane (80% DDA et 42 kDa, N/P = 5) qui varie de 20 à 160 nm. Enfin, cette technique recueille des fractions à des temps d'élution différents pour analyser la taille et la morphologie des particules dans chaque fraction par microscopie électronique à balayage.

À l'aide de la méthode que nous avons développée et qui combine la technique AF4 avec des détecteurs UV/Vis, MALS et DLS, nous avons étudié l'effet du ratio N/P, de la concentration de l'ADN et des caractéristiques moléculaires du chitosane (DDA, M_n) sur la fraction de chitosane libre et les paramètres structuraux des complexes, tels que la taille, la distribution de la taille, la composition et la conformation des particules (chapitre 6). Ces paramètres ont été sélectionnés car ils peuvent influencer l'efficacité de transfection des complexes ADN/chitosane. Le système AF4 combiné avec les différents détecteurs nous a permis de déterminer en une seule étape tous ces paramètres pour chaque formulation de complexes ADN/chitosane. Dans les formulations analysées, nous avons trouvé que les complexes mesuraient tous de 15 à 160 nm de rayon hydrodynamique mais se différenciaient par leur distribution en taille. L'augmentation de la concentration d'ADN durant la préparation ou l'augmentation de la masse molaire du chitosane favorise la formation d'une plus grande proportion de grosses particules. Nous avons également trouvé une grande majorité de chitosane libre en solution dans les dispersions qui ont été préparées avec un excès de chitosane. La fraction de chitosane libre augmente de 53 à 92% lorsque le ratio N/P dans les dispersions varie de 3 à 15. À partir de ces résultats, nous avons calculé la composition réelle des complexes, exprimée en ratio N/P afin de faciliter la comparaison. Nous étions surpris de trouver que les complexes avaient tous un ratio N/P presque constant de 1.4, peu importe l'excès de chitosane utilisé dans la préparation et les caractéristiques du chitosane. Étant donné de l'impact de ces résultats sur la transfection, nous avons décidé de les valider par une méthode alternative. Nous avons donc centrifugé par ultracentrifugation chaque dispersion de complexes ADN/chitosane afin de précipiter les

complexes et recueillir le surnageant contenant le chitosane libre. Les surnageants ont été ensuite analysés par colorimétrie pour déterminer la concentration de chitosane libre. Les résultats obtenus par cette méthode ont bien confirmé les résultats obtenus par le système AF4. Nous avons démontré dans cette étude que le système AF4 est un outil puissant pour la caractérisation des complexes ADN/chitosane. De plus, cette étude a révélé l'importance de quantifier le polycation libre des formulations pour la transfection et de comprendre son rôle dans la livraison de gènes.

Après la caractérisation de l'affinité chitosane-ADN par ITC et des propriétés physico-chimiques des complexes ADN/chitosane, nous avons déterminé leur stabilité en présence de différents biopolymères anioniques (annexe 2). Ces polyanions compétiteurs peuvent dissocier les complexes ADN/chitosane pour se lier au chitosane par des interactions électrostatiques et relâcher l'ADN en solution. La spectroscopie de fluorescence a été utilisée pour détecter et quantifier l'ADN dissocié du chitosane en utilisant le Picogreen comme marqueur fluorescent pour l'ADN. Nous avons trouvé que la stabilité des complexes ADN/chitosane dépend de plusieurs facteurs : la densité de charge du polyanion compétiteur ainsi que la masse molaire, le DDA et la concentration du chitosane (ratio N/P). La stabilité des complexes ADN/chitosane est bien reliée à l'affinité du chitosane pour l'ADN que nous avons caractérisée dans le chapitre 4. Elle augmente avec le DDA et la masse molaire du chitosane. Parmi les polyanions compétiteurs utilisés, l'héparine qui possède la plus grande densité de charge, était le seul à pouvoir dissocier les complexes ADN/chitosane. Ceci est expliqué par sa constante d'affinité avec le chitosane (déterminée par ITC) qui est seulement deux fois plus élevée comparée à celle du couple chitosane-ADN. Les autres polyanions compétiteurs ne peuvent pas causer la rupture des complexes ADN/chitosane car leur affinité pour le chitosane est très faible par rapport au couple chitosane-ADN, soit 40 à 200 fois moins élevé selon les conditions utilisées.

La stabilité des complexes ADN/chitosane en présence d'héparine dépend également du ratio N/P dans la dispersion. La quantité d'ADN dissocié des complexes par l'héparine diminue avec l'augmentation du ratio N/P. À un certain ratio N/P, il y a suffisamment de chitosane pour l'ADN et l'héparine, sans que les complexes soient dissociés. Ceci a été vérifié par la quantification du chitosane libre dans les dispersions avant de les exposer à l'héparine. Cependant, le ratio N/P dans les dispersions doit augmenter avec la concentration d'héparine en solution afin d'avoir plus de chitosane libre pour interagir avec l'héparine et éviter la dissociation des complexes. Cependant, une concentration trop élevée de polycation libre pourrait nuire à l'internalisation des complexes ADN/polycation, et induire une toxicité selon le type de polycation. Cette étude a permis de corréler la stabilité des complexes ADN/chitosane à l'affinité des composantes et a également révélé l'importance du chitosane libre pour la livraison de gènes. Le chitosane libre pourrait prévenir la dissociation prématurée des complexes ADN/chitosane lors des interactions avec les composantes extracellulaires ou pourrait contribuer à la rupture des endosomes selon l'hypothèse du *proton sponge effect*.

CONCLUSION ET RECOMMANDATIONS

Une étude thermodynamique de l'association entre le chitosane et l'ADN a été réalisée pour la première fois en utilisant la microcalorimétrie de titrage isotherme (ITC). Nous avons trouvé que la formation des complexes ADN/chitosane est gouvernée par des interactions électrostatiques. Elle est également couplée par un transfert de protons du système tampon au chitosane induit par le caractère fortement anionique de l'ADN. Ce transfert permet la formation de complexes à un pH supérieur au p*K*a du chitosane, dans des conditions où le chitosane en solution est faiblement ionisé. Les changements d'ionisation du chitosane et du système tampon associés au transfert de protons contribuent entièrement à l'enthalpie d'interaction mesurée. Nous avons trouvé que la constante d'affinité entre le chitosane et l'ADN est fortement influencée par le pH ainsi que la masse molaire et le degré de désacétylation (DDA) du chitosane.

Une grande affinité entre l'ADN et un chitosane avec une masse molaire ou une valeur de DDA élevée favorise des complexes stables qui seront résistants à la dissociation par des composantes biologiques chargées négativement. Par contre, ils seront trop stables pour pouvoir relâcher l'ADN à l'intérieur du noyau afin de permettre l'expression des gènes. D'un autre côté, une affinité trop faible entre l'ADN et un chitosane avec une masse molaire ou un DDA faible mène à la formation de complexes peu stables qui vont se dissocier avant même l'internalisation dans les cellules. Cette relation entre l'affinité du chitosane pour l'ADN et la stabilité de leurs complexes a été vérifiée par une étude où nous avons utilisés des polyanions compétiteurs pour induire la dissociation des complexes. Nous avons trouvé que les polyanions fortement chargés, comme l'héparine, peuvent dissocier les complexes. Quant aux polyanions avec une faible densité de charges comme l'acide hyaluronique, ils ne peuvent pas déstabiliser les complexes en

raison de leur affinité beaucoup plus faible pour le chitosane par rapport celle de l'ADN. Les résultats dérivés de ces deux études corrèlent bien avec l'efficacité de transfection des complexes ADN/chitosane. Ils représentent des lignes directrices pour le développement de systèmes de livraison de gènes efficaces qui seront suffisamment stables pour éviter une dissociation prématurée et, en même temps, permettront à l'ADN de se libérer dans le noyau des cellules pour la transcription des gènes.

Les propriétés physico-chimiques des complexes ADN/chitosane telles que la taille et la charge de surface des particules, peuvent également influencer la livraison de gènes. Il est donc important de bien les caractériser afin d'établir une corrélation avec l'efficacité de transfection des complexes. Dans le cadre de ce projet, nous avons développé une nouvelle approche pour la caractérisation des complexes ADN/polycation, combinant la technique de fractionnement par flux-force avec flux asymétrique (AF4) avec un spectrophotomètre UV-visible, un détecteur de diffusion de lumière multi-angles (MALS) et un détecteur de diffusion dynamique de lumière (DLS). Ce système AF4 a permis de caractériser, en une seule étape et avec précision, plusieurs propriétés physico-chimiques d'une dispersion de complexes ADN/chitosane : la taille, la distribution de taille et la conformation des particules ainsi que la fraction de chitosane libre permettant le calcul de la composition réelle des particules.

Nous avons utilisé ce système pour déterminer l'effet de plusieurs facteurs importants sur ces propriétés, tels que le ratio N/P, la concentration d'ADN, la masse molaire et le DDA du chitosane. Nous avons utilisé un excès de chitosane par rapport à l'ADN (ratio N/P) dans la préparation des complexes, une condition nécessaire pour condenser l'ADN et avoir des particules chargées positivement. De plus, plusieurs études ont montré de meilleures efficacités de transfection avec des ratios N/P très élevés. Nous n'avons pas observé de différences concernant l'intervalle de tailles hydrodynamiques mesurées entre les différentes formulations.

Par contre, la proportion de grosses particules augmente avec la concentration d'ADN et la masse molaire du chitosane. Nous avons trouvé que la majorité du chitosane était libre en solution. Peu importante l'excès de chitosane ajouté, la composition des complexes était la même et correspondait à un ratio N/P de 1.4. Les résultats de cette étude montrent l'importance de quantifier le polycation libre dans les dispersions de complexes ADN/polycation afin de comprendre son rôle dans la livraison de gènes.

Différentes recommandations peuvent être faîtes pour poursuivre ce travail. Tout d'abord, il serait important d'étudier la stabilité colloïdale des complexes ADN/chitosane dans des conditions physiologiques. Le système AF4 serait très utile pour cette étude. Il serait intéressant de déterminer comment les paramètres d'interaction avec l'ADN seront influencés par la modification du chitosane (par exemple, la pegylation pour la stabilisation stérique, le greffage de ligands pour une livraison de gènes ciblée et l'ajout de peptides endosomolytiques). D'autres types d'interactions pourraient être identifiés par ITC selon leur contribution à la chaleur mesurée. Une étude thermodynamique de l'association entre le chitosane et différents types d'acides nucléiques (oligonucléotides, ARN) serait également intéressante. Elle permettrait d'obtenir des informations très utiles pour le développement de systèmes dédiés à la livraison d'ARN d'interférences pour le silençage génique. Le système AF4 pourrait également être utilisé pour la caractérisation de ces systèmes.

BIBLIOGRAPHIE

Andersson, M., Wittgren, B. et Wahlund, K.-G. (2001). Ultrahigh molar mass component detected in ethylhydroxyethyl cellulose by asymmetrical flow field-flow fractionation coupled to multiangle light scattering. *Anal. Chem., 73*(20), 4852-4861.

Andersson, M., Wittgren, B. et Wahlund, K.-G. (2003). Accuracy in multiangle light scattering measurements for molar mass and radius estimations. Model calculations and experiments. *Anal. Chem., 75*(16), 4279-4291.

Augsten, C., Kiselev, M. A., Gehrke, R., Hause, G. et Mäder, K. (2008). A detailed analysis of biodegradable nanospheres by different techniques - a combined approach to detect particle sizes and size distributions. *J. Pharm. Biomed. Anal., 47*(1), 95-102.

Augsten, C. et Maeder, K. (2008). Characterizing molar mass distributions and molecule structures of different chitosans using asymmetrical flow field-flow fractionation combined with multi-angle light scattering. *Int. J. Pharm., 351*(1-2), 23-30.

Behr, J.-P. (1997). The proton sponge: A trick to enter cells the viruses did not exploit. *Chimia, 51*, 34-36.

Berry, G. C. (1966). Thermodynamic and conformational properties of polystyrene. I. Light-scattering studies on dilute solutions of linear polystyrenes. *J. Chem. Phys., 44*(12), 4550-4564.

Bertschinger, M., Backliwal, G., Schertenleib, A., Jordan, M., Hacker, D. L. et Wurm, F. M. (2006). Disassembly of polyethylenimine-DNA particles in vitro: Implications for polyethylenimine-mediated DNA delivery. *J. Control. Release, 116*(1), 96-104.

Bloomfield, V. A., Crothers, D. M. et Tinoco, I., Jr. (2000). *Nucleic acids: Structures, properties and functions*. Sausalito, CA: University Science Books.

Boeckle, S., von Gersdorff, K., van der Piepen, S., Culmsee, C., Wagner, E. et Ogris, M. (2004). Purification of polyethylenimine polyplexes highlights the role of free polycations in gene transfer. *J. Gene Med., 6*(10), 1102-1111.

Bootz, A., Vogel, V., Schubert, D. et Kreuter, J. (2004). Comparison of scanning electron microscopy, dynamic light scattering and analytical ultracentrifugation for the sizing of poly(butyl cyanoacrylate) nanoparticles. *Euro. J. Pharm. Biopharm., 57*(2), 369-375.

Boussif, O., Lezoualc'h, F., Zanta, M. A., Mergny, M. D., Scherman, D., Demeneix, B. et Behr, J. P. (1995). A versatile vector for gene and oligonucleotide transfer into cells in culture and in vivo: Polyethylenimine. *Proc. Natl. Acad. Sci. USA, 92*(16), 7297-7301.

Bronich, T., Kabanov, A. V. et Marky, L. A. (2001). A thermodynamic characterization of the interaction of a cationic copolymer with DNA. *J. Phys. Chem. B, 105*(25), 6042-6050.

Burchard, W. (1983). Static and dynamic light scattering from branched polymers and biopolymers. *Adv. Polym. Sci., 48*, 1-124.

Burchard, W. (1996). Combined static and dynamic light scattering. In W. Brown, (éd.), *Light scattering: Principles and development* (pp. 439-476). New York: Oxford University Press.

Casu, B. et Gennaro, U. (1975). Conductimetric method for the determination of sulfate and carboxyl groups in heparin and other mucopolysaccharides. *Carbohydrate Research, 39*(1), 168-176.

Chen, W., Turro, N. J. et Tomalia, D. A. (2000). Using ethidium bromide to probe the interactions between DNA and dendrimers. *Langmuir, 16*(1), 15-19.

Choosakoonkriang, S., Lobo, B. A., Koe, G. S., Koe, J. G. et Middaugh, C. R. (2003). Biophysical characterization of PEI/DNA complexes. *J. Pharm. Sci., 92*(8), 1710-1722.

Chu, B. (1991). *Laser light scattering: Basic principles and practice* (2e éd.). Boston: Academic Press.

Citkowicz, A., Petry, H., Harkins, R. N., Ast, O., Cashion, L., Goldmann, C., Bringmann, P., Plummer, K. et Larsen, B. R. (2008). Characterization of virus-like particle assembly for DNA delivery using asymmetrical flow field-flow fractionation and light scattering. *Anal. Biochem., 376*(2), 163-172.

Clamme, J. P., Azoulay, J. et Mely, Y. (2003). Monitoring of the formation and dissociation of polyethylenimine/DNA complexes by two photon fluorescence correlation spectroscopy. *Biophys. J., 84*(3), 1960-1968.

Crini, G., Guibal, É., Morcellet, M., Torri, G. et Badot, P.-M. (2009). Chitine et chitosane. Préparation, propriétés et principales applications. In *Chitine et chitosane du biopolymère à l'application* (pp. 19-54). Besançon: Presses universitaires de Franche-Comté.

Danielsen, S., Maurstad, G. et Stokke, B. T. (2005). DNA-polycation complexation and polyplex stability in the presence of competing polyanions. *Biopolymers, 77*(2), 86-97.

Danielsen, S., Strand, S., de Lange Davies, C. et Stokke, B. T. (2005). Glycosaminoglycan destabilization of DNA-chitosan polyplexes for gene delivery depends on chitosan chain length and GAG properties. *Biochim. Biophys. Acta Gen. Subj., 1721*(1-3), 44-54.

Danielsen, S., Varum, K. M. et Stokke, B. T. (2004). Structural analysis of chitosan mediated DNA condensation by afm: Influence of chitosan molecular parameters. *Biomacromolecules, 5*(3), 928-936.

Darras, V., Nelea, M., Winnik, F. M. et Buschmann, M. D. (2010). Chitosan modified with gadolinium diethylenetriaminepentaacetic acid for magnetic resonance imaging of DNA/chitosan nanoparticles. *Carbohydr. Polym., 80*(4), 1137-1146.

Dean, J. A. (1999). *Lange's handbook of chemistry* (15e éd.). New York: McGraw-Hill.

Debye, P. (1947). Molecular-weight determination by light scattering. *J. Phys. Colloid Chem., 51*(1), 18-32.

Dickerson, R. E., Drew, H. R., Conner, B. N., Wing, R. M., Fratini, A. V. et Kopka, M. L. (1982). The anatomy of A-, B-, and Z-DNA. *Science, 216*(4545), 475-485.

Drogoz, A., David, L., Rochas, C., Domard, A. et Delair, T. (2007). Polyelectrolyte complexes from polysaccharides: Formation and stoichiometry monitoring. *Langmuir, 23*(22), 10950-10958.

Duceppe, N. et Tabrizian, M. (2009). Factors influencing the transfection efficiency of ultra low molecular weight chitosan/hyaluronic acid nanoparticles. *Biomaterials, 30*(13), 2625-2631.

Ehtezazi, T., Rungsardthong, U. et Stolnik, S. (2003). Thermodynamic analysis of polycation-DNA interaction applying titration microcalorimetry. *Langmuir, 19*(22), 9387-9394.

Erbacher, P., Bettinger, T., Brion, E., Coll, J.-L., Plank, C., Behr, J.-P. et Remy, J.-S. (2004). Genuine DNA/polyethylenimine (PEI) complexes improve transfection properties and cell survival. *J. Drug Targeting, 12*(4), 223 - 236.

Filion, D., Lavertu, M. et Buschmann, M. D. (2007). Ionization and solubility of chitosan solutions related to thermosensitive chitosan/glycerol-phosphate systems. *Biomacromolecules, 8*(10), 3224-3234.

Fraunhofer, W., Winter, G. et Coester, C. (2004). Asymmetrical flow field-flow fractionation and multiangle light scattering for analysis of gelatin nanoparticle drug carrier systems. *Anal. Chem., 76*(7), 1909-1920.

Funhoff, A. M., van Nostrum, C. F., Koning, G. A., Schuurmans-Nieuwenbroek, N. M. E., Crommelin, D. J. A. et Hennink, W. E. (2004). Endosomal escape of polymeric gene delivery complexes is not always enhanced by polymers buffering at low pH. *Biomacromolecules, 5*(1), 32-39.

Gabrielson, N. P. et Pack, D. W. (2006). Acetylation of polyethylenimine enhances gene delivery via weakened polymer/DNA interactions. *Biomacromolecules, 7*(8), 2427-2435.

Germershaus, O., Mao, S., Sitterberg, J., Bakowsky, U. et Kissel, T. (2008). Gene delivery using chitosan, trimethyl chitosan or polyethylenglycol-graft-trimethyl chitosan block copolymers: Establishment of structure-activity relationships in vitro. *J. Control. Release, 125*(2), 145-154.

Godbey, W. T., Wu, K. K. et Mikos, A. G. (2001). Poly(ethylenimine)-mediated gene delivery affects endothelial cell function and viability. *Biomaterials, 22*(5), 471-480.

Goldberg, R. N., Kishore, N. et Lennen, R. M. (2002). Thermodynamic quantities for the ionization reactions of buffers. *J. Phys. Chem. Ref. Data, 31*(2), 231-370.

Hinz, H. J., Shiao, D. D. F. et Sturtevant, J. M. (1971). Calorimetric investigation of inhibitor binding to rabbit muscle aldolase. *Biochemistry, 10*(8), 1347-1352.

Howard, K. A., Paludan, S. R., Behlke, M. A., Besenbacher, F., Deleuran, B. et Kjems, J. (2008). Chitosan/siRNA nanoparticle-mediated tnf-[alpha] knockdown in peritoneal macrophages for anti-inflammatory treatment in a murine arthritis model. *Mol. Ther., 17*(1), 162-168.

Huang, D., Korolev, N., Eom, K. D., Tam, J. P. et Nordenskiöld, L. (2008). Design and biophysical characterization of novel polycationic ε-peptides for DNA compaction and delivery. *Biomacromolecules, 9*(1), 321-330.

Huang, M., Fong, C.-W., Khor, E. et Lim, L.-Y. (2005). Transfection efficiency of chitosan vectors: Effect of polymer molecular weight and degree of deacetylation. *J.Control. Rel., 106*(3), 391-406.

Hupfeld, S., Moen, H. H., Ausbacher, D., Haas, H. et Brandl, M. (2010). Liposome fractionation and size analysis by asymmetrical flow field-flow fractionation/multi-angle light scattering: Influence of ionic strength and osmotic pressure of the carrier liquid. *Chem. Phys. Lipids, 163*(2), 141-147.

Ilich, P., Mishra, P. K., Macura, S. et Burghardt, T. P. (1996). Direct observation of rhodamine dimer structures in water. *Spectrochim. Acta A: Mol. Biomol. Spectrosc., 52*(10), 1323-1330.

Ise, N. et Okubo, T. (1966). Mean activity coefficient of polyelectrolytes. III. Measurements of hydrochlorides of polyethylenimine and its low molecular weight analogs. *J. Phys. Chem., 70*(7), 2400-2405.

Ise, N. et Okubo, T. (1968). Mean activity coefficient of polyelectrolytes. X. Activity coefficients of polyphosphates of various gegenions. *J. Phys. Chem., 72*(4), 1370-1373.

Ishii, T., Okahata, Y. et Sato, T. (2001). Mechanism of cell transfection with plasmid/chitosan complexes. *Biochim. Biophys. Acta Biomembr., 1514*(1), 51-64.

Ito, T., Iida-Tanaka, N., Niidome, T., Kawano, T., Kubo, K., Yoshikawa, K., Sato, T., Yang, Z. et Koyama, Y. (2006). Hyaluronic acid and its derivative as a multi-functional gene expression enhancer: Protection from non-specific interactions, adhesion to targeted cells, and transcriptional activation. *J. Control. Release, 112*(3), 382-388.

Izume, M., Nagae, S., Kawagishi, H., Mitsutomi, M. et Ohtakara, A. (1992). Action pattern of bacillus SP NO-7-M chitosanase on partially N-acetylated chitosan. *Biosci. Biotech. Biochem., 56*(3), 448-453.

Izumrudov, V. A., Zhiryakova, M. V. et Goulko, A. A. (2002). Ethidium bromide as a promising probe for studying DNA interaction with cationic amphiphiles and stability of the resulting complexes. *Langmuir, 18*(26), 10348-10356.

Jahn, A., Vreeland, W. N., DeVoe, D. L., Locascio, L. E. et Gaitan, M. (2007). Microfluidic directed formation of liposomes of controlled size. *Langmuir, 23*(11), 6289-6293.

Jean, M., Smaoui, F., Lavertu, M., Methot, S., Bouhdoud, L., Buschmann, M. D. et Merzouki, A. (2009). Chitosan-plasmid nanoparticle formulations for im and sc delivery of recombinant FGF-2 and PDGF-BB or generation of antibodies. *Gene Therapy, 16*(9), 1097-1110.

Kang, D. Y., Kim, M. J., Kim, S. T., Oh, K. S., Yuk, S. H. et Lee, S. (2008). Size characterization of drug-loaded polymeric core/shell nanoparticles using asymmetrical flow field-flow fractionation. *Anal. Bioanal. Chem., 390*(8), 2183-2188.

Kiang, T., Wen, J., Lim, H. W. et Leong, K. W. (2004). The effect of the degree of chitosan deacetylation on the efficiency of gene transfection. *Biomaterials, 25*(22), 5293-5301.

Kim, T.-H., Jiang, H.-L., Jere, D., Park, I.-K., Cho, M.-H., Nah, J.-W., Choi, Y.-J., Akaike, T. et Cho, C.-S. (2007). Chemical modification of chitosan as a gene carrier in vitro and in vivo. *Prog. Polym. Sci., 32*(7), 726-753.

Kim, W., Yamasaki, Y. et Kataoka, K. (2006). Development of a fitting model suitable for the isothermal titration calorimetric curve of DNA with cationic ligands. *J. Phys. Chem. B, 110*(22), 10919-10925.

Koetz, J., Linow, K. J., Philipp, B., Hu, L. P. et Vogl, O. (1986). Effects of charge density and structure of side-chain branching on the composition of polyanion-polycation complexes. *Polymer, 27*(10), 1574-1580.

Koping-Hoggard, M., Tubulekas, I., Guan, H., Edwards, K., Nilsson, M., Varum, K. M. et Artursson, P. (2001). Chitosan as a nonviral gene delivery system. Structure-property relationships and characteristics compared with polyethylenimine in vitro and after lung administration in vivo. *Gene Therapy, 8*(14), 1108-1121.

Koping-Hoggard, M., Varum, K. M., Issa, M., Danielsen, S., Christensen, B. E., Stokke, B. T. et Artursson, P. (2004). Improved chitosan-mediated gene delivery based on easily dissociated chitosan polyplexes of highly defined chitosan oligomers. *Gene Therapy, 11*(19), 1441-1452.

Koyama, Y., Yamashita, M., Iida-Tanaka, N. et Ito, T. (2006). Enhancement of transcriptional activity of DNA complexes by amphoteric PEG derivative. *Biomacromolecules, 7*(4), 1274-1279.

Kujawa, P., Schmauch, G., Viitala, T., Badia, A. et Winnik, F. M. (2007). Construction of viscoelastic biocompatible films via the layer-by-layer assembly of hyaluronan and phosphorylcholine-modified chitosan. *Biomacromolecules, 8*(10), 3169-3176.

Kulkarni, R. P., Mishra, S., Fraser, S. E. et Davis, M. E. (2005). Single cell kinetics of intracellular, nonviral, nucleic acid delivery vehicle acidification and trafficking. *Bioconj. Chem., 16*(4), 986-994.

Kumler, W. D. et Eiler, J. J. (1943). The acid strength of mono and diesters of phosphoric acid. The N-alkyl esters from methyl to butyl, the esters of biological importance, and the natural guanidine phosphoric acids. *J. Am. Chem. Soc., 65*(12), 2355-2361.

Lavertu, M., Filion, D. et Buschmann, M. D. (2008). Heat-induced transfer of protons from chitosan to glycero phosphate produces chitosan precipitation and gelation. *Biomacromolecules, 9*(2), 640-650.

Lavertu, M., Methot, S., Tran-Khanh, N. et Buschmann, M. D. (2006). High efficiency gene transfer using chitosan/DNA nanoparticles with specific combinations of molecular weight and degree of deacetylation. *Biomaterials, 27*(27), 4815-4824.

Lavertu, M., Xia, Z., Serreqi, A. N., Berrada, M., Rodrigues, A., Wang, D., Buschmann, M. D. et Gupta, A. (2003). A validated ^{1}H NMR method for the determination of the degree of deacetylation of chitosan. *J. Pharm. Biomed. Anal., 32*(6), 1149-1158.

Layman, J. M., Ramirez, S. M., Green, M. D. et Long, T. E. (2009). Influence of polycation molecular weight on poly(2-dimethylaminoethyl methacrylate)-mediated DNA delivery in vitro. *Biomacromolecules, 10*(5), 1244-1252.

Le Cerf, D., Simon, S., Argillier, J.-F. et Picton, L. (2007). Contribution of flow field flow fractionation with on line static and dynamic light scattering to the study of hydrosoluble polyelectrolyte complexes. *Anal. Chim. Acta, 604*(1), 2-8.

Le Pecq, J. B. et Paoletti, C. (1967). A fluorescent complex between ethidium bromide and nucleic acids. Physical-chemical characterization. *J. Mol. Biol., 27*(1), 87-106.

Lee, H., Williams, S. K. R., Allison, S. D. et Anchordoquy, T. J. (2001). Analysis of self-assembled cationic lipid-DNA gene carrier complexes using flow field-flow fractionation and light scattering. *Anal. Chem., 73*(4), 837-843.

Lee, S., Rao, S. P., Moon, M. H. et Giddings, J. C. (1996). Determination of mean diameter and particle size distribution of acrylate latex using flow field-flow fractionation, photon correlation spectroscopy, and electron microscopy. *Anal. Chem., 68*(9), 1545-1549.

Liu, M. K. et Giddings, J. C. (1993). Separation and measurement of diffusion coefficients of linear and circular DNAs by flow field-flow fractionation. *Macromolecules, 26*(14), 3576-3588.

Liu, W., Sun, S., Cao, Z., Zhang, X., Yao, K., Lu, W. W. et Luk, K. D. K. (2005). An investigation on the physicochemical properties of chitosan/DNA polyelectrolyte complexes. *Biomaterials, 26*(15), 2705-2711.

Liu, X., Howard, K. A., Dong, M., Andersen, M. O., Rahbek, U. L., Johnsen, M. G., Hansen, O. C., Besenbacher, F. et Kjems, J. (2007). The influence of polymeric properties on chitosan/siRNA nanoparticle formulation and gene silencing. *Biomaterials, 28*(6), 1280-1288.

Liu, Y. et Reineke, T. M. (2010). Degradation of poly(glycoamidoamine) DNA delivery vehicles: Polyamide hydrolysis at physiological conditions promotes DNA release. *Biomacromolecules, 11*(2), 316-325.

Liu, Y. et Sturtevant, J. M. (1997). Significant discrepancies between van't hoff and calorimetric enthalpies. Iii. *Biophys. Chem., 64*(1-3), 121-126.

Lobo, B. A., Koe, G. S., Koe, J. G. et Middaugh, C. R. (2003). Thermodynamic analysis of binding and protonation in DOTAP/DOPE (1:1): DNA complexes using isothermal titration calorimetry. *Biophys. Chem., 104*(1), 67-78.

Lukacs, G. L., Haggie, P., Seksek, O., Lechardeur, D., Freedman, N. et Verkman, A. S. (2000). Size-dependent DNA mobility in cytoplasm and nucleus. *J. Biol. Chem., 275*(3), 1625-1629.

Lundback, T. et Hard, T. (1996). Salt dependence of the free energy, enthalpy, and entropy of nonsequence specific DNA binding. *J. Phys. Chem., 100*(44), 17690-17695.

Luzio, J. P., Mullock, B. M., Pryor, P. R., Lindsay, M. R., James, D. E. et Piper, R. C. (2001). Relationship between endosomes and lysosomes. *Biochem. Soc. Trans., 29*(4), 476-480.

Ma, O., Lavertu, M., Sun, J., Nguyen, S., Buschmann, M. D., Winnik, F. M. et Hoemann, C. D. (2008). Precise derivatization of structurally distinct chitosans with rhodamine B isothiocyanate. *Carbohydr. Polym., 72*(4), 616-624.

Ma, P. L., Buschmann, M. D. et Winnik, F. M. (2010a). One-step analysis of DNA/chitosan complexes by field-flow fractionation reveals particle size and free chitosan content. *Biomacromolecules, 11*(3), 549-554.

Ma, P. L., Buschmann, M. D. et Winnik, F. M. (2010b). Simultaneous determination of unbound polycation and particle size of DNA/chitosan complexes by asymmetrical flow field-flow fractionation. *Anal. Chem., Submitted*.

Ma, P. L., Lavertu, M., Winnik, F. M. et Buschmann, M. D. (2009). New insights into chitosan-DNA interactions using isothermal titration microcalorimetry. *Biomacromolecules, 10*(6), 1490-1499.

MacLaughlin, F. C., Mumper, R. J., Wang, J., Tagliaferri, J. M., Gill, I., Hinchcliffe, M. et Rolland, A. P. (1998). Chitosan and depolymerized chitosan oligomers as condensing carriers for in vivo plasmid delivery. *J. Control. Release, 56*(1-3), 259-272.

Mao, H. Q., Roy, K., Troung-Le, V. L., Janes, K. A., Lin, K. Y., Wang, Y., August, J. T. et Leong, K. W. (2001). Chitosan-DNA nanoparticles as gene carriers: Synthesis, characterization and transfection efficiency. *J. Control. Release, 70*(3), 399-421.

Mao, S., Augsten, C., Maeder, K. et Kissel, T. (2007). Characterization of chitosan and its derivatives using asymmetrical flow field-flow-fractionation: A comparison with traditional methods. *J. Pharm. Biomed. Anal., 45*(5), 736-741.

Mao, S., Shuai, X., Unger, F., Wittmar, M., Xie, X. et Kissel, T. (2005). Synthesis, characterization and cytotoxicity of poly(ethylene glycol)-graft-trimethyl chitosan block copolymers. *Biomaterials, 26*(32), 6343-6356.

Marshall, E. (1999). Gene therapy death prompts review of adenovirus vector. *Science, 286*(5448), 2244.

Maurstad, G., Danielsen, S. et Stokke, B. T. (2007). The influence of charge density of chitosan in the compaction of the polyanions DNA and xanthan. *Biomacromolecules, 8*(4), 1124-1130.

McGhee, J. D. et von Hippel, P. H. (1974). Theoretical aspects of DNA-protein interactions: Co-operative and non-co-operative binding of large ligands to a one dimensional homogeneous lattice. *J. Mol. Biol., 86*, 469-489.

MicroCal LLC. (2004). *Itc data analysis in origin, tutorial guide, version 7.* . Northampton, MA.

Mima, S., Miya, M., Iwamoto, R. et Yoshikawa, S. (1983). Highly deacetylated chitosan and its properties. *J. Appl. Polym. Sci., 28*(6), 1909-1917.

Mintzer, M. A. et Simanek, E. E. (2009). Nonviral vectors for gene delivery. *Chem. Rev., 109*(2), 259-302.

Mislick, K. A. et Baldeschwieler, J. D. (1996). Evidence for the role of proteoglycans in cation-mediated gene transfer. *Proc. Natl. Acad. Sci. USA, 93*(22), 12349-12354.

Misra, V. K., Hecht, J. L., Yang, A.-S. et Honig, B. (1998). Electrostatic contributions to the binding free energy of the lambda ci repressor to DNA. *Biophys. J., 75*(5), 2262-2273.

Misra, V. K. et Honig, B. (1995). On the magnitude of the electrostatic contribution to ligand-DNA interactions. *Proc. Natl. Acad. Sci. USA, 92*(10), 4691-4695.

Miyata, K., Kakizawa, Y., Nishiyama, N., Harada, A., Yamasaki, Y., Koyama, H. et Kataoka, K. (2004). Block catiomer polyplexes with regulated densities of charge and disulfide cross-linking directed to enhance gene expression. *J. Am. Chem. Soc., 126*(8), 2355-2361.

Moret, I., Esteban Peris, J., Guillem, V. M., Benet, M., Revert, F., Dasí, F., Crespo, A. et Aliño, S. F. (2001). Stability of PEI-DNA and DOTAP-DNA complexes: Effect of alkaline pH, heparin and serum. *J. Control. Release, 76*(1-2), 169-181.

Morille, M., Passirani, C., Vonarbourg, A., Clavreul, A. et Benoit, J.-P. (2008). Progress in developing cationic vectors for non-viral systemic gene therapy against cancer. *Biomaterials, 29*(24-25), 3477-3496.

Mumper, R. J., Wang, J., Claspell, J. M. et Rolland, A. P. (1995). Novel polymeric condensing carriers for gene delivery. *Proceedings of the 22nd International Symposium on Controlled Release of Bioactive Materials*, *Seattle, WA* (Vol. 22, pp. 178-179)Controlled Release Society.

Nguyen, B., Stanek, J. et Wilson, W. D. (2006). Binding-linked protonation of a DNA minor-groove agent. *Biophys. J., 90*(4), 1319-1328.

Nguyen, S., Winnik, F. M. et Buschmann, M. D. (2009). Improved reproducibility in the determination of the molecular weight of chitosan by analytical size exclusion chromatography. *Carbohydr. Polym., 75*(3), 528-533.

Ogris, M., Steinlein, P., Kursa, M., Mechtler, K., Kircheis, R. et Wagner, E. (1998). The size of DNA/transferrin-PEI complexes is an important factor for gene expression in cultured cells. *Gene Therapy, 5*(10), 1425-1433.

Oupicky, D., Konak, C., Ulbrich, K., Wolfert, M. A. et Seymour, L. W. (2000). DNA delivery systems based on complexes of DNA with synthetic polycations and their copolymers. *J. Control. Release, 65*(1-2), 149-171.

Pasternack, R. F., Caccam, M., Keogh, B., Stephenson, T. A., Williams, A. P. et Gibbs, E. J. (1991). Long-range fluorescence quenching of ethidium ion by cationic porphyrins in the presence of DNA. *J. Am. Chem. Soc., 113*(18), 6835-6840.

Pauck, T. et Colfen, H. (1998). Hydrodynamic analysis of macromolecular conformation. A comparative study of flow field flow fractionation and analytical ultracentrifugation. *Anal. Chem., 70*(18), 3886-3891.

Philipp, B., Dautzenberg, H., Linow, K. J., Koetz, J. et Dawydoff, W. (1989). Polyelectrolyte complexes - recent developments and open problems. *Prog. Polym. Sci., 14*(1), 91-172.

Prestel, H., Niessner, R. et Panne, U. (2006). Increasing the sensitivity of asymmetrical flow field-flow fractionation: slot outlet technique. *Anal. Chem., 78*(18), 6664-6669.

Prevette, L. E., Kodger, T. E., Reineke, T. M. et Lynch, M. L. (2007). Deciphering the role of hydrogen bonding in enhancing pDNA-polycation interactions. *Langmuir, 23*(19), 9773-9784.

Prevette, L. E., Lynch, M. L., Kizjakina, K. et Reineke, T. M. (2008). Correlation of amine number and pDNA binding mechanism for trehalose-based polycations. *Langmuir, 24*(15), 8090-8101.

Rawn, J. D. (1990). *Traité de biochimie*. Bruxelles: De Boeck Université.

Reitan, N. K., Maurstad, G., de Lange Davies, C. et Strand, S. P. (2009). Characterizing DNA condensation by structurally different chitosans of variable gene transfer efficacy. *Biomacromolecules, 10*(6), 1508-1515.

Ren, X. et Xu, Q.-H. (2008). Label-free DNA sequence detection with enhanced sensitivity and selectivity using cationic conjugated polymers and picogreen. *Langmuir, 25*(1), 43-47.

Rinaudo, M. (2006). Chitin and chitosan: Properties and applications. *Prog. Polym. Sci., 31*(7), 603-632.

Roberts, G. A. F. (1992). *Chitin chemistry*. London: Macmillan.

Romoren, K., Pedersen, S., Smistad, G., Evensen, O. et Thu, B. J. (2003). The influence of formulation variables on in vitro transfection efficiency and physicochemical properties of chitosan-based polyplexes. *Int. J. Pharm., 261*(1-2), 115-127.

Rungsardthong, U., Ehtezazi, T., Bailey, L., Armes, S. P., Garnett, M. C. et Stolnik, S. (2003). Effect of polymer ionization on the interaction with DNA in nonviral gene delivery systems. *Biomacromolecules, 4*(3), 683-690.

Ruponen, M., Honkakoski, P., Ronkko, S., Pelkonen, J., Tammi, M. et Urtti, A. (2003). Extracellular and intracellular barriers in non-viral gene delivery. *J. Control. Release, 93*(2), 213-217.

Ruponen, M., Ronkko, S., Honkakoski, P., Pelkonen, J., Tammi, M. et Urtti, A. (2001). Extracellular glycosaminoglycans modify cellular trafficking of lipoplexes and polyplexes. *J. Biol. Chem., 276*(36), 33875-33880.

Ruponen, M., Yla-Herttuala, S. et Urtti, A. (1999). Interactions of polymeric and liposomal gene delivery systems with extracellular glycosaminoglycans: Physicochemical and transfection studies. *Biochim. Biophys. Acta Biomembr., 1415*(2), 331-341.

Sato, T., Ishii, T. et Okahata, Y. (2001). In vitro gene delivery mediated by chitosan. Effect of pH, serum, and molecular mass of chitosan on the transfection efficiency. *Biomaterials, 22*(15), 2075-2080.

Saul, J. M., Wang, C. H. K., Ng, C. P. et Pun, S. H. (2008). Multilayer nanocomplexes of polymer and DNA exhibit enhanced gene delivery. *Advanced Materials, 20*(1), 19-25.

Schaffer, D. V., Fidelman, N. A., Dan, N. et Lauffenburger, D. A. (2000). Vector unpacking as a potential barrier for receptor-mediated polyplex gene delivery. *Biotechnol. Bioeng., 67*(5), 598-606.

Schimpf, M. E., Caldwell, K., Giddings, J. C. et Eds. (2000). *Field-flow fractionation handbook*. New York: John Wiley & Sons.

Schwarz, S., Jaeger, W., Bratskaya, S., Bohrisch, J., Schimmel, T., Mende, M., Oelmann, M. et Boyko, V. (2006). Formation of polyelectrolyte complexes in a polycarboxybetaine/weak polyanion system. *Colloid. Surf. A: Physicochem. Eng. Asp., 276*(1-3), 65-71.

Selwyn, J. E. et Steinfeld, J. I. (1972). Aggregation of equilibriums of xanthene dyes. *J. Phys. Chem., 76*(5), 762-774.

Singer, V. L., Jones, L. J., Yue, S. T. et Haugland, R. P. (1997). Characterization of picogreen reagent and development of a fluorescence-based solution assay for double-stranded DNA quantitation. *Anal. Biochem., 249*(2), 228-238.

Smith, M. H., South, A. B., Gaulding, J. C. et Lyon, L. A. (2010). Monitoring the erosion of hydrolytically-degradable nanogels via multiangle light scattering coupled to asymmetrical flow field-flow fractionation. *Anal.Chem., 82*(2), 523-530.

Storkle, D., Duschner, S., Heimann, N., Maskos, M. et Schmidt, M. (2007). Complex formation of DNA with oppositely charged polyelectrolytes of different chain topology: Cylindrical brushes and dendrimers. *Macromolecules, 40*(22), 7998-8006.

Strand, S. P., Danielsen, S., Christensen, B. E. et Varum, K. M. (2005). Influence of chitosan structure on the formation and stability of DNA-chitosan polyelectrolyte complexes. *Biomacromolecules, 6*(6), 3357-3366.

Strand, S. P., Issa, M. M., Christensen, B. E., Varum, K. M. et Artursson, P. (2008). Tailoring of chitosans for gene delivery: Novel self-branched glycosylated chitosan oligomers with improved functional properties. *Biomacromolecules, 9*(11), 3268-3276.

Strand, S. P., Lelu, S., Reitan, N. K., de Lange Davies, C., Artursson, P. et Varum, K. M. (2010). Molecular design of chitosan gene delivery systems with an optimized balance between polyplex stability and polyplex unpacking. *Biomaterials, 31*(5), 975-987.

Takahashi, R., Al-Assaf, S., Williams, P. A., Kubota, K., Okamoto, A. et Nishinari, K. (2003). Asymmetrical-flow field-flow fractionation with on-line multiangle light scattering detection. 1. Application to wormlike chain analysis of weakly stiff polymer chains. *Biomacromolecules, 4*(2), 404-409.

Tan, J. F., Too, H. P., Hatton, T. A. et Tam, K. C. (2006). Aggregation behavior and thermodynamics of binding between poly(ethylene oxide)-block-poly(2-(diethylamino)ethyl methacrylate) and plasmid DNA. *Langmuir, 22*(8), 3744-3750.

Tang, M. X. et Szoka, F. C. (1997). The influence of polymer structure on the interactions of cationic polymers with DNA and morphology of the resulting complexes. *Gene Therapy, 4*(8), 823-832.

Thomas, M. et Klibanov, A. M. (2003). Non-viral gene therapy: Polycation-mediated DNA delivery. *Appl. Microbiol. Biotech., 62*(1), 27-34.

Tiera, M. J., Qiu, X.-P., Bechaouch, S., Shi, Q., Fernandes, J. C. et Winnik, F. M. (2006). Synthesis and characterization of phosphorylcholine-substituted chitosans soluble in physiological pH conditions. *Biomacromolecules, 7*(11), 3151-3156.

Tsuchida, E., Osada, Y. et Abe, K. (1974). Formation of polyion complexes between polycarboxylic acids and polycations carrying charges in the chain backbone. *Makromolekulare Chemie, 175*(2), 583-592.

Varum, K. M., Anthonsen, M. W., Grasdalen, H. et Smidsrod, O. (1991). High-field nmr-spectroscopy of partially n-deacetylated chitins (chitosans) .1. Determination of the degree of N-acetylation and the distribution of N-acetyl groups in partially N-deacetylated chitins (chitosans) by high-field NMR-spectroscopy. *Carbohydrate Research, 211*(1), 17-23.

Velázquez-Campoy, A. (2006). Ligand binding to one-dimensional lattice-like macromolecules: Analysis of the mcghee-von hippel theory implemented in isothermal titration calorimetry. *Anal. Biochem., 348*(1), 94-104.

Viebke, C. et Williams, P. A. (2000). The influence of temperature on the characterization of water-soluble polymers using asymmetric flow field-flow-fractionation coupled to multiangle laser light scattering. *Anal. Chem., 72*(16), 3896-3901.

Wahlund, K. G. et Giddings, J. C. (1987). Properties of an asymmetrical flow field-flow fractionation channel having one permeable wall. *Anal. Chem., 59*(9), 1332-1339.

Wight, T. N., Heinegard, D. K. et Hascall, V. C. (1991). Proteoglycans: Structure and function. In E. D. Hay, (éd.), *Cell biology of extracellular matrix* (pp. 45-78). New York: Plenum Press.

Wink, T., De Beer, J., Hennink, W. E., Bult, A. et Van Bennekom, W. P. (1999). Interaction between plasmid DNA and cationic polymers studied by surface plasmon resonance spectrometry. *Anal. Chem., 71*(4), 801-805.

Wiseman, T., Williston, S., Brandts, J. F. et Lin, L. N. (1989). Rapid measurement of binding constants and heats of binding using a new titration calorimeter. *Anal. Biochem., 179*(1), 131-137.

Xu, P., Quick, G. K. et Yeo, Y. (2009). Gene delivery through the use of a hyaluronate-associated intracellularly degradable crosslinked polyethyleneimine. *Biomaterials, 30*(29), 5834-5843.

Yan, X., Grace, W. K., Yoshida, T. M., Habbersett, R. C., Velappan, N., Jett, J. H., Keller, R. A. et Marrone, B. L. (1999). Characteristics of different nucleic acid staining dyes for DNA fragment sizing by flow cytometry. *Anal. Chem., 71*(24), 5470-5480.

Yang, S. et May, S. (2008). Release of cationic polymer-DNA complexes from the endosome: A theoretical investigation of the proton sponge hypothesis. *J. Chem. Phys., 129*(18), 185105-185109.

Yin, M., Ding, K., Gropeanu, R. A., Shen, J., Berger, R., Weil, T. et Müllen, K. (2008). Dendritic star polymers for efficient DNA binding and stimulus-dependent DNA release. *Biomacromolecules, 9*(11), 3231-3238.

Yohannes, G., Holappa, S., Wiedmer, S. K., Andersson, T., Tenhu, H. et Riekkola, M.-L. (2005). Polyelectrolyte complexes of poly(methacryloxyethyltrimethylammonium chloride) and poly(ethylene oxide)-block-poly(sodium methacrylate) studied by asymmetrical flow field-flow fractionation and dynamic light scattering. *Anal. Chim. Acta, 542*(2), 222-229.

Yohannes, G., Pystynen, K.-H., Riekkola, M.-L. et Wiedmer, S. K. (2006). Stability of phospholipid vesicles studied by asymmetrical flow field-flow fractionation and capillary electrophoresis. *Anal. Chim. Acta, 560*(1-2), 50-56.

Zelikin, A. N., Trukhanova, E. S., Putnam, D., Izumrudov, V. A. et Litmanovich, A. A. (2003). Competitive reactions in solutions of poly-L-histidine, calf thymus DNA, and synthetic polyanions: Determining the binding constants of polyelectrolytes. *J. Am. Chem. Soc., 125*(45), 13693-13699.

Zhang, Z.-Y. et Smith, B. D. (2000). High-generation polycationic dendrimers are unusually effective at disrupting anionic vesicles: Membrane bending model. *Bioconjugate Chem., 11*(6), 805-814.

Zhao, X., Pan, F., Zhang, Z., Grant, C., Ma, Y., Armes, S. P., Tang, Y., Lewis, A. L., Waigh, T. et Lu, J. R. (2007). Nanostructure of polyplexes formed between cationic diblock copolymer and antisense oligodeoxynucleotide and its influence on cell transfection efficiency. *Biomacromolecules, 8*(11), 3493-3502.

Zhao, X., Zhang, Z., Pan, F., Waigh, T. A. et Lu, J. R. (2008). Plasmid DNA complexation with phosphorylcholine diblock copolymers and its effect on cell transfection. *Langmuir, 24*(13), 6881-6888.

Zillies, J. C., Zwiorek, K., Winter, G. et Coester, C. (2007). Method for quantifying the pegylation of gelatin nanoparticle drug carrier systems using asymmetrical flow field-flow fractionation and refractive index detection. *Anal. Chem., 79*(12), 4574-4580.

Zimm, B. H. (1948). Apparatus and methods for measurement and interpretation of the angular variation of light scattering; preliminary results on polystyrene solutions. *J. Chem. Phys., 16*(12), 1099-1116.

Zipper, H., Brunner, H., Bernhagen, J. et Vitzthum, F. (2004). Investigations on DNA intercalation and surface binding by SYBR green I, its structure determination and methodological implications. *Nucleic Acids Research, 32*(12), e103/101-e103/110.

ANNEXES

ANNEXE 1 CALCULS DES MASSES MOLAIRES ET DU RAYON DE GIRATION

D'après la théorie de la diffusion de la lumière, pour une particule dont le rayon de giration est inférieur à la longueur d'onde de la lumière incidente, on a :

$$R(\theta)/Kc = M_w P(\theta)\left[1 - 2A_2 M_w P(\theta) + \ldots\right] \qquad \textbf{(A.1.1)}$$

où $R(\theta)$ est le rapport de Rayleigh qui est directement proportionnel au rapport de la lumière diffusée à un angle θ et l'intensité incidente ; c est la concentration massique des espèces diffusées ; A_2 est le second coefficient de Viriel qui renseigne de l'affinité polymère-soluté ; $K = \frac{4\pi^2 n_0^2}{N_A \lambda_0^4}\left(\frac{dn}{dc}\right)^2$ est une constante optique et $P(\theta) = 1 - \left(16\pi^2/3\lambda^2\right) R_g \sin^2(\theta/2)$ est la fonction de diffusion de la particule dans le cas où l'angle de diffusion est faible. Étant donné que les fractions sont en concentration très diluées, on peut négliger le terme entre les crochets dans l'équation A.1.1 (tend vers 1). On a donc :

$$R(\theta)/Kc = M_w\left(1 - \left(16\pi^2/3\lambda^2\right) R_g \sin^2(\theta/2)\right) \qquad \textbf{(A.1.2)}$$

Cette équation suppose une valeur d'angle de diffusion proche de 0. Or d'un point de vue pratique, on ne peut accéder à la valeur de l'intensité diffusée à cet angle. La méthode couramment employée en SEC est de mesurer des intensités à de multiple valeurs d'angles et ensuite extrapoler la valeur à un angle de 0° en appliquant différents modèles. Il existe trois grands modèles d'extrapolation. Le premier est le modèle de Debye (1947) et utilise l'équation

A.1.2. En traçant $R(\theta)/Kc$ en fonction de $\sin^2(\theta/2)$, on obtient une droite dont la pente est à $-(16\pi^2/3\lambda^2)R_g$ et l'ordonnée à l'origine est M_w. Dans le cas de la méthode de Zimm (1948), l'équation A.1.2 est transformée en :

$$\frac{Kc}{R(\theta)} = \frac{1}{M_w} + \frac{16\pi^2}{3\lambda^2}\frac{1}{M_w}R_g \sin^2(\theta/2) \qquad \textbf{(A.1.3)}$$

Dans ce modèle, la droite est $\frac{Kc}{R(\theta)} = f\left(\sin^2(\theta)\right)$ avec une pente égale à $16\pi^2 R_g/3\lambda^2 M_W$ et une ordonnée à l'origine égale à $1/M_w$. La méthode de Berry (1966) est une variante de la méthode de Zimm :

$$\sqrt{\frac{Kc}{R(\theta)}} = \sqrt{\frac{1}{M_w} + \frac{16\pi^2}{3\lambda^2}\frac{1}{M_w}R_g \sin^2(\theta/2)} \qquad \textbf{(A.1.4)}$$

Dans ce cas, $(Kc/R(\theta))^{1/2}$ est tracé en fonction de $\sin^2(\theta/2)$ pour obtenir la valeur $1/M_w^{1/2}$ comme ordonnée à l'origine et la pente $8\pi^2 R_g/3\lambda^2 M_W^{1/2}$. Le détecteur MALS permet donc par différentes méthodes d'expolation d'accéder à la masse molaire moyenne en masse mais comme indiqué dans l'équation A.1.1, il est nécessaire de connaître deux autres paramètres : la concentration de chaque fraction et le dn/dc qui est la variation de l'indice de réfraction par rapport à la concentration. Le dn/dc est propre au polymère et dépend du solvant et de la longueur d'onde de la lumière incidente et de la concentration. Cette information est connue en temps réel grâce au réfractomètre qui, à partir du dn/dc mesuré, va nous renseigner en temps réel de la concentration de chaque fraction.

Les différents calculs de masses molaires sont résumés ci-dessous. Si M_i est la masse molaire de chaque fraction mesurée par diffusion de lumière et c_i leur concentration mesurée par réfractométrie, on a :

$$\overline{M_n} = \frac{\sum n_i M_i}{\sum n_i} = \frac{\sum c_i}{\sum c_i / M_i} \text{ et } \overline{M}_w = \frac{\sum n_i M_i^2}{\sum n_i M_i} = \frac{\sum c_i M_i}{\sum c_i} \qquad \textbf{(A.1.5)}$$

ANNEXE 2 STABILITÉ DES COMPLEXES ADN/CHITOSANE EN PRÉSENCE DE POLYANIONS COMPÉTITEURS

Cette annexe présente l'étude de la stabilité des complexes ADN/chitosane en présence de polyanions compétiteurs qui peuvent induire la dissociation des complexes en se liant au chitosane par des interactions électrostatiques. Cet article est en cours de préparation pour soumettre à la revue scientifique *Langmuir*.

STABILITY OF DNA/CHITOSAN COMPLEXES EXPOSED TO COMPETING POLYANIONS

Pei Lian Ma, Françoise M. Winnik, and Michael D. Buschmann

Department of Chemical and Biomedical Engineering, Ecole Polytechnique de Montréal, PO 6079 Succ. Centre-Ville, Montreal, Quebec, H3C 3A7, Canada, and Department of Chemistry and Faculty of Pharmacy, Université de Montréal, PO 6128 Succ. Centre-Ville, Montreal, Quebec, H3C 3J7, Canada.

A.2.1 Abstract

The stability of DNA/chitosan complexes upon exposure to hyaluronan (HA), chondroitin sulfate (CS), and heparin (Hp), was assessed by fluorescence spectroscopy using Picogreen as the probe to quantify the release of DNA from binding to chitosan. Only the highly charged heparin was found to destabilize the DNA/chitosan complexes and release DNA from chitosan.

Isothermal titration microcalorimetry (ITC) was used to further determine the binding constants of chitosan with DNA and with each competing polyanion in MES buffer at pH 6.5 and 150 mM of total ionic strength. The binding constant of chitosan-DNA was approximately 40-fold and 2-fold greater compared to those of chitosan-CS and chitosan-Hp, respectively. Negligible heat was detected during titrations of chitosan into HA, possibly due to the absence of proton transfer from the buffer to chitosan. However, significant heat changes upon chitosan binding to HA were measured at a lower ionic strength of 18 mM, but resulting in an isotherm with a binding constant that was still about 200-fold lower compared to chitosan-DNA. The ability of the competing polyanions to release DNA from the DNA/chitosan complexes was related to the binding affinities of chitosan with the different polyanions (including DNA). The stability of the DNA/chitosan complexes exposed to heparin increased with chitosan DDA and molecular weight, in agreement with increasing binding affinities to DNA previously determined by ITC. Heparin was unable to dissociate the complexes in dispersions with high N/P ratios, where a significant amount of free chitosan was initially detected and quantified by subjecting the dispersions to ultracentrifugation and subsequent analysis of the supernatant by the Orange II depletion method. For example, the free chitosan content was 60% in a dispersion prepared at an N/P ratio of 6 and further diluted in the MES buffer at pH 6.5 and 150 mM of ionic strength. This amount of free chitosan was found to be sufficient for binding to both DNA and heparin at limited concentrations. However, higher N/P ratios in the dispersions providing higher amounts of free chitosan were required to achieve similar protection with increasing heparin concentration in the samples. These findings suggest that free polycation can prevent premature dissociation of DNA/polycation complexes upon interactions with anionic components in the extracellular matrix and provide critical information relating complex stability which effects DNA protection and transfection efficiency.

A.2.2 Introduction

Cationic polymers have been extensively investigated as vectors for nonviral gene delivery due to the low immunogenicity, a better safety profile compared to their viral counterparts, and the ease of their preparation. Significant progress has been made in understanding complex formation between polycations and DNA, the internalization of the complexes into the cells and subsequent trafficking into the cell nucleus. It is commonly accepted that DNA/polycation complexes are taken up by cells via endocytosis but further stages of their endosomal release into the cytoplasm, their transport to the nucleus, and the release of the genes for their expression are less well understood. One mechanism of endosomal release of the complexes into the cytoplasm is based on the proton sponge hypothesis (Boussif et al., 1995; Behr, 1997). According to this hypothesis, several cationic polymers, such as polyethyleneimine (PEI) and dendrimers, have the ability to buffer endosomal acidification causing an accumulation of protons and an influx of chloride anions, resulting in an increase of osmotic pressure with entry of water and thereby the disruption of the endosome. However, the effectiveness of this mechanism is not always present since some polymers with high buffering capacity do not escape the endosome (Funhoff et al., 2004; Kulkarni et al., 2005; Gabrielson et Pack, 2006). For example, PEI is well known for its high buffering capacity but the acetylation of its primary amines (up to 57%) was found to enhance significantly the transfection efficiency, although buffering capacity is reduced (Gabrielson et Pack, 2006). Once outside the endosome, DNA has to dissociate from the polycation and be transported into the nucleus for transcription. The intracellular DNA unpackaging from its vector has been demonstrated to be a limiting factor for efficient gene expression in nonviral systems (Schaffer et al., 2000). In line with this finding, the acetylation of PEI was seen to decrease the DNA-polycation interactions leading to more facile

unpackaging of the complexes (Gabrielson et Pack, 2006). Gene expression levels were decreased or inhibited when DNA was either tightly or loosely bound to the polycation, such as PEI (Gabrielson et Pack, 2006; Ito et al., 2006; Koyama et al., 2006) and chitosan (Sato et al., 2001; Lavertu et al., 2006; Strand et al., 2010). Tightly bound and highly stable complexes will be readily endocytosed but possibly not disassembled to access the transcription machinery. On the other hand, DNA weakly bound to the polycation forms complexes that will dissociate prematurely in the medium and not even be endocytosed into cells. The increased gene delivery activity has been related to an appropriate balance between the DNA-polycation binding strength and the ability to dissociate intracellularly for gene expression (Lavertu et al., 2006; Ma, P.L. et al., 2009; Strand et al., 2010) .

Gene delivery can be affected by non-specific interactions of DNA/polycation complexes with anionic biological components, including serum proteins, cytoplasmic RNA and glycoaminoglycans. Glycosaminoglycans, such as hyaluronan (HA), chondroitin sulfate, and heparin, are linear and negatively charged polymers of repeating disaccharides that are found abundantly in the extracellular matrix, intracellularly, and on the plasma membrane associated with cell surface receptors and adhesion molecules (Wight et al., 1991) . They can destabilize the DNA/polycation complexes by competing with DNA for binding to the polycation, resulting in the dissociation of the complexes and premature release of DNA extracellularly (Danielsen, Strand et al., 2005). Labeled heparan sulfate was found previously to decrease the cellular uptake and gene expression of DNA/PEI complexes, and was mostly bound to the polycation inside the cells as detected by confocal microscopy (Ruponen et al., 2001). However, the binding of HA to positively charged DNA/polycation complexes was recently found to mediate gene delivery without disrupting the complexes (Ito et al., 2006; Duceppe et Tabrizian, 2009; Xu et al., 2009). This approach aimed at protecting the complexes from non-specific interactions with serum

proteins and loosen the tight binding between DNA and the polycation to facilitate intracellular unpackaging. The stability of DNA/polycation complexes in the presence of serum proteins and competing polyanions, such as HA and heparin, has been commonly assessed by gel electrophoresis to detect released DNA (Bertschinger et al., 2006; Layman et al., 2009; Strand et al., 2010) . In the majority of cases, only the highly charged heparin was able to dissociate the complexes. Fluorescence spectroscopy together with ethidium bromide as a probe for DNA was also used to investigate the formation of DNA/polycation complexes (Izumrudov et al., 2002; Rungsardthong et al., 2003; Zelikin et al., 2003; Strand et al., 2005) and their dissociation by competing polyanions (Danielsen, Maurstad et al., 2005; Danielsen, Strand et al., 2005). Yet, the majority of studies on the stability of DNA/polycation complexes in the presence of biological polyanions were descriptive and provided little if any quantitative information about the release of DNA as well as the binding affinity of the polycation with DNA and with the competing polyanions.

We report here the stability behavior of DNA/chitosan complexes upon exposure to biological polyanions using fluorescence spectroscopy. Chitosan was selected as the polycation because it is the most frequently used natural polymer for the delivery of plasmid DNA and siRNA in the emerging field of gene silencing. The biological polyanions used to compete with DNA for binding to chitosan include HA, chondroitin sulfate, and heparin, which differ in sulfate content and charge density. Isothermal titration microcalorimetry (ITC) was used to study the interaction of chitosan with DNA and with each competing polyanion. The binding constants of the binary systems determined from ITC measurements were then compared and correlated with the ability of the competing polyanions to disrupt DNA/chitosan complexes. The effect of several parameters on the stability of these complexes was assessed, including the chitosan molecular weight and charge density via the degree of deacetylation (DDA) as well as the

chitosan amine to DNA phosphate ratio used in the formulations. These parameters are known to influence the binding affinity of chitosan with DNA (Ma, P.L. et al., 2009) and the transfection efficiency of the complexes (MacLaughlin et al., 1998; Koping-Hoggard et al., 2001; Sato et al., 2001; Lavertu et al., 2006; Strand et al., 2010).

A.2.3 Experimental Section

A.2.3.1 Materials

The 6.4 kb plasmid EGFPLuc (Clontech Laboratories) was amplified in DH5α bacteria and purified using the Qiagen Plasmid Mega Kit. A stock solution of this plasmid (0.33 mg/mL) was prepared in deionized water and stored at –20 ^{o}C before use. Ultrapure heterogeneously deacetylated chitosans (Ultrasan^{TM}) with a DDA of 72%, 80%, and 98% were provided by Biosyntech Inc. (Laval, Qc, Canada) and were depolymerized according to Lavertu et al. (2006) using nitrous acid to achieve specific number-average molecular weight (M_n) of 11, 80, and 153 kDa. Table A.2.1 summarizes the M_n and polydispersity index of chitosans measured by gel permeation chromatography (GPC)(Darras et al., 2010) as well as the DDA determined by ^{1}H.(Lavertu et al., 2003) Chitosan stock solutions of 5 mg/mL were prepared by dissolving the samples overnight in deionized water and hydrochloric acid (from 1 M HCl solution), such as to reach an HCl/glucosamine ratio of 1.

Chondroitin-6-sulfate sodium salt (CS) from shark cartilage (Sigma-Aldrich, C4384) and heparin sodium salt (Hp) from porcine intestinal mucosa (Sigma-Aldrich, H3149) were used as the competing polyanions. A high molecular weight hyaluronic acid sodium salt (HA1, >1000 kDa) from Sigma-Aldrich (H5388) and a hyaluronic acid sodium salt with a M_n of 21 kDa (HA2) from Lifecore USA were also used. The M_n and polydispersity index of these polyanions

determined by GPC(Kujawa et al., 2007) are shown in Table A.2.1. The structure of HA, CS, and Hp disaccharides are illustrated in Figure A.2.1. Stock solutions of the polyanion (1 mg/mL) were prepared in deionized water. Picogreen was provided (Invitrogen) as a 320 mM concentrated stock solution in DMSO. Orange II was from Sigma-Aldrich (195235).

A.2.3.2 Preparation of DNA/Chitosan Complexes

Prior to mixing, chitosan solutions were diluted with deionized water to reach the desired molar N/P ratio (chitosan protonable amine to DNA phosphate ratio) when 50 μL of chitosan would be mixed with 50 μL of DNA solution, the latter always at a concentration of 0.33 mg/ml in deionized water. The mixing was done quickly by up and down pipetting of the dispersions. Samples were allowed to incubate at room temperature 30 min before analysis.

Table A.2.1 Molecular Characteristics of Chitosan and Polyanions.

Polyelectrolyte	DDA	M_n (kDa)	M_w/M_n
Chitosan	72%	86	3.5
	80%	11	1.4
	80%	76	1.6
	80%	153	1.6
	98%	79	1.6
Hp		32	2.8
CS		25	1.4
HA1[a]		---	---
HA2		21	1.7

[a] Molecular weight > 1000 kDa as provided by Sigma-Aldrich

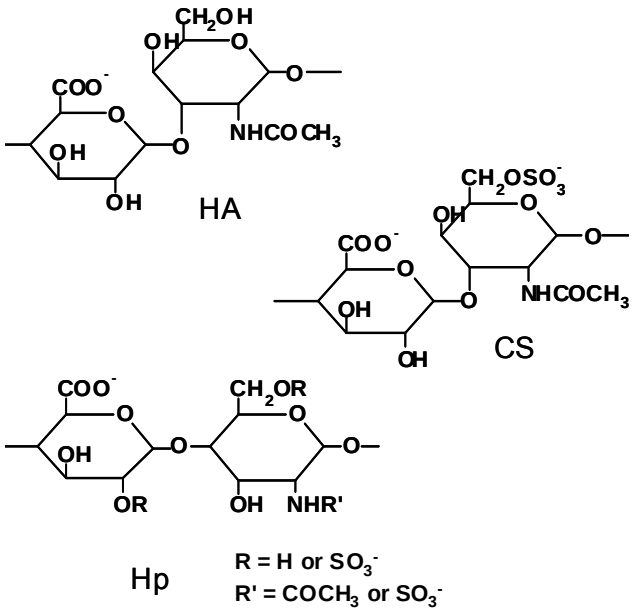

Figure A.2.1. Structure of Hyaluronan (HA), Chondroitin-6-Sulfate (CS), and Heparin (Hp) disaccharides.

A.2.3.3 Polyanion Competition Binding Assay

Dispersions of DNA/chitosan complexes (50 μL) were diluted with 25 mM MES buffer (1.2 mL) at pH 6.5 with a total ionic strength of 150 mM (adjusted by addition of NaCl). These samples were allowed to equilibrate for 30 min in the pH-adjusted MES buffer before analysis. We used 96-well black plates (Fisher, no.CS003915) for this assay and added 30 μL of each sample to each well. We then added 70 μL of competing polyanion solution at a concentration of 5 or 24 μg/mL prepared by diluting the stock solution (1 mg/mL) in MES buffer adjusted to pH 6.5. For controls (no competing polyanion), 70 μL of MES buffer was added to the wells. The mixing was done on a rocking agitation table for 60 min at 150 rpm. Picogreen was then used to quantify the free or released DNA before and after exposure to the competing polyanions. A 200-fold dilution of the Picogreen stock solution was prepared in MES buffer and a volume of 100 μL was added to each well. The mixing was done quickly by up and down pipetting of the

mixtures. The final volume and the DNA concentration in each well were 200 μL and 0.99 μg/mL, respectively. After 2 min of incubation, the fluorescence intensity of the samples was measured using a microplate spectrofluorometer (Spectramax Gemini XS, Molecular Devices, Sunnyvale, CA) at excitation and emission wavelengths of 485 and 535 nm, respectively. The blank containing 100 μL of MES buffer and 100 μL of diluted Picogreen solution was subtracted from the measurements. The reported fluorescence intensity for each N/P ratio is relative to the control containing 0.99 μg/mL of DNA without chitosan (N/P = 0) and represents the mean value (± S.D.) of three independent measurements.

A.2.3.4 Isothermal Titration Calorimetry

Binding studies were performed using a VP-ITC microcalorimeter from MicroCal (Northampton, MA) with a cell volume of 1.428 mL at 25^{o}C. Samples were degassed in a ThermoVac system (MicroCal) prior to use. The reference cell was filled with 25 mM MES buffer (pH 6.5, total ionic strength of 150 mM adjusted by addition of NaCl) solution only. The sample cell was filled either with the DNA solution (40 μg/mL), Hp solution (33 μg/mL), CS solution (60 μg/mL), or HA2 solution (78 μg/mL), all prepared using the MES buffer. The chitosan stock solution (80% DDA, M_n = 11 kDa; 5 mg/mL) was diluted using the MES buffer to a concentration of 154 μg/mL in the titrations of chitosan into DNA or Hp, and to a concentration of 462 μg/mL in the titrations of chitosan into CS or HA2. The solution of chitosan was introduced into the thermostated cell by means of a syringe which also stirred at 250 rpm. Each titration consisted of an initial 2 μL injection (neglected in the analysis) followed by 28 subsequent 10 μL injections each of which were 20 s in duration and were programmed to occur at 400 s intervals. The heats of dilution from titrations of chitosan solution into buffer only

(without DNA or competing polyanion) were subtracted from the heats obtained from titrations of chitosan solution into the DNA or competing polyanion solution to obtain net binding heats. All experiments were carried out in duplicate.

A.2.3.5 Analysis of Binding Isotherms

Raw ITC data of chitosan binding to a polyanion (DNA, Hp, CS, or HA) polyanion was processed with the Origin software provided by the manufacturer (MicroCal, Northampton, MA). The isotherms were fit as previously described (Ma, P.L. et al., 2009) using the Single Set of Identical Sites (SSIS) model by a nonlinear least-squares analysis (Wiseman et al., 1989; MicroCal LLC., 2004) . The equilibrium binding constant, *K*, between a free molecule of chitosan and a free binding site on the polyanion is represented by Equation A.2.1, assuming independent binding sites.

$$\text{Free binding site on polyanion} + \text{Free chitosan} \underset{}{\overset{K}{\rightleftharpoons}} \text{Bound chitosan}$$

$$K = \frac{[\text{Bound chitosan}]}{[\text{Free binding sites}][\text{Free chitosan}]} \qquad \textbf{(A.2.1)}$$

From the heat changes (ΔQ) detected by the instrument, we determined the binding affinity, *K*, the enthalpy of binding, ΔH, and the number of binding sites for chitosan, *n*. These parameters are reported as the mean of two measurements with errors representing their minimum and maximum.

A.2.3.6 Quantification of Free Chitosan by Ultracentrifugation and Orange II Dye

Dispersions of DNA/chitosan (80% DDA, 80 kDa) complexes (100 µL) were diluted with 400 µL of either deionized water or 25 mM MES buffer (pH 6.5, total ionic strength of 150 mM adjusted by addition of NaCl). These samples were allowed to rest for 30 min before subjecting them to ultracentrifugation at 65 000 rpm for 30 min (Beckman, Optima MAX-E, TLA-110 fixed rotor). The supernatant of each sample was then recovered to determine the concentration of free chitosan by the Orange II dye depletion method (Drogoz et al., 2007). A volume of 100 µL of supernatant was collected and further diluted 6 to 15 fold with 50 mM acetic acid/sodium acetate buffer at pH 4.0, such that the concentration of chitosan amine groups to be assayed would be always lower than that of Orange II at mixing. The diluted supernatant was then mixed with 0.1 volume of 1 mM Orange II solution (in the acetic acid/sodium acetate buffer) by vortexing. After 15 min of incubation, the suspension of chitosan/Orange II was centrifuged (20 000g for 30 min) to precipitate the complexes and recover the supernatant containing the unbound dye. The absorbance of the supernatant was then measured at 484 nm using a UV/Vis spectrophotometer (Beckman DU-600). The free chitosan content in DNA/chitosan dispersions was calculated from calibration curves obtained with solutions of chitosan. The reported values are the average (± standard deviation) of at least three samples.

A.2.3.7 Polyacrylamide Gel Electrophoresis

Dispersions of DNA/chitosan complexes were diluted 5-fold with 25 mM MES buffer at pH 6.5 and left at rest for 30 min. 25 µL of each of these samples was then mixed with 5 µL of 40% sucrose solution. The mixing was briefly done by pipetting. A sample volume of 20 µL

(0.66 μg of DNA equivalence) was then loaded into a 6% polyacrylamide gel (20 mM MES, 8 mM sodium acetate, pH 6.5). Electrophoresis was carried out at 90 V for 60 min. Chitosan was then stained by immersing the gel in a Coomassie blue staining solution (10:45:45 glacial acetic acid/methanol/deionized water and 0.25% w/v Coomassie brilliant blue R250 (Biorad, M1226)) for 45 min in a shaker followed by washing with a destaining solution (10:30:60 glacial acetic acid/methanol/deionized water) for 4 hours in a shaker. Images of the gel were taken using a ChemImager 5500 system (Alpha Innotech).

A.2.3.8 Zeta Potential Measurements

Dispersions of DNA/complexes (100 μL) were diluted 4 times in 25 mM MES buffer (pH 6.5, total ionic strength of 150 mM adjusted by addition of NaCl) prior to analysis with a Malvern Zetasizer Nano ZS (Worcestershire, UK). The zeta potential of the complexes was calculated from the electrophoretic mobility values using the Smoluchowski equation.

A.2.4 Results and Discussion

A.2.4.1 Effect of Charge Density of the Competing Polyanions on the Stability of the Complexes

The biological polyanions selected to compete with DNA for binding to chitosan include hyaluronan (HA), chondroitin sulfate (CS), and heparin (Hp). They were fully ionized under the conditions used in this study. Among these anionic polysaccharides, HA has the lowest negative charge density bearing only one carboxyl group on each repeating disaccharide unit while CS has one additional sulfate group per disaccharide unit Figure A.2.1. Hp has the highest negative

charge density compared to these two polyanions because it can have multiple sulfate groups per disaccharide unit in addition to a carboxyl group (Figure A.2.1). The carboxyl and sulfate content of Hp was determined by carrying out conductimetric titrations of the acid form of heparin with a solution of NaOH (See Supporting Information, Figure A.2.SI-1). We found a sulfate to carboxyl ratio of 2, indicating an average of two sulfate and one carboxyl groups on each repeating disaccharide unit of Hp.

The ability of these competing polyanions to destabilize and dissociate the DNA/chitosan complexes was assessed by detecting and quantifying the unbound or released DNA. For this purpose, we used Picogreen, a cyanine dye suitable for plasmid DNA, because it preferentially binds to double stranded DNA and has an absorption coefficient about 12-fold greater than ethidium bromide (Singer et al., 1997; Ren et Xu, 2008). The dye itself in the unbound state has actually no fluorescence while the dye bound to DNA undergoes fluorescence enhancement. Compared to ethidium bromide, Picogreen was previously shown to be more sensitive in the quantification of released DNA from gene delivery systems (Moret et al., 2001). We first prepared dispersions of DNA/chitosan (80% DDA, 76 kDa) complexes at different N/P ratios and then mixed each of them with a solution of Picogreen for detection of unbound DNA prior to exposure to competing polyanions. These samples without addition of any competing polyanion correspond to the controls of Figure A.2.2, showing the fluorescence intensities of Picogreen bound to uncomplexed DNA as a function of the N/P ratio in the dispersions. The reported values are relative to the fluorescence intensity measured upon addition of Picogreen to a solution of DNA at the same concentration as in each dispersion but without chitosan (N/P = 0). The decrease of the fluorescence intensity observed with increasing N/P ratio indicates increasing amounts of DNA complexed with chitosan, in agreement with the zeta potential measurements of the complexes showing gradual neutralisation of the DNA phosphate groups by chitosan Figure

A.2.3. The relative fluorescence intensity of the dye reached an almost constant value of 5% in the dispersions with N/P ratios above 1.5 (Figure A.2.2), where DNA was fully complexed with chitosan as confirmed by the positive zeta potentials (Figure A.2.3). This residual fluorescence intensity of bound Picogreen, although negligible, may result from some limited access of Picogreen to DNA inside the complexes.

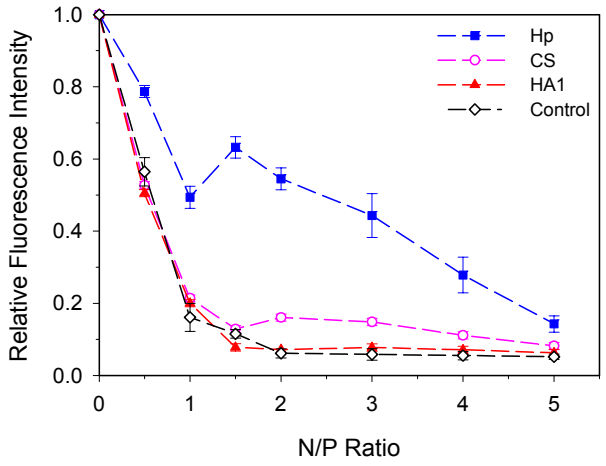

Figure A.2.2. Fluorescence intensity of Picogreen bound to DNA released from DNA/chitosan (80% DDA, 76 kDa) complexes upon exposure to different competing polyanions (Hp, CS, and HA1). The complexes were exposed to 1.8 µg/mL of competing polyanion, except for the controls.

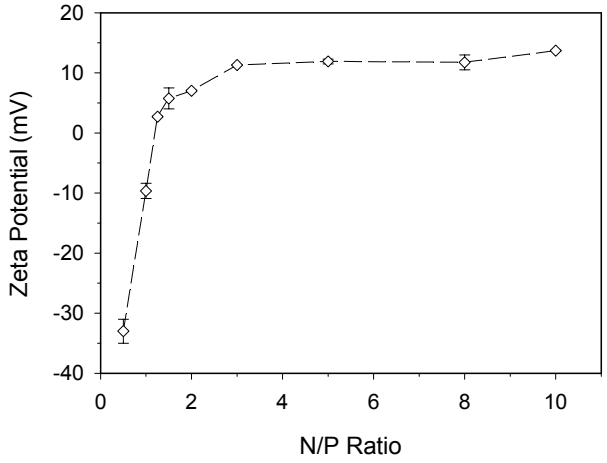

Figure A.2.3. Zeta Potentials of DNA/chitosan (80% DDA, 76 kDa) complexes prepared at different N/P ratios (in 25 mM MES buffer, pH 6.5, total ionic strength of 150 mM adjusted by addition of NaCl).

The initially prepared dispersions of DNA/chitosan (80% DDA, 76 kDa) complexes were then exposed to 1.8 μg/mL of either HA1, CS, or Hp. At this concentration, the amount of negative charge of the competing polyanion was always in excess compared to that of DNA phosphate groups in the samples. These polyanions did not interfere in the detection and quantification of free DNA by Picogreen, in agreement with a previous report (Singer et al., 1997). The relative fluorescence intensities of Picogreen bound to DNA in dispersions of DNA/chitosan complexes with addition of a competing polyanion are also shown in Figure A.2.2. The DNA/chitosan complexes exposed to HA1 resulted in similar fluorescence intensities of the dye as in the controls without any added competing polyanion. Increasing the concentration up to 17 μg/mL of HA1 in the samples also did not result in any significant changes in the measured fluorescence intensities (data not shown). These observations indicate that HA was unable to disrupt the DNA/chitosan binding, in agreement with a previous report using fully deacetylated chitosans to form complexes with DNA (Danielsen, Strand et al., 2005). The exposure of

DNA/chitosan complexes to CS resulted in a slight but not significant increase of the fluorescence intensity of bound Picogreen, compared to the controls in the range of N/P ratios between 2 and 4 (Figure A.2.2). We did not detect further release of DNA from these complexes upon increasing the amount of competing CS in the samples. Similar results in the presence of HA1 or CS were found when complexes were prepared with a chitosan of 80% DDA and a M_n of 11 kDa (data not shown). In contrast to the competition with HA and CS, exposure of DNA/chitosan complexes to 1.8 μg/mL of Hp resulted in significant destabilization upon exposure, as indicated by the increased fluorescence intensities relative to the controls (Figure A.2.2). The destabilization of the complexes was even observed in the dispersion with an N/P ratio of 0.5 where the DNA/chitosan complexes were negatively charged with a zeta potential of -33 (±2) mV (Figure A.2.3). The charge repulsion by a negative zeta potential did not prevent Hp from disrupting the complexes and consequently releasing DNA in solution for binding with the dye. However, not all DNA was released. These observations suggest strong competition between Hp and DNA for binding to chitosan as well as strong binding affinities of chitosan with both DNA and Hp.

The ability of competing polyanions to destabilize the DNA/chitosan complexes appears related to their negative charge density, or equivalently the number of charge groups per dissaccharide, as suggested in previous studies on polymeric and liposomal based gene delivery systems (Ruponen et al., 1999; Ruponen et al., 2001; Ruponen et al., 2003; Danielsen, Strand et al., 2005) HA did not destabilize the DNA/chitosan complexes most probably due to its low negative charge density with only one carboxyl group per disaccharide unit. The additional sulfate group on the disaccharide unit of CS compared to HA had a slight effect on DNA release while only heparin with two sulfates and one carboxyl group per disaccharide was able to

significantly compete with DNA for chitosan binding resulting in the disruption of the complexes.

A.2.4.2 Binding Affinity Between Chitosan and Different Polyanions

The competition binding assay using Picogreen to detect released DNA from the complexes does not provide a direct measurement of the binding affinity between oppositely charged polyelectrolytes, but rather information about the stability of the complexes against competition with polyanions. We did however determine binding constants using isothermal titration microcalorimetry (ITC) for chitosan interacting with different polyanions, including DNA, Hp, CS, and HA2, from analysis of the heat changes measured upon binding. We used a chitosan with a DDA of 80% and a M_n of 11 kDa for ITC measurements. The isotherms are presented in Figure A.2.4 showing the heats of binding normalized to the amount of chitosan titrated into each solution of polyanion, all in 25 mM MES buffer at pH 6.5 with a total ionic strength of 150 mM, and presented as a function of the number of glucosamine units in chitosan to the number negative charges in the polyanion. The interactions of chitosan-DNA, chitosan-Hp, and chitosan-CS were exothermic in the MES buffer that was also used in the competition binding assay. The titrations of chitosan into the solution of HA2 yielded negligible heat changes compared to the other studied binary systems.

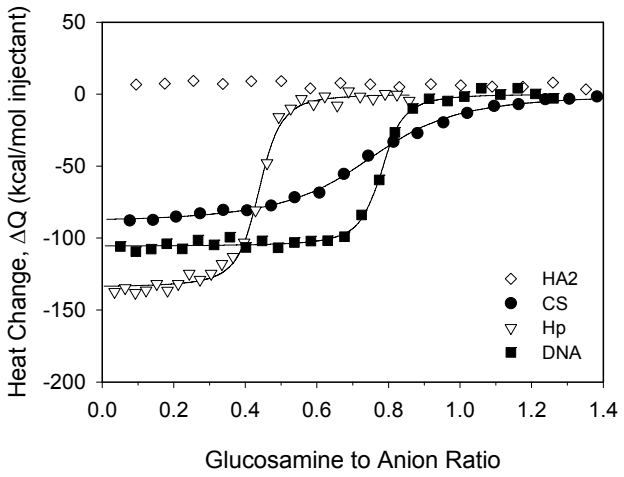

Figure A.2.4. Heats of interaction from calorimetric titrations of chitosan (80% DDA, 11 kDa) into different types of polyanions: HA2, CS, Hp, and DNA (in 25 mM MES buffer, pH 6.5, and total ionic strength of 150 mM adjusted by addition of NaCl). Solid lines represent best-fits generated from the SSIS model.

The enthalpy of binding, ΔH_{obs}, the binding stoichiometry, n, and the binding constant, K_{obs}, determined from fitting the SSIS model to the ITC isotherms of the different systems are summarized in Table A.2.2. The degree of ionization of chitosan in the unbound state was 46% in the MES buffer at pH 6.5 with a total ionic strength of 150 mM, calculated as previously described (Filion et al., 2007; Ma, P.L. et al., 2009). However, we have demonstrated in a previous study that DNA induces proton transfer from the buffer to chitosan, as revealed by the dependence of the measured heat release on the nature of the buffer (Ma, P.L. et al., 2009). The observed enthalpy of binding (ΔH_{obs}) was found in that study to be almost entirely accounted for by the heats associated with proton transfer. Therefore, the values of ΔH_{obs} determined here for the interactions of chitosan-DNA, chitosan-Hp, and chitosan-CS are not the intrinsic enthalpy of binding because they can contain contributions from the ionization changes of the buffer and of

chitosan. The ionization state of chitosan can be increased to a greater extent in the complexed form because of proton transfer. The use of buffers with different enthalpy of ionization is required for the determination of the number of transferred protons (Hinz et al., 1971; Ma, P.L. et al., 2009), which was not within the scope of this study. In contrast to ΔH_{obs}, the binding constant and the stoichiometry of binding are parameters found to be independent of buffer choice (Ehtezazi et al., 2003; Ma, P.L. et al., 2009). The binding constant between chitosan and DNA was 3.8 x 10^8 M^{-1} determined from fitting the corresponding isotherm in Figure A.2.4. This value is about 40-fold higher than the constant obtained for chitosan binding to CS, which clearly explains the observed inability of CS to disrupt the DNA/chitosan complexes. On the other hand, heparin was able to disrupt the DNA/chitosan complexes and release DNA into solution because the binding affinities of chitosan-Hp and chitosan-DNA are similar; the latter value being only 2-fold higher. This finding suggests that any extracellular and intracellular components with similar or higher binding affinities for chitosan could disrupt the DNA/chitosan complexes. Such components can include cellular RNA which was found to dissociate DNA/PEI complexes and was suggested to be involved in the intracellular disassembly of these complexes (Bertschinger et al., 2006).

The negligible heat changes detected during titrations of chitosan into a solution of HA2 (Figure A.2.4) suggest that this low charge density polyanion, compared to DNA and Hp, did not induce proton transfer from the buffer to chitosan under conditions of pH 6.5 and total ionic strength of 150 mM. Since binding is electrostatically driven, we seeked to increase it by decreasing the ionic strength to 18 mM and carrying out ITC measurements. The heat changes at 18 mM ionic strength were significantly higher (Figure A.2.5), than at an ionic strength of 150 mM which screened electrostatic attraction of oppositely charged polyelectrolytes. In both ionic strengths, we can not exclude possible interactions between chitosan and HA, that are athermal

and thereby not detectable by ITC, since negligible heat changes have been previously reported for fully ionized oppositely charged polyelectrolytes undergoing complexation (Rungsardthong et al., 2003; Ma, P.L. et al., 2009). The binding constant of chitosan-HA2 determined at 18mM of ionic strength was 1 x 10^{-7} M. This value is still about 200-fold lower than the binding constant of chitosan-DNA under similar conditions of pH and ionic strength (Figure A.2.5 and Table A.2.2) indicating a weak ability of HA to compete with DNA for chitosan binding, in agreement with results obtained from the competition binding assay using Picogreen.

Table A.2.2. Parameters of Interaction from fitting of the SSIS Model to Isotherms of Chitosan (80% DDA, 11 kDa) with different Polyanions in 25 mM MES Buffer at pH 6.5 with different ionic strengths.

Polyanion	n^a	$n_{N:Anion}{}^b$	ΔH_{obs} **(kcal/mol)**	K_{obs} **(x 10^7 M^{-1})**
A) Total Ionic Strength = 150 mM				
DNA	180 ± 9	0.72 ± 0.03	-107 ± 1	38 ± 1
Hp	1.4 ± 0.0	0.42 ± 0.01	-156 ± 22	19 ± 5
CS	1.4 ± 0.0	0.74 ± 0.01	-87 ± 2	1 ± 0
HA2	---	---	---	---
B) Total Ionic Strength = 18 mM				
DNA	199 ± 11	0.80 ± 0.04	-194 ± 2	206 ± 93
HA2	1.0 ± 0.0	0.98 ± 0.00	-91 ± 0	1 ± 0

[a] The number of moles of binding sites for chitosan on each mole of polyanion. [b] The ratio of glucosamine to anion groups in the complex when all binding sites are occupied at saturation (calculated from n). The parameters n, ΔH_{obs} and K_{obs} were determined from the SSIS model fit using the molar concentration of chitosan and polyanion as the binding entities and not their glucosamine and anions groups. Means are shown with error representing minimum and maximum of duplicates.

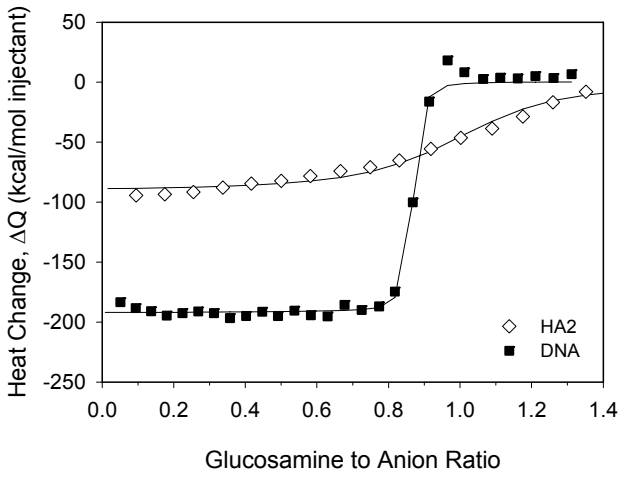

Figure A.2.5. Heats of interaction from calorimetric titrations of chitosan (80% DDA, 11 kDa) into HA2 and DNA (in 25 mM MES buffer, pH 6.5, without NaCl). Solid lines represent best-fits generated from the SSIS model.

A.2.4.3 Effect of the Chitosan Degree of Deacetylation and Molecular Weight on the Stability of the Complexes

The charge density of chitosan can be modulated by its degree of deacetylation (DDA) defined as the fractional content of glucosamine monomers. Increasing the DDA of chitosan increases the charge density along the molecular chain of chitosan, which was previously found to enhance the binding affinity for DNA by ITC (Ma, P.L. et al., 2009) and ethidium displacement assay (Strand et al., 2005). The effect of DDA on the stability of DNA/chitosan complexes upon exposure to heparin was assessed using Picogreen for detection of DNA release. Dispersions of DNA/chitosan complexes were prepared at different N/P ratios using chitosans having a similar M_n of ~ 80 kDa but different DDA values ranging from 72% to 98%. These complexes were then exposed to increasing concentrations of Hp from 0 to 8.4 μg/mL. The fluorescence intensities of these samples measured after addition of Picogreen are shown in

Figure A.2.6 A, B, and C. The exposure of the complexes to 1.8 μg/mL of Hp clearly destabilized the complexes and released DNA to an extent dependent on DDA and N/P ratio. Increasing the chitosan DDA from 72% to 80% did not significantly improve the stability of the complexes against disruption by Hp at this concentration since similar amounts of DNA released from the complexes were bound to Picogreen. However, the chitosan of 98% DDA clearly renders the complexes more stable and less vulnerable to the dissociation by heparin. The ability to resist dissociation by Hp is an indication of stronger binding between DNA and chitosan of 98% DDA. These observations are in agreement with our previous study in which the binding constant determined for chitosan-DNA did not change significantly as the DDA increased from 72% to 80% but increased almost 3-fold with a DDA of 98% (Ma, P.L. et al., 2009).

Heparin also destabilized the DNA complexes prepared with chitosans having a constant DDA of 80% but different M_n values, as shown in Figure A.2.7 A, B, and C. However, the ability of these complexes to resist dissociation by heparin was enhanced with increasing chitosan molecular weight from 11 to 153 kDa. Similar findings were previously reported using also heparin to disrupt DNA complexes prepared with fully deacetylated chitosans of different molecular weights (Danielsen, Strand et al., 2005). This increased stability is attributed to the higher affinity of DNA for binding to longer chitosans as previously demonstrated by ITC (Ma, P.L. et al., 2009).

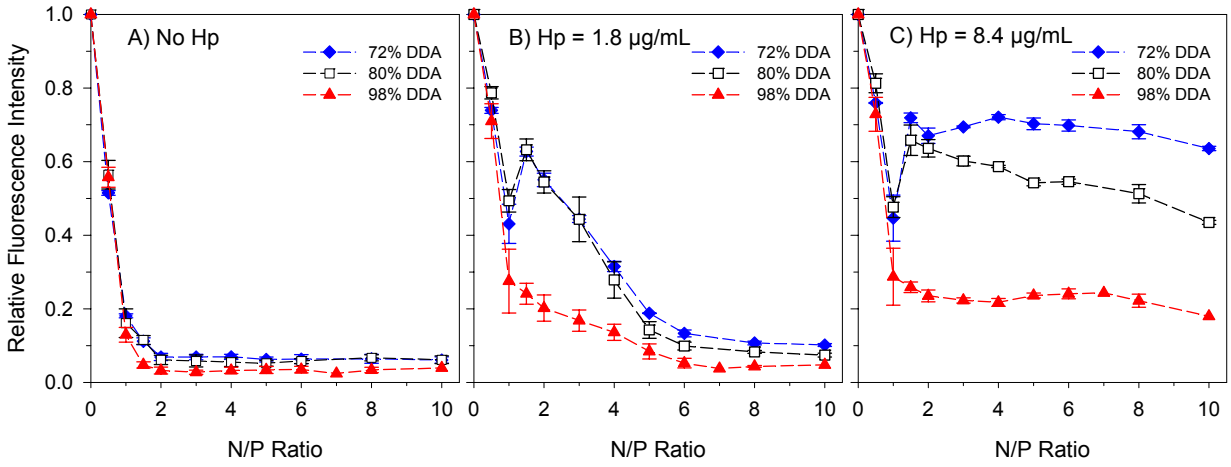

Figure A.2.6. Fluorescence intensity of Picogreen bound to DNA released from DNA/chitosan complexes upon exposure to heparin. The complexes were prepared with chitosans of different DDA (M_n ~ 80 kDa) and then exposed to (A) no Hp, (B) 1.8 µg/mL of Hp, and (C) 8.4 µg/mL of Hp.

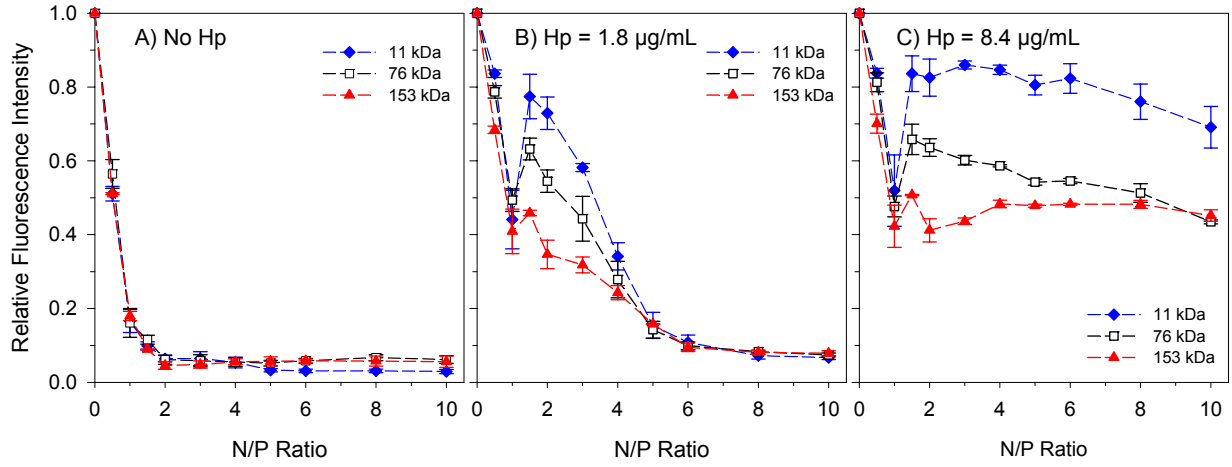

Figure A.2.7. Fluorescence intensity of Picogreen bound to DNA released from DNA/chitosan complexes upon exposure to heparin. The complexes were prepared with chitosans of different M_n (DDA = 80%) and then exposed to (A) no Hp, (B) 1.8 µg/mL of Hp, and (C) 8.4 µg/mL of Hp.

Strong bindings of DNA with chitosans of high DDA or molecular weights are desirable to resist against nuclease degradation and premature dissociation by competing polyanions but yields, on the other hand, complexes that are too stable to transfect cells since they cannot disassemble inside the cells for gene expression. The level of gene expression was previously found to decrease substantially when the chitosan DDA increased from 80% to 98% with similar M_n of about 80 kDa (Lavertu et al., 2006). However, the decrease of the DDA from 90% to 70% and 62% of a chitosan of 390 kDa resulted also in reduced gene expression levels, which were attributed to the observed destabilization of DNA/chitosan complexes by serum proteins when the DDA was lower than 90%.(Kiang et al., 2004) Chitosans with DDA values > 90% combined with high molecular weights (> 100 kDa) (Sato et al., 2001; Lavertu et al., 2006; Strand et al., 2010) showed poor transfection efficacy. These formulations that were found to be highly stable against disruption by heparin (Danielsen, Strand et al., 2005; Strand et al., 2010) resulted also in slow increases of gene expression with time, suggesting slow and inefficient release of DNA from the complexes once inside the cells (Strand et al., 2010). On the other hand, complexes formed with chitosans of too low molecular weights (< 5 kDa) were found to dissociate prematurely in transfection medium as determined by gel electrophoresis and resulted in both low cellular uptake and low efficacy of transfection (Strand et al., 2010). The release of DNA found in our study, which was induced by addition of heparin, is consistent with these previous findings relating transfection efficiency to DDA and M_n via stability arguments. A balance between complex stability and protection of DNA but retaining the ability to dissociate inside the cell must be achieved for efficient gene delivery, as previously found via observation of the coupling of either low M_n with high DDA or high M_n with low DDA values of chitosans (Lavertu et al., 2006). Results published by other groups suggesting that this balance of stability could also be

achieved by modification of polycations, such as chitosan (Strand et al., 2010) and PEI (Gabrielson et Pack, 2006), with uncharged groups to lower the binding affinity to DNA.

A.2.4.4 Role of Free Chitosan in Dispersions of DNA/Chitosan Complexes Exposed to Competing Polyanions

The amount of DNA released upon disruption of the DNA/chitosan complexes by heparin was dependent on the N/P ratio used to prepare the dispersions (Figure A.2.6 B and C; Figure A.2.7 B and C). The drop of the fluorescence intensity observed for formulations prepared at an N/P ratio of 1, and followed by a sudden increase in intensity at an N/P ratio of 1.5, was probably due to precipitation of most DNA/chitosan complexes formed near the point of charge neutralization prior to addition of Hp. Near the point of neutralization (N/P ≈ 1), lower amounts of chitosan and DNA were consequently available in solution for the competition binding with Hp, in comparison to the dispersions with an excess of DNA (N/P < 1) or chitosan (N/P >1) that generate sufficiently charged complexes to prevent precipitation (Figure A.2.3). For the dispersions exposed to 1.8 μg/mL of Hp (Figure A.2.6 B; Figure A.2.7 B), the fluorescence intensity reached its highest value at N/P = 1.5 and decreased with higher chitosan content until reaching values comparable with those measured for the samples without addition of heparin at N/P ratios above 6. Dispersions of DNA/polycation complexes prepared under similiar conditions were found to contain a significant amount of free polycation in solution (Clamme et al., 2003; Boeckle et al., 2004; Reitan et al., 2009; Ma, P.L. et al., 2010a). Free chitosan was eventually detected in our dispersions with N/P ratios at above 5 from analysis by polyacrylamide gel electrophoresis coupled with coomassie blue staining (Figure A.2.8). This finding together with the negligible amounts of DNA released from the complexes at N/P ratios above 6 suggests

that sufficient amounts of chitosan were available for binding to both DNA and heparin (1.8 μg/mL) and prevent disruption of the complexes. In the presence of a higher concentration of Hp (8.4 μg/mL), larger amounts of chitosan in the dispersions were required to prevent dissociation of the DNA/chitosan complexes (Figure A.2.6 C; Figure A.2.7 C). Heparin therefore seems to first bind to free chitosan and then to disrupt the complexes by binding to chitosan in the complexes once the free fraction has been saturated.

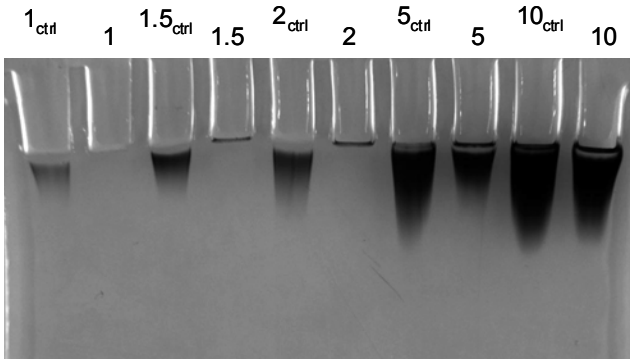

Figure A.2.8. Polyacrylamide gel electrophoresis of DNA/chitosan (80% DDA, 76 kDa) complexes prepared at N/P ratios from 1 to 10, showing the bands of free chitosan stained with coomassie brilliant blue. The controls (ctrl) correspond to solutions of chitosan at the same concentrations as in the dispersions but without DNA.

To further explore the role of free chitosan content in dispersions of DNA/chitosan complexes, we quantified free chitosan content by subjecting the samples to the depletion method with the Orange II dye employed by Drogoz et al. (2007) for the characterization of dextran-sulfate/chitosan complexes. Since the filtration step suggested by Drogoz et al. resulted in material build-up and inefficient removal of DNA/chitosan complexes, we used ultracentrifugation to spin-down the complexes and recover the supernatant containing free chitosan. The concentration of free chitosan was then determined from a calibration curve

obtained from the interaction of chitosan with the sulfonated Orange II dye. The free chitosan contents presented in Figure A.2.9 A were determined for dispersions of DNA/chitosan (80% DDA, 76 kDa) complexes after dilution with deionized water and after equilibration in MES buffer at pH 6.5 (total ionic strength of 150 mM). The dilution of the dispersions with water enabled the quantification of free chitosan under conditions that do not alter the physical properties of the DNA/chitosan complexes initially formed in a solution pH of 4.0-5.5. Under such conditions, the free chitosan content increased from 40% to 85% as the N/P ratio increased from 2 to 10 in the dispersions. These data are similar to those previously determined by asymmetrical flow field-flow fractionation (AF4) (Ma, P.L. et al., 2010a; Ma, P.L. et al., 2010b). Compared to the dispersions diluted with water, the dilution of the same dispersions but with the MES buffer yielded lower fractions of free chitosan ranging from 26% to 76% as the N/P ratio increased from 2 to 10, indicating further incorporation of chitosan into the initially formed complexes. Based on free chitosan content, we calculated the N/P ratio of the complexes themselves and found ranges of N/P of 1.3-1.5 in the dispersions diluted with water and 2.0-2.5 in MES buffer at pH 6.5. These values were essentially independent of the N/P ratio used to prepare the dispersions in the range of 3 to 10 (Figure A.2.9 B). Therefore, the dispersions with an N/P ratio of 6 contained about 60% of free chitosan in the MES buffer (Figure A.2.9 A). This fraction of free chitosan avoided the disruption of the DNA/chitosan complexes by heparin (Figure A.2.6 B; Figure A.2.7 B) since the amount of free chitosan was sufficient to accommodate the binding of 1.8 μg/mL of Hp (corresponding to an amount of negative charges that was 3-fold higher than the DNA charges in the samples). However, the free chitosan content was not sufficient when the dispersions were exposed to 8.3 μg/mL of Hp (Figure A.2.6 C; Figure A.2.7 C). To prevent the dissociation of the complexes by Hp at this concentration, the N/P ratio in the formulations must be increased substantially to increase the concentration of free

polycation in the dispersions, beyond the maximal N/P of 10 used in this study. Notably, increasing the amount of polycation above an optimal N/P ratio was found to decrease the cellular uptake of the complexes, delay the onset of gene expression, and lower gene expression levels (Boeckle et al., 2004; Strand et al., 2010). We demonstrated here that the free polycation may beneficially prevent premature dissociation of the complexes by competing polyanions but, on the other hand, it may reduce biological effectiveness if in great excess (Boeckle et al., 2004; Strand et al., 2010).

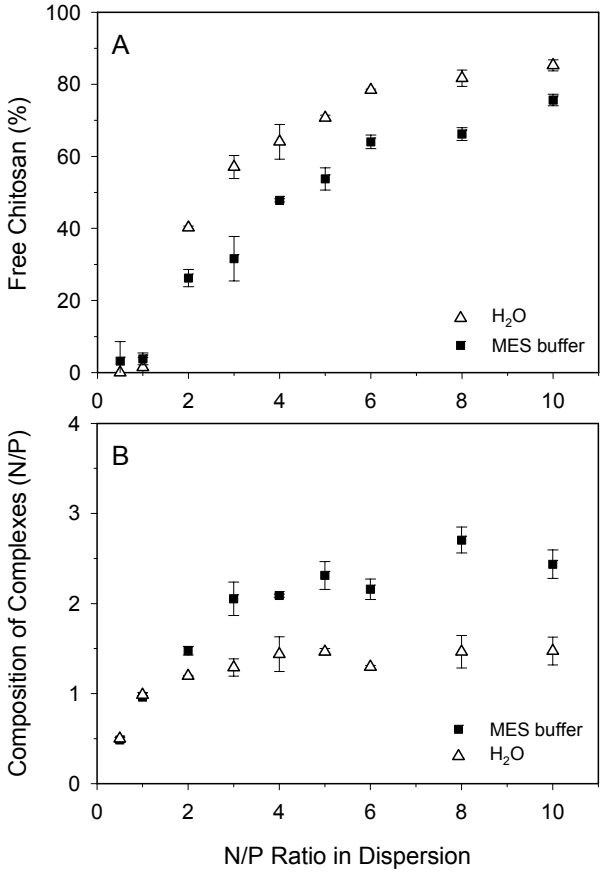

Figure A.2.9. Free chitosan content (A) and composition of complexes in terms of N/P ratio (B) in dispersions of DNA/chitosan (80% DDA, 76 kDa) complexes initially prepared at different N/P ratios and further diluted with deionized water or 25 mM MES buffer at pH 6.5 (total ionic strength of 150 mM). The fractions of free chitosan were determined by subjecting the samples to ultracentrifugation and the collected supernatants were analyzed by the Orange II depletion method.

A.2.5 Conclusions

We have demonstrated the correlation relationship between the ability of biological polyanions to disrupt DNA/chitosan complexes and their binding affinity for chitosan. The inability of hyaluronan and chondroitin sulfate to destabilize DNA/chitosan complexes is attributed to their substantially lower binding constants with chitosan compared to the chitosan-DNA binding constant as determined by ITC. Among the competing polyanions investigated here, only heparin with the highest charge density has a binding affinity with chitosan that is comparable to that of chitosan-DNA. Heparin was able to displace DNA to an extent that was dependent on the concentration of heparin and on the N/P ratio in the dispersions. The higher stability of DNA/chitosan complexes with higher N/P ratios when exposed to heparin was due to the presence of free chitosan. We found that the competing heparin first binds to free chitosan without disrupting the DNA/chitosan complexes and once the free chitosan component is saturated with heparin, further addition begins to release DNA from the complexes through competitive binding to chitosan in physiological media. This finding suggests that free polycation can prevent premature dissociation of the complexes upon interactions with anionic biological components in the extracellular matrix. Literature suggests that this free polycation fraction can increase the transfection efficiency of the complexes while excessive amounts can impede cellular uptake and induce cytotoxicity depending on polycation type. The stability of the complexes also depends on the chitosan DDA and molecular weight, in agreement with the transfection efficiency and binding affinity dependence on these parameters where increasing DDA or molecular weight increases binding affinity to DNA and thereby complex stability. Increasing chitosan DDA or molecular weight resulted in more stable complexes while decreasing these parameters led to unstable complexes in the presence of heparin. These findings

provide guidelines for the design of effective gene delivery systems where the balance between the polycation-DNA binding strength and the intracellular ability to dissociate complexes and release DNA for gene expression is required.

A.2.6 Acknowledgments

This work was supported by the Canadian Institutes of Health Research (CIHR) and by the Natural Sciences and Engineering Research Council of Canada (NSERC). Pei Lian Ma received a doctoral fellowship from the Fonds québécois de la recherche sur la nature et les technologies (FQRNT).

A.2.7 Supporting Information

Quantification of the Sulphate and Carboxyl Groups of Heparin by Conductimetric Titration.

Conductimetric titrations of heparin were performed by titrating the acid form of heparin with a solution of NaOH. We followed the procedure reported by Casu and Gennaro(1975) with some modifications. To work with the acid form of heparin, 30 mg of heparin sodium salt was dissolved in 30 mL of deionized water and then mixed with 1 g of Amberlite IR-120(H^+) ion exchange resin (Sigma, no.216534), initially washed with deionized water until reaching a constant pH to remove excess of H^+. The mixing was done under agitation for 60 min prior to the recovery of the resin by filtration. The resin was then rinsed with 10 mL of deionized water. The titration curve of the solution containing the acid form of heparin was obtained by measuring the conductivity upon addition of 0.1 M NaOH using a digital conductivity meter (VWR

Scientific). The sulfate content was determined from the first equivalence point evaluated by extrapolating the first two branches of the conductimetric titration curve. The amount of NaOH required to neutralize the carboxyl groups of heparin was determined by subtracting the amount required to neutralize the sulfate groups from the total amount of NaOH added at the second inflexion point.

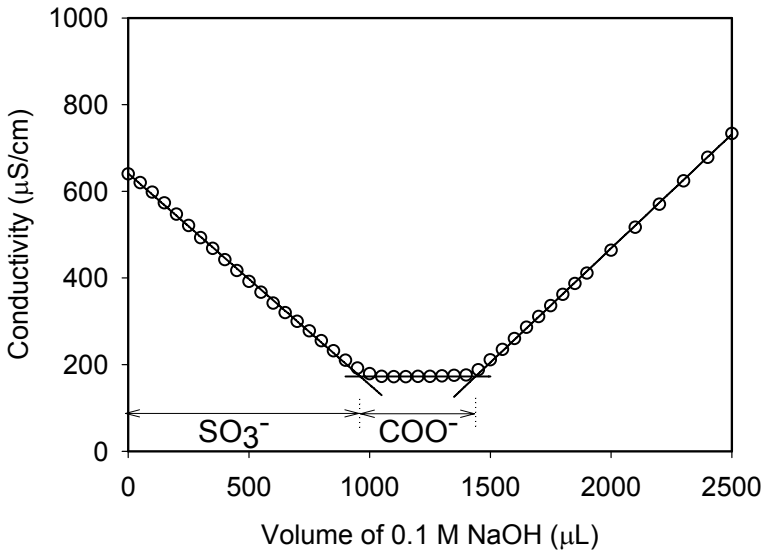

Figure A.2.SI-1. Quantification of the sulfate and carboxyl groups of heparin by conductimetric titration with 0.1 M NaOH. The content of charged groups was 3.3 moles of SO_3^-/g of heparin and 1.6 moles of COO^-/g of heparin, corresponding to a SO_3^-/COO^- ratio of 2.